C.P. No. 512
(21,429)
A.R.C. Technical Report

C.P. No. 512
(21,429)
A.R.C. Technical Report

MINISTRY OF AVIATION

AERONAUTICAL RESEARCH COUNCIL

CURRENT PAPERS

The Shapes and Lift-Dependent Drags of some Sweptback Wings designed for $M_o = 1{\cdot}2$

by

J. A. Bagley, B.Sc. and J. A. Beasley

LONDON: HER MAJESTY'S STATIONERY OFFICE

1960

PRICE 11s. 6d. NET

C.P. No. 512

U.D.C. No. 533.693.2 : 533.6.013.12 : 533.6.011.35/5 : 533.6.048.1

Report No. Aero.2620

June, 1959.

R O Y A L A I R C R A F T E S T A B L I S H M E N T

THE SHAPES AND LIFT-DEPENDENT DRAGS OF SOME SWEPTBACK WINGS DESIGNED FOR $M_o = 1.2$

by

J.A. Bagley, B.Sc.,

and

J.A. Beasley

SUMMARY

The camber and twist distributions needed to produce a constant spanwise C_L-distribution and certain linear chordwise load distributions have been calculated by linearised supersonic theory at $M_o = 1.2$ for a set of 34 thin sweptback wings. The wing planforms cover a range of aspect ratios from 2.0 to 3.5 and leading-edge sweep angles from 55° to 70°. Both leading and trailing edges are subsonic at the design Mach number, and the slenderness parameter $\beta s/\ell$ is between 0.19 and 0.40.

The lift-dependent vortex and wave drags associated with these loadings have also been calculated, and appear not to be excessive in almost all the cases considered.

LIST OF CONTENTS

LIST OF APPENDICES

LIST OF ILLUSTRATIONS

1 INTRODUCTION

In Ref.1, an attempt was made to set down the aerodynamic principles which should be employed in the design of a swept-winged aircraft intended to operate at low supersonic speeds, and to show in particular how a suitable design might be evolved for a long-range transport aeroplane. Predominant among these aerodynamic principles is the need to design the wing so that essentially shock-free flow is maintained over the whole wing in the cruising condition. Unless this is done, there is a considerable risk that separated or unsteady flows will be obtained, and it is likely that the drag will be large.

In the particularly simple case of a swept wing with constant sections and infinite span (the so-called "infinite sheared wing"), it is well-known that a shock-free "sub-critical" flow which gives no normal-pressure drag can be obtained at zero lift provided the Mach number component normal to the wing isobars nowhere exceeds unity. The isobars on such a wing are naturally straight lines, parallel to the leading- and trailing-edges. A considerable body of theoretical and experimental work has shown that similar sub-critical flows can be obtained on swept wings of finite span, by combining them with suitably designed fuselages, and that again there is essentially no normal-pressure drag arising on the wing itself at zero lift. The 'wave drag' of such a wing-fuselage combination need not be much more than that of the fuselage itself.

In Ref.1 the suggestion is made, and applied, that a lifting wing-fuselage combination should also be designed so that the isobars on the wing are straight and the local Mach number component perpendicular to them nowhere exceeds unity, in which case a sub-critical, essentially shock-free, flow should again be obtained on the wing. Such a flow should certainly be well-behaved, but this does not imply that the normal-pressure drag will still be negligible as it is is on the constant-section wing at zero lift.

By using linearised supersonic theory, the drag associated with any distribution of lift forces can be calculated. It can be shown (see, for example, Ref.2, p.222) that this drag can be separated into two terms: one depending on the spanwise lift distribution, and one depending on the lengthwise lift distribution. The former, the so-called "vortex drag", is independent of Mach number; while the latter term, the "lift-dependent wave drag", appears only at supersonic speeds and increases with $(M_o^2 - 1)$. This lift-dependent wave drag must appear as a normal-pressure drag on the configuration, and one purpose of the present work is to investigate how large this drag term is likely to be on wings which are intended to have sub-critical flows at lift.

The present work has, in fact, a dual origin. In the first place, there was a requirement to find out what camber shapes would be needed on a wide range of wing planforms to obtain the type of load distribution proposed in Ref.1 - namely a constant spanwise C_L-distribution with straight isobars. This purpose has largely controlled the choice of wing planforms and loadings which have been dealt with. Secondly, there was the desire to have more examples of the lift-dependent wave drag calculated on reasonably "practical" wings, and to relate these to calculations of the spanwise drag distributions to see where the normal-pressure drag is actually concentrated.

In principle, a wing of given planform can be cambered and twisted to have any prescribed load distribution at a specified speed. This load distribution will not, of course, be maintained at incidences other than the design value. In the present work, supersonic thin-wing theory has been used to calculate the warp distributions needed on 34 wing planforms to produce certain load distributions at $M_o = 1.2$. To reduce the computations to

manageable proportions, only simple loadings have been considered: these are of the form

$$-\Delta C_p(x,y) = A + B\xi$$

where A and B are constants and $\xi = \dfrac{x - x_L}{x_T - x_L}$; $x_L(y)$ and $x_T(y)$ being the equations of the wing leading- and trailing-edges. All the results have been calculated, and are presented here, for a lift coefficient $C_L = 0.25$. The wing slopes are all proportional to the lift coefficient, so the camber and twist needed on wings designed for a lower C_L would be proportionately reduced.

The simple load distributions considered will only give an approximation to the desired type of pressure distribution with straight isobars, except on wing-fuselage combinations with a special thickness distribution such that the zero-lift pressure distribution also has straight isobars, and then only within linearised theory. Another deficiency of these loadings is that, in the linearised theory, the finite load specified at the leading-edge leads to a logarithmic singularity in the wing slope there. Even though this singularity is removed (in a rather arbitrary fashion) by the calculation method adopted here, the shapes calculated offer no guarantee that the flow will be attached at the leading-edge in the design conditions, and there is considerable risk of the flow separating from the lower surface. In practice, this difficulty can probably be overcome by suitably modifying the wing sections, particularly near the nose, but this will in itself further modify the wing isobar pattern.

A further simplification had perforce to be adopted in these calculations: they were all made for isolated wings, since no practical method exists for calculating the influence of a fuselage at supersonic speeds. In Appendix 1 (which is an extension of work by Weber[3]) slender-body theory is applied to calculate the shape needed for the junction section of an untapered sweptback wing mounted on a cylindrical fuselage at zero incidence. This is compared with the shape calculated for the centre of an isolated wing designed to carry the same load distribution. It is concluded that the shapes calculated for isolated wings should provide an acceptable approximation to the shapes needed on wing-fuselage combinations with near-circular fuselage cross-sections. It is clearly not permissible to assume (as has sometimes been done) that the extremely twisted part of the wing near the centre will be covered in practice by the fuselage of a wing-fuselage combination.

The wing planforms which have been considered are detailed in section 2; they cover a range of aspect ratios from 2.0 to 3.5, and leading-edge sweeps from 55° to 70°. The minimum trailing-edge sweep considered is 35°, so all the wings have subsonic leading- and trailing-edges at $M_o = 1.2$. All the wings are members of a particular family with curved leading-edges over the outer part, and streamwise tips.

The calculation of the camber distributions is described in section 3.1, with some discussion of the significance of the results in section 3.2. The determination of lift-dependent drags from the spanwise and lengthwise load distributions is presented in sections 4.1 and 4.2. The spanwise drag distribution has been calculated for a few of the wings in section 4.3, and these are integrated to compare with the other method of estimating lift-dependent drags.

From the lengthwise loading, the centre of pressure position can also be determined, and in section 5 these positions are compared with calculated positions of the low-speed aerodynamic centre. Any large difference between these positions implies that a trimming load is needed, since the centre of gravity of an aircraft must be close to the low-speed aerodynamic centre if it is to be stable at low speeds. The comparison presented may therefore be of some value in assessing the relative difficulty of trimming wings with different planforms, although it is not possible to make estimates of the actual trim-drag penalties.

2 THE RANGE OF PLANFORMS CONSIDERED

The family of swept wings considered in this survey (originally described by Beasley in an unpublished R.A.E. note) are shown in Fig.2, with an explanation of the symbols used in defining them in Fig.1. This family is a fairly arbitrary selection of planforms which represents an attempt to extend the small number of wings considered in Ref.1 to cover the range of aspect ratios and sweep angles thought to be of interest for the design of transport aeroplanes intended to cruise at low supersonic speeds.

All the wings considered have edges swept back at more than the Mach angle for the design speed $M_o = 1.2$; all have straight trailing-edges and leading-edges composed of a straight inner half with a parabolic curved tip. This particular parabolic shape has no peculiar merit - any curved edge which fairs into a streamwise tip would probably also be aerodynamically satisfactory. An experiment by Hall and Rogers[4] on a particular wing with a square-cut tip has illustrated the complicated flow patterns which develop at transonic speeds near the tip. Most of these complicated features appear to be connected with the presence of the discontinuity at the square tip, and this lends support to the arguments which have been put forward (e.g. in Ref.1) in favour of curved tip shapes. It is also worth noting that Lock's work[8], referred to in section 3.2 below, also leads to similar curved tip shapes.

Each planform of the family is defined by four parameters: the sweep-back angles of the leading-edge, φ_o, and of the trailing-edge, φ_1; the aspect ratio A; and the fraction of the semi-span occupied by the straight segment of the leading-edge, η_t. (For all the wings considered here, $\eta_t = \frac{1}{2}$; in practice a range $0.3 \leqslant \eta_t \leqslant 0.7$ might cover all cases of practical interest, and within this range changes in the calculated warp distribution are not likely to be significant.)

Other geometrical parameters of interest are the semi-span s, root chord c_o, overall length (in the x-direction) ℓ, and the "projected tip chord", c_t, defined as shown in Fig.1 by extending the straight part of the leading-edge. None of the more conventional definitions of "taper ratio" appears to be convenient for wings of this sort, so a taper ratio T defined as c_t/c_o is used here.

Let x, y, z be right-handed Cartesian coordinates with x measured streamwise, y spanwise, z upwards and the origin at the apex. Then the leading-edge of any planform in the family is given by

$$\left.\begin{aligned} x &= m_o y && \text{for} \quad 0 < y < \eta_t s \\ x &= m_o y + c_t\, f(\eta) && \text{for} \quad \eta_t s < y < s \end{aligned}\right\} \qquad (1)$$

where $$f(\eta) = 1 - 2\sqrt{\frac{1-\eta}{1-\eta_t}} + \frac{1-\eta}{1-\eta_t}$$

$$m_o = \tan\varphi_o\,, \qquad m_1 = \tan\varphi_1\,, \qquad \eta = y/s$$

The trailing-edge is given by

$$x = c_o + m_1 y \tag{2}$$

It can easily be shown that

$$A = \frac{4\frac{s}{c_o}}{1 + \left\{1 - \frac{s}{c_o}(m_o - m_1)\right\}\left(\frac{2+\eta_t}{3}\right)}$$

or $$\frac{c_o}{s} = \frac{\frac{12}{A} + (m_o - m_1)(2 + \eta_t)}{5 + \eta_t} \tag{3}$$

Also, $$T = \frac{\frac{12}{A} - 3(m_o - m_1)}{\frac{12}{A} + (2 + \eta_t)(m_o - m_1)} \tag{4}$$

and $$\frac{s}{\ell} = \frac{5 + \eta_t}{\frac{12}{A} + m_o(2 + \eta_t) + 3m_1} \tag{5}$$

Values of these parameters for the 34 wings shown in Fig.2 are tabulated in Table 1. It may be worth drawing attention to the fact that all the wings considered are aerodynamically fairly slender; at the design speed $M_o = 1.2$, the slenderness parameter $\beta s/\ell$ lies between 0.19 and 0.40 for all the wings considered.

3 CAMBER AND TWIST DISTRIBUTIONS

3.1 Calculation methods

As is shown for example in Sears[2], Section D.10, pp.148 et seq, a thin wing in a supersonic stream of velocity V_o and Mach number M_o which carries a load distribution $\Delta C_p(x,y)$ can be represented by a planar distribution of vortices which produce a perturbation velocity potential

$$\phi(x,y,z) = -\frac{V_o}{4\pi}\iint_{\tau}\frac{z.(x-x_1)\,\Delta C_p(x_1,y_1)\,dx_1\,dy_1}{\left[(y-y_1)^2+z^2\right]\left[(x-x_1)^2-\beta^2(y-y_1)^2-\beta^2z^2\right]^{\frac{1}{2}}} \qquad (6)$$

where $\beta^2 = M_o^2 - 1$, and the integration is carried out over all points (x_1,y_1) on the wing plane lying within the Mach forecone of the point (x,y,z). The wing shape can be calculated as a stream surface of this velocity field: applying a linearised boundary condition gives

$$\frac{\partial z}{\partial x}(x,y) = \frac{v_z(x,y,z)}{V_o} = \frac{1}{V_o}\frac{\partial \phi}{\partial z}(x,y,z)$$

To find the wing shape needed to support a prescribed load distribution thus requires first an integration to determine the potential ϕ, which is differentiated with respect to z to obtain the distribution of surface slope on the wing.

By considering only load distributions of the form $-\Delta C_p(x,y) = A + B\xi$, the practical application of equation (6) can be simplified (at the expense of certain disadvantages pointed out in section 1). Two slightly different techniques for dealing with equation (6) have been used to produce the present results.

By performing the integration on the right-hand side of (6) first with respect to x_1, differentiating with respect to z and taking the limit as $z \to 0$, Roper[5] has obtained an expression involving a singular integral with respect to y_1, which is valid for wings of zero thickness. A numerical method of performing the final integration and obtaining the desired limit has been developed by Watt[6], in a form suitable for calculation on a digital computer, and the DEUCE computers of Mathematical Services Department, R.A.E. have been used to perform these calculations for the present work.

Using this approach, the value of $\partial z/\partial x$ becomes logarithmically infinite at points on the centre-line $y = 0$, and on the leading- and trailing-edges unless $\Delta C_p = 0$ there.

The singularities at the leading- and trailing-edges do not appear in the results reproduced in Figs.3 to 40. Values of $\partial z/\partial x$ were calculated on DEUCE for the points $\xi = 0.01$, 0.03, 0.05 and 0.1 (0.1) 0.9; these were used in an interpolation and integration routine (described by Watt[6]) which extrapolates to give finite values at $\xi = 0$ and $\xi = 1$, and this process produces the values of $z(x,y)$ shown in Figs.3 to 40.

On most wings, results were obtained for the spanwise stations $y/s = 0.05$, 0.1, 0.2, 0.4, 0.6, 0.8 and 0.9; on a few wings extra points were calculated which are included in the appropriate figures. It may be of interest to record that the actual time needed to produce the standard set of 84 values of $\partial z/\partial x$ on the DEUCE was about $2\frac{1}{2}$ hours for each wing and each load distribution.

To avoid the logarithmic singularity at the centre of the wing, in the case of a constant-chord wing, Weber[3] has dealt with equation (6) by integrating first with respect to y_1, differentiating with respect to z, and taking $z = z_t(\xi)$ in the result, where $z_t(\xi)$ are the ordinates of an appropriate uncambered wing of finite thickness. For points on the centre-line y = 0 the resulting integrals with respect to x_1 can be obtained in closed form for loadings of the specified type, and explicit expressions for the slope of the wing centre-line are derived. Cooke[7] has developed this method to obtain approximate results at the centre-line of wings with tapered planforms. Results from Refs.3 and 7 for the wings considered here are included in Figs.3 to 40; these calculations were made (on desk calculating machines) using values of z_t appropriate to a 6% thick RAE 101 wing section.

Cooke's results[7] are strictly valid only for wings on which the curved part of the leading edge does not intrude into the Mach forecone of the centre-line trailing-edge point, i.e. for wings of the family described in section 2 for which

$$\frac{c_o}{s} \leqslant \frac{m_o + \beta}{2m_o\beta}$$

This condition is not satisfied for most of the smaller aspect-ratio wings, but the errors should be small and confined to the neighbourhood of the trailing-edge.

3.2 Discussion of results

Two particular chordwise load distributions have been taken for the examples calculated here:

(a) a triangular loading given by

$$-\Delta C_p = 0.5 - 0.5\xi$$

(b) a uniform loading given by

$$-\Delta C_p = 0.25$$

Both give a sectional lift coefficient $C_L = 0.25$, and, of course, an overall wing lift coefficient $\overline{C_L} = 0.25$.

For the triangular loading, the camber shapes needed for all 34 planforms shown in Fig.2 have been calculated; for the uniform loading only four wings (wings 3, 5, 17 and 24 in Fig.2 and Table 1) have been considered. The results are shown in Figs.3 to 40: of these, Figs.6, 9, 22 and 30 show the results for the wings carrying uniform load.

These figures show that the most significant feature of all these wing shapes is the large incidence required at the wing centre, and the large spanwise twist variation. The values of centre-line incidence, α_c, for the various planforms are summarised in Fig.41(a), from Ref.7; as explained above, these results are strictly valid only for wings on which

$$\frac{c_o}{s} \leqslant \frac{m_o + \beta}{2m_o\beta}$$

Furthermore, these results have been calculated assuming a 6% thick RAE 101 wing section, and different results would be obtained if a different thickness distribution were assumed. The effect of changing the thickness-chord ratio on one particular planform is shown in Fig.41(b), taken from Ref.3.*

Comparison between the results presented for two different loadings on wings 3, 5, 17 and 24 shows that there is a broad similarity between the shapes needed to produce different loadings, but the section camber-lines are naturally quite different and the spanwise twist distributions do differ to a certain extent. The variation in shape of the camber-lines is illustrated in Fig.42, showing results for a particular wing. (In this figure, the actual camber-line ordinates are plotted; the local twist which is included in Figs.3 to 40 is here subtracted at each station.)

The differences in spanwise twist variations associated with the triangular and uniform chordwise loadings is illustrated in Fig.43. This shows results for the inner half of wing 3, compared with some calculations made (at $M_o = 1$) for a wing of infinite span, obtained by integrating equation (67) of Ref.3. It is noteworthy that the values for the 'infinite sheared wing' (obtained as $y \to \infty$) are approached very slowly. Even at $y/c = 2$, which would represent mid-semispan on an untapered wing of aspect ratio 8, the local incidence is still $\frac{1}{4}^o$ higher than on the infinite wing.

To examine further the changes in wing shape required to produce different chordwise loadings, calculations were made at $M_o = 1$ of the centre-section shapes associated with the two chordwise load distributions already discussed and also with the loading $-\Delta C_p = C/\sqrt{\xi}$ which is of the same type as that of a flat plate at incidence. These calculations are described in Appendix 2, and the results for an untapered wing with 55^o sweep are shown in Fig.52. These confirm that the main feature is the large local incidence required at the wing root.

In this context, some work by Lock[8] is also relevant. He has considered the problem of designing the planform of a flat thin wing so that, at incidence, the singularity in the load distribution at the leading-edge has a constant strength outboard of a specified point. The chordwise load distributions then have a leading term of the form $-\Delta C_p = C/\sqrt{\xi}$, and the coefficient C is constant over the outer part of the wing.

Lock prescribed an untapered inner part of the wing, and found that the planform needed over the outer part comprised a curved leading-edge and a streamwise tip. The planform obtained is similar to wing 3 of the family shown in Fig.2. Not only is the leading-edge singularity constant over the curved part, but the whole chordwise load distribution is found to be almost the same over the outer part of the wing.

Thus, Lock has obtained a wing on which nearly constant chordwise loadings are associated with constant (uncambered, untwisted) wing shapes over the whole outer part of the planform. However, the load distributions over the inner part of the planform do vary considerably; to maintain the

---

* The results in Fig.41(b) are actually from calculations made at $M_o = 1$, but it is shown in Ref.3 that the differences from calculations at $M_o = 1.2$ are small.

same chordwise loading there also, camber and twist would be needed. It follows from the results shown in Fig.52 that the centre-section incidence would have to be of the same order as is shown in Figs.5 and 6 for wing 3 with triangular and uniform chordwise loadings.

4 CALCULATION OF LIFT-DEPENDENT DRAGS

The total lift-dependent drag on any wing can be defined as being equal to the momentum transported through a cylindrical control surface surrounding the wing (see e.g. Ref.2, p.222). This can conveniently be separated into "vortex drag" and "wave drag" components, which are equal to the momentum transported through the parts of the control surface respectively perpendicular and parallel to the stream direction.

4.1 Vortex drag

The vortex drag can be shown to be

$$D_V = -\tfrac{1}{2}\rho \int_{-s}^{s} \Gamma\, w_\infty \, dy$$

where

$$\Gamma = \tfrac{1}{2} V_o \, C_L \, c$$

is the circulation round a section of the wing

and

$$w_\infty = \frac{1}{2\pi} \int_{-s}^{s} \frac{d\Gamma}{dy_1} \frac{dy_1}{y - y_1}$$

is the downwash in the Trefftz plane far downstream of the wing.
It is noteworthy that this relation does not depend on Mach number.

Thus the vortex drag coefficient, based on wing area S, is

$$C_{DV} = \frac{D_V}{\tfrac{1}{2}\rho V_o^2 S} = \frac{1}{8\pi A} \int_{-1}^{1} C_L \frac{c}{\bar{c}} \left\{ \int_{-1}^{1} \frac{d}{d\eta_1} \left(C_L \frac{c}{\bar{c}} \right) \frac{d\eta_1}{\eta - \eta_1} \right\} d\eta \qquad (7)$$

where $\bar{c}$ is the (geometric) mean chord of the wing.

For wings designed, as here, to have constant $C_L(y) = \overline{C_L}$, the vortex drag factor K_V is then:

$$K_V = \frac{C_{DV}}{\overline{C_L}^2/\pi A} = \frac{1}{8} \int_{-1}^{1} \frac{c}{\bar{c}} \left\{ \int_{-1}^{1} \frac{d}{d\eta_1} \left(\frac{c}{\bar{c}} \right) \frac{d\eta_1}{\eta - \eta_1} \right\} d\eta \qquad (8)$$

This is simply a function of the planform shape, and for the present series of wings with η_t constant it is clear from equations (1) and (4) that K_V is a function of the taper ratio T only. Equation (8) has been integrated numerically, and the result is shown in Fig.44.

It is noteworthy, that, except for wings with $T < 0.25$, values of K_V less than 1.1 are obtained. There is clearly a considerable range of planforms on which it should be possible to design for straight isobars without incurring an excessive vortex drag penalty.

If equation (7) is integrated by parts, it yields

$$C_{DV} = -\frac{A}{32\pi} \int_{-1}^{1} \int_{-1}^{1} \frac{d}{d\eta}\left(\frac{C_L c}{s}\right) \frac{d}{d\eta_1}\left(\frac{C_L c}{s}\right) \ell n|\eta - \eta_1| \, d\eta \, d\eta_1 \qquad (9)$$

This symmetrical form is analogous to the expression (equation (10)) obtained for the wave drag. The vortex drag can thus be obtained from the spanwise load distribution by using Eminton's method[9] originally developed for calculating the zero-lift wave drag of slender bodies. As a matter of interest, this method was applied to several examples from the present series of wings, and points were obtained agreeing very closely with the curve in Fig.44.

4.2 Lift-dependent wave drag

A lifting wing at supersonic speeds can be represented in a linearised theory by a planar distribution of doublets, and their influence at large distances (in particular the momentum transport across a cylindrical control surface which can be equated to the wave drag) can be represented by a set of equivalent distributions of singularities along a streamwise line. Using this principle, Heaslet, Lomax and Spreiter[10] have expressed the lift-dependent wave drag of a wing as a triple integral involving the streamwise distributions of the lift intercepted by oblique planes, in direct analogy to the 'supersonic area rule' used for calculating the wave drag due to thickness of non-lifting bodies. This result can be expanded[11] as a series of terms involving powers of a slenderness parameter $(\beta s/\ell)^2$; the leading term in this series involves only the distribution of the cross-load $L(x)$ defined by

$$L(x) = \tfrac{1}{2}\rho V_o^2 \int_{-\sigma}^{\sigma} (-\Delta C_p) \, dy$$

where $\sigma(x)$ is the local semispan.

For sufficiently small values of $(\beta s/\ell)^2$, the lift-dependent wave drag is then given by

$$\frac{D_W}{\frac{1}{2}\rho V_o^2} = \frac{-(M_o^2 - 1)}{16\pi} \int_0^{\ell} \int_0^{\ell} \frac{L'(x)}{\frac{1}{2}\rho V_o^2} \frac{L'(x_1)}{\frac{1}{2}\rho V_o^2} \ell n|x - x_1| \, dx \, dx_1 \qquad (10)$$

$$\left(\text{where } L'(x) \text{ denotes } \frac{dL(x)}{dx}\right),$$

provided that $L(o) = L(\ell) = 0$. This condition is satisfied by all the wings treated here.

If the cross-load distribution is elliptical, equation (10) yields R.T. Jones' lower bound to the lift-dependent wave drag for a wing of given semispan and overall length and small $(\beta s/\ell)^2$:

$$C_{DW} = \frac{\overline{C_L}^2}{\pi A} \cdot 2 \left(M_o^2 - 1 \right) \left(\frac{s}{\ell} \right)^2 \qquad (11)$$

If the cross-load distribution is not elliptical, it is sometimes convenient to write

$$C_{DW} = K_W \frac{\overline{C_L}^2}{\pi A} \cdot 2 \left(M_o^2 - 1 \right) \left(\frac{s}{\ell} \right)^2 \qquad (12)$$

where the factor K_W is a measure of the extent to which the actual cross-load distribution differs from an ellipse. (This factor is not in general a function of any particular simple geometrical parameter.)

On the wings of the present series, the slenderness parameter $\beta s/\ell$ has values up to 0.40, which is probably small enough for equation (10) to give an adequate approximation since the lift-dependent wave drag at $M_o = 1.2$ is only about 20% of the total lift-dependent drag, which is itself only about one-third of the total drag of a practical aeroplane in cruising conditions. The error in using equation (10) might be more significant for other planforms, for example M-wings, and the full result obtained by Heaslet, Lomax and Spreiter[10] involving the oblique loading should then be used.

A convenient method of evaluating the double integral in equation (10) is to use the numerical method developed by Eminton[9] for dealing with the corresponding problem for non-lifting bodies. This was done by Beasley in the present case, and is discussed in more detail in Appendix 3. The results of the calculations are shown in the form of a drag factor

$$\frac{C_{DW}}{\overline{C_L}^2/\pi A} \qquad \text{at} \qquad M_o = 1.2$$

in Figs.45(a) and 45(b) for triangular and uniform chordwise loadings respectively.

The results are also related to R.T. Jones' lower bound in Fig.46 which shows the factor K_W of equation (12). (As was pointed out above, there is no reason to expect any relation between K_W and T - the choice of T as ordinate in Fig.46 is merely for convenience). It appears that K_W lies between about 1.2 and 1.4 for all the wings and loadings considered here. This suggests that no excessive penalty in lift-dependent wave drag would be incurred by designing wings to have straight isobars.

Combining the vortex and wave drags gives the total lift-dependent drag factor

$$K = \frac{C_{DV} + C_{DW}}{\overline{C_L}^2/\pi A}$$

which is shown in Figs.47(a) and 47(b) for the two chordwise loadings considered. For wings of given aspect ratio and leading-edge sweep, it seems that minimum drag should be obtained at about T = 0.7, but there is little significant change in drag over the range $0.5 \leq T \leq 1.0$. On the other hand, highly-tapered wings designed to have constant chordwise loading are at a definite disadvantage.

4.3 Spanwise drag distribution

Although the division of lift-dependent drag into vortex and wave-drag elements just presented is convenient for many purposes, it is also instructive to consider the spanwise distribution of streamwise forces acting on the wing. This can be done by multiplying the local load by the local surface slope and integrating to obtain the sectional drag coefficients:

$$C_D(y) = - \int_{x_L}^{x_T} \Delta C_p(x,y) \frac{dz}{dx} \, dx$$

The results obtained in this way for several wings are shown in Fig.48.

For comparison, the spanwise distributions of sectional drag coefficients for wings with the same planforms which are cambered to produce the same load distributions at $M_o = 0$ are also shown. These were obtained by Vickers-Armstrongs Ltd.[12] in a programme of calculations undertaken in parallel with the present investigation, and are calculated from the relation

$$C_D(y) = C_L(y) \, \alpha_i(y)$$

where the induced incidence distribution $\alpha_i(y)$ was calculated by Multhopp's method.*

It is noteworthy that at supersonic wings there is a marked concentration of local normal-pressure drag near the centre of the wing, and that in fact some thrust force is carried on the outer part of the wing.

By integrating the spanwise distributions of $C_D(c/\bar{c})$ in Fig.48, the overall drag coefficient can be obtained and compared with the values obtained above for the separate vortex and wave drag elements. In principle, the value obtained from the integration of local forces should be more accurate than the other, since the theory used in section 5.2 to obtain the lift-dependent wave drag involves the additional assumption that the wing is slender. However, in practice the numerical result for the overall drag is obtained by a succession of graphical integrations, in which the singularities at the edges of the planforms are not properly dealt with, and it is impossible to obtain very accurate results from the limited number of points available. The order of agreement shown in Fig.49 for a number of the wings therefore seems to be reasonable, and it serves to some extent to provide an independent check of the shapes calculated in section 2. It is clearly not possible to use these comparisons as a check on the validity of the assumption, made in section 4.2, that equation (10) could be used although some of the wings may not be strictly slender.

---

* An exact calculation of $\alpha_i(y)$ would have shown a logarithmic singularity at the centre of the tapered wings; Multhopp's method evades this by effectively modifying the wing planform near the centre.

5 CENTRES OF PRESSURE AND LOW-SPEED AERODYNAMIC CENTRE POSITIONS

On a complete aeroplane, the requirement for low-speed longitudinal stability demands that the aerodynamic centre is close to the aircraft centre of gravity. Therefore, unless the centre of pressure at cruise is also close to the low-speed aerodynamic centre, some form of trimming load is required. This can be done in various ways: for example by a tailplane or foreplane, or by a suitable distribution of load along the fuselage, and the consequent drag penalty will depend on the precise method of doing it. (It need not even be a penalty, as has been pointed out by Richardson[13].)

It is thus not practicable to compare the trim drags associated with the various planforms considered here in the quantitative fashion which can be done for the other lift-dependent drag terms. Some form of comparison seemed to be desirable, however, so in Fig.2 there are shown the centres of pressure associated with the triangular and uniform loadings on each of the 34 wings, together with the low-speed aerodynamic centre position. These positions are also tabulated in Table 1. The centres of pressure at $M_o = 1.2$ were calculated from the cross-load distribution, as explained in Appendix 3: the two loadings considered probably represent reasonably adequately the range of loadings likely to be used in practical cases.

The low-speed aerodynamic centre positions were calculated by Küchemann's method[14], assuming that attached flow will be maintained in the low-speed condition, and taking no account of the loading likely to be obtained by deflecting flaps or similar devices. With these limitations, however, it may be fair to conclude from the results shown in Fig.2 that for a fairly wide range of sweep and aspect ratio it should not be difficult to arrange that the design centre of pressure is close to the low-speed aerodynamic centre, and hence to the aircraft centre of gravity, so that little or no trim load should be needed in cruising flight.

6 CONCLUSIONS

Supersonic thin-wing theory has been used to calculate the camber and twist distributions which would be needed to obtain, at $M_o = 1.2$, a constant spanwise C_L-distribution and particular chordwise loadings on a particular family of sweptback wing planforms. The shapes needed to produce triangular chordwise load distributions have been calculated for 34 wings, and the shapes needed for uniform loading have also been calculated for four of these. This programme of calculations was originally projected as an extension of the work of Ref.1, to survey a wide range of wing planforms which might be applicable to the design of transport aeroplanes cruising at low supersonic speeds.

The resulting wing shapes are all generally similar in character, having a large incidence at the centre-line and a considerable variation in incidence across the span.

Although the shapes presented here were all calculated for $M_o = 1.2$, Weber has shown[3] that the centre-section shapes of constant-chord wings designed to have a linear chordwise load distribution at $M_o = 0$, 1.0 and 1.2 are all very similar. In addition, a series of calculations made at $M_o = 0$ for the same planforms and load distributions as the present series (by Vickers-Armstrongs Ltd.[12]) has also produced wing shapes very similar to the $M_o = 1.2$ results given here. It is therefore suggested that the general character of these results would be found also in calculations made at other speeds.

The lift-dependent vortex and wave drags associated with both triangular and uniform chordwise load distributions on this family of wing planforms have been calculated, and the values obtained are not much greater than the lower bounds for wings of these planforms. The vortex drag factors, K_V, lie between 1.01 and 1.12 for all wings with taper ratio less than 5 to 1, and the lift-dependent wave drag factor K_W is between 20% and 40% greater than R.T. Jones' lower bound. This indicates that wings designed to have constant C_L and chordwise loading (hence straight isobars) need not have high lift-dependent drags, unless they have highly tapered planforms.

Since these calculated drags are not much greater than the lower-bound values, there does not seem to be much scope for attempts to find wing shapes with lower theoretical drags. The objects of future research in this field should rather be to find out how closely the theoretical values can be approximated in practice in a real flow on thick wings; and possibly to find less extravagant shapes with similar characteristics. In the latter context, the use of asymmetric body waisting which should reduce the large local incidences needed in the wing root appears particularly attractive.

The calculated vortex drag factors are independent of Mach number, and thus refer to wings of this family, designed to have constant spanwise C_L-distributions at any speed. The lift-dependent wave drag factors are calculated using a theory[11] which assumed that the slenderness parameter $\beta s/\ell$ is small; they should be correct for wings designed to have these load distributions at low supersonic speeds for values of $\beta s/\ell$ similar to those considered here (i.e. up to 0.40). At higher supersonic speeds the lift-dependent wave drag forms a higher proportion of the total drag of a practical aircraft, and the use of equation (10) would be valid only for smaller values of $\beta s/\ell$.

To provide some indication of possible trimming problems, the centre of pressure associated with these load distributions has been calculated, and compared with the aerodynamic centre position at low speeds calculated for attached flow. It appears that, on some of the wings at least, there should be no great difficulty in arranging for the design centre of pressure at $M_o = 1.2$ to be close to the low-speed aerodynamic centre, in which case trimming problems should not be serious.

7 ACKNOWLEDGEMENTS

The authors are particularly indebted to Mr. J.M. Watt and Miss E. Eminton of R.A.E., who prepared the programmes for the DEUCE computer referred to in section 3, and to Dr. J. Weber for the analysis presented in Appendices 1 and 2.

LIST OF REFERENCES

No.	Author	Title, etc.
1	Bagley, J.A.	An aerodynamic outline of a transonic transport aeroplane. Unpublished M.O.A. Report ARC.19,205.
2	Sears, W.R. (ed)	High-speed aerodynamics and jet propulsion. Vol.VI. General theory of high-speed aerodynamics. Oxford University Press, 1955.
3	Weber, J.	The shape of the centre part of a sweptback wing with a required load distribution. R & M.3098.
4	Hall, I.M., Rogers, E.W.E.	The flow pattern on a tapered sweptback wing at Mach numbers between 0.6 and 1.6. ARC.19,691, Nov. 1957.
5	Roper, G.M.	Formulae for calculating the camber surfaces of thin sweptback wings with subsonic leading edges and subsonic or supersonic trailing edges. Unpublished M.O.A. Report. ARC.21,430.
6	Watt, J.M.	The calculation of ordinates of twisted and cambered high-speed wings. Unpublished M.O.A. Report.
7	Cooke, J.C.	The centre section shape of swept tapered wings with a linear chordwise load distribution. C.P.470. September, 1958.
8	Lock, R.C.	The design of wing planforms for transonic speeds. ARC.21,480. December, 1959.
9	Eminton, E.	On the minimisation and numerical evaluation of wave drag. Unpublished M.O.A. Report. ARC.19,212. November, 1955.
10	Heaslet, M.A., Lomax, H., Spreiter, J.R.	Linearised compressible-flow theory for sonic flight speeds. NACA Report 956, 1950. NACA T.N.1824.
11	Adams, M.C., Sears, W.R.	Slender body theory - review and extension. Journal Aero. Sciences, Vol.20, p.85, Feb. 1953.
12	Blake, M.	Results of some calculations on camber and twist distributions for swept wings at M = 0. Vickers-Armstrongs (Aircraft) Ltd., Supermarine Works, Report No. A.570.2, (Sept.) 1959.
13	Richardson, J.R.	Notes on drag-due-to-lift and trim drag. Handley Page Ltd. Report HP/Aero/279, Feb. 1957.

LIST OF REFERENCES (Contd.)

No.	Author	Title, etc.
14	Küchemann, D.	A simple method of calculating the span- and chord-wise loading on straight and swept wings of any given aspect ratio at subsonic speeds. R & M.2935, August, 1952.
15	-	DEUCE Programme News - No.19. English Electric Co. Nelson Research Laboratories Report NSy86, Jan. 1958.

APPENDIX 1

THE SHAPE OF A SWEPTBACK WING WHICH PRODUCES A CONSTANT SPANWISE LOAD DISTRIBUTION WHEN COMBINED WITH A CYLINDRICAL FUSELAGE

A combination comprising a sweptback wing mounted in the mid-wing position on a cylindrical fuselage at zero incidence to the free stream is considered. The wing is cambered and twisted so that the spanwise load distribution is constant across the wing of the combination. It was suggested in Ref.3 that an acceptable approximation to the camber and twist needed in and near the wing-fuselage junction might be obtained by taking the wing shape calculated at and near the centre of an isolated wing carrying the same load distribution.

To investigate the propriety of such a procedure, the shape of the junction section of an untapered sweptback wing combined with a cylindrical fuselage of circular cross-section is calculated, using slender-body theory (i.e. for $M_o = 1$). The apex of the wing planform (extended inside the body) is taken as the origin of right-handed Cartesian coordinates x, y, z with x measured streamwise and y spanwise. The wing chord is taken as unity, the body radius as R, the wing sweepback as φ and $\xi = x - |y| \tan \varphi$.

As in the main text of this report, only linear chordwise load distributions of the form

$$- \Delta C_p(x,y) = A + B\xi$$

are considered. With this given load distribution, the discontinuity in the velocity potential between the upper and lower surfaces of the wing, $\Delta\phi = \phi_{US} - \phi_{LS}$, is also prescribed:

$$\frac{\partial}{\partial x}\left(\frac{\Delta\phi(x,y)}{V_o}\right) = -\frac{1}{2}\Delta C_p(x,y)$$

$$\frac{\Delta\phi(x,y)}{V_o} = \frac{1}{2}A\xi + \frac{1}{4}B\xi^2 = \frac{A}{2}(x - |y| \tan\varphi) + \frac{B}{4}(x - |y| \tan\varphi)^2 \qquad (13)$$

The task is to determine, for each cross-sectional plane x = const., the two-dimensional flow which has a vanishing normal velocity component at the body contour and satisfies the condition (13) for the velocity potential at the wing contour.

This two-dimensional problem can be solved by transforming the plane x = const.

$$\zeta = y + iz$$

into a $\bar{\zeta}$ plane by the transformation

$$\bar{\zeta} = \zeta - \frac{R^2}{\zeta}$$

so that the body contour, $|\zeta| = R$, is transformed into the slit $\bar{y} = 0$, $|\bar{z}| < 2R$. The wing is transformed into the straight line $|\bar{y}| < \bar{s}(x) = s(x) - R^2/s(x)$, $\bar{z} = 0$, where $s(x) = x/\tan\varphi$. Points on the original and the transformed wing contour are related by:-

$$y = \frac{1}{2}\left[\bar{y} + \sqrt{\bar{y}^2 + 4R^2}\right] \tag{14}$$

The transformation does not alter the value of the discontinuity in the velocity potential so that by equations (13) and (14):-

$$\frac{\Delta\phi(\bar{y}, \bar{z}=0;\ x)}{V_o} = \frac{A}{4}\left[2x - |\bar{y}|\tan\varphi - \tan\varphi\sqrt{\bar{y}^2 + 4R^2}\right] + \frac{B}{16}\left[2x - |\bar{y}|\tan\varphi - \tan\varphi\sqrt{\bar{y}^2 + 4R^2}\right]^2 \tag{15}$$

The flow which satisfies equation (15) induces at the point $\bar{y}$, $\bar{z}$ the downwash:-

$$\frac{\bar{v}_{\bar{z}}(\bar{y}, \bar{z};\ x)}{V_o} = -\frac{1}{2\pi}\int_{-\bar{s}(x)}^{\bar{s}(x)} \frac{\partial}{\partial\bar{y}'}\left(\frac{\Delta\phi(\bar{y}')}{V_o}\right)\frac{\bar{y} - \bar{y}'}{(\bar{y} - \bar{y}')^2 + \bar{z}^2}\, d\bar{y}'$$

For $\bar{y} = 0$, i.e. points corresponding to the body circumference, the downwash is thus given by:-

$$\frac{\bar{v}_{\bar{z}}(x, \bar{y}=0, \bar{z})}{V_o} = \frac{1}{\pi}\int_0^{\bar{s}(x)} \frac{\partial}{\partial\bar{y}'}\left(\frac{\Delta\phi(\bar{y}')}{V_o}\right)\frac{\bar{y}'}{\bar{y}'^2 + \bar{z}^2}\, d\bar{y}'$$

$$= -\frac{\tan\varphi}{4\pi}(A + Bx)\int_0^{\bar{s}(x)}\left[1 + \frac{\bar{y}'}{\sqrt{\bar{y}'^2 + 4R^2}}\right]\frac{\bar{y}'}{\bar{y}'^2 + \bar{z}^2}\, d\bar{y}'$$

$$+ \frac{\tan^2\varphi}{4\pi} B\int_0^{\bar{s}(x)}\left[\bar{y}' + \sqrt{\bar{y}'^2 + 4R^2} - \frac{2R^2}{\sqrt{\bar{y}'^2 + 4R^2}}\right]\frac{\bar{y}'}{\bar{y}'^2 + \bar{z}^2}\, d\bar{y}'$$

For $\bar{z} \to 0$, $\bar{v}_z$ (and with it the downwash in the original plane, v_z) tends to a logarithmically infinite value. Therefore, v_z is calculated at a finite distance $z_t(x)$, corresponding to half the local wing thickness; the argument for this procedure is discussed in detail in Ref.3. For $|z| < R$, i.e. $|\bar{z}| < 2R$, performing the integration gives

$$\frac{\bar{v}_{\bar{z}}(x,\ \bar{y}=0,\ \bar{z})}{V_o} = -\frac{\tan\varphi}{4\pi}(A + Bx)\left[\log\frac{\sqrt{\bar{s}^2+\bar{z}^2}\left[\bar{s}+\sqrt{\bar{s}^2+4R^2}\right]}{2R\bar{z}} - \frac{\bar{z}}{\sqrt{4R^2-\bar{z}^2}}\tan^{-1}\frac{\bar{s}\sqrt{4R^2-\bar{z}^2}}{\bar{z}\sqrt{\bar{s}^2+4R^2}}\right]$$

$$+\frac{\tan^2\varphi}{4\pi}B\left\{\bar{s}+\sqrt{\bar{s}^2+4R^2}-2R-\bar{z}\tan^{-1}\frac{\bar{s}}{\bar{z}} + \frac{-2R^2+\bar{z}^2}{2\sqrt{4R^2-\bar{z}^2}}\log\frac{\left[\sqrt{\bar{s}^2+4R^2}+\sqrt{4R^2-\bar{z}^2}\right]\left[2R-\sqrt{4R^2-\bar{z}^2}\right]}{\left[\sqrt{\bar{s}^2+4R^2}-\sqrt{4R^2-\bar{z}^2}\right]\left[2R+\sqrt{4R^2-\bar{z}^2}\right]}\right\} \quad (16)$$

The v_z-velocity in the original plane is related to $\bar{v}_{\bar{z}}$ in the transformed plane by the mapping ratio $|d\bar{\zeta}/d\zeta|$:-

$$v_z(x,y,z) = \bar{v}_{\bar{z}}(x,\bar{y},\bar{z})\left|\frac{d\bar{\zeta}}{d\zeta}\right|$$

For the wing-body junction ($y = y_J$, $z = z_t(x)$) the mapping ratio is:-

$$\left|\frac{d\bar{\zeta}}{d\zeta}\right| = 2\sqrt{1-\left(\frac{z_t}{R}\right)^2}$$

and

$$\bar{z} = 2z_t$$

The downwash in the wing-body junction is thus given by the relation:-

$$\frac{v_z(x,\, y_J,\, z_t)}{V_o} = -\frac{\tan\varphi}{2\pi}(A + Bx)\left[\sqrt{1-\left(\frac{z_t}{R}\right)^2}\,\log\frac{\sqrt{\bar{s}^2+4z_t^2}\left[\bar{s}+\sqrt{\bar{s}^2+4R^2}\right]}{4z_tR} - \frac{z_t}{R}\tan^{-1}\frac{\bar{s}\sqrt{R^2-z_t^2}}{z_t\sqrt{\bar{s}^2+4R^2}}\right]$$

$$+\frac{\tan^2\varphi}{2\pi}B\left\{\sqrt{1-\left(\frac{z_t}{R}\right)^2}\left[\bar{s}+\sqrt{\bar{s}^2+4R^2}-2R-2z_t\tan^{-1}\frac{\bar{s}}{2z_t}\right]\right.$$

$$\left.-R\left[1-2\left(\frac{z_t}{R}\right)^2\right]\log\frac{\left[\sqrt{\bar{s}^2+4R^2}+2\sqrt{R^2-z_t^2}\right]z_t}{\sqrt{\bar{s}^2+4z_t^2}\left[R+\sqrt{R^2-z_t^2}\right]}\right\} \qquad (17)$$

where $$\bar{s} = \bar{s}(x) = \frac{x}{\tan\varphi} - \frac{R^2\tan\varphi}{x}$$

The shape of the junction section of the wing is obtained by integrating this downwash:-

$$\frac{z(\xi)}{c} = \int_{\xi}^{1}\frac{v_z(\xi')}{V_o}\,d\xi'$$

Some numerical calculations have been carried out for a 4.5% thick wing with RAE 101 thickness distribution and 55° sweep. The results are given in Figs.50 and 51 for triangular and uniform chordwise load distributions respectively, together with those for the centre section of the isolated wing which are equivalent to those derived for an infinite body radius. (The same limit is not obtained as R/c → 0 since equation (17) is valid only for $|z_t| < R$.)

The wing shapes required in the wing-fuselage junctions are qualitatively similar to those calculated for the centre of the isolated wing, but the local wing incidence has to be somewhat greater when the body is present. In most practical cases, the ratio R/c will lie between the values 0.1 and 0.2 which are considered in Figs.50 and 51.

These results were obtained for wings mounted on a fuselage which is at zero incidence. If the fuselage is at positive incidence (or is cambered so that it carries a positive load), the upwash which it produces in the wing-body junction should reduce the local wing incidence needed there. These considerations, in conjunction with the demonstration in Ref.3 that calculations of the wing shape needed to produce a given loading at $M_o = 1.0$

and at $M_o = 1.2$ give very similar results, suggest that the wing shapes presented in the main text of this report should be satisfactory approximations to the wing shapes needed for combinations with near-circular fuselage cross-sections.

APPENDIX 2

THE SHAPE OF THE CENTRE-SECTION OF A SWEPTBACK WING DESIGNED TO HAVE VARIOUS CHORDWISE LOAD DISTRIBUTIONS

In the main report only load distributions of the form $-\Delta C_p = A + B\xi$ have been considered. It is however of interest to know how much the results depend on the chosen load distribution, in particular to know whether the large angles of twist required at the centre section are a consequence of this choice.

A variety of load distributions is easily investigated at $M_o = 1$. Sweptback wings of constant chord are considered, which are cambered and twisted so that the spanwise load distributions are constant. The symbols used are the same as in Appendix 1 and Ref.3. For $M_o = 1$, the downwash at points on the centre-section of such a wing is:-

$$\frac{v_z(x,\ 0,\ z_t)}{V_o} = \frac{1}{2\pi}\int_0^x \Delta C_p(\xi') \frac{(x-\xi')\tan\varphi}{(x-\xi')^2 + z_t^2\tan^2\varphi}\, d\xi'$$

In Ref.3, load distributions which can be written as polynomials in ξ were considered, and explicit expressions for the section slope were obtained. It is also of interest to investigate load distributions which have the same singular behaviour near the leading-edge as the load distribution for the two-dimensional flat plate, i.e. load distributions whose leading term is proportional to $1/\sqrt{\xi}$. Putting

$$-\Delta C_p(x,y) = C\frac{1}{\sqrt{\xi}}$$

in the expression above and performing the integration gives

$$\frac{v_z}{V_o} = \frac{C\tan\varphi}{4\pi(x^2+z_t^2\tan^2\varphi)^{\frac{1}{4}}}\left\{\cos\Theta\,\log\frac{x+(x^2+z_t^2\tan^2\varphi)^{\frac{1}{2}} - 2\sqrt{x}(x^2+z_t^2\tan^2\varphi)^{\frac{1}{4}}\cos\Theta}{x+(x^2+z_t^2\tan^2\varphi)^{\frac{1}{2}} + 2\sqrt{x}(x^2+z_t^2\tan^2\varphi)^{\frac{1}{4}}\cos\Theta}\right.$$

$$\left. - 2\sin\Theta\tan^{-1}\frac{2\sqrt{x}(x^2+z_t^2\tan^2\varphi)^{\frac{1}{4}}\sin\Theta}{x-(x^2+z_t^2\tan^2\varphi)^{\frac{1}{2}}}\right\}$$

where $$\Theta = \tfrac{1}{2}\tan^{-1}\left(\frac{z_t\tan\varphi}{x}\right)$$

Over most of the chord $z_t\tan\varphi \ll x$ and it is convenient to use the following expression, obtained by expanding in powers of $\dfrac{z_t\tan\varphi}{x}$, for practical calculation:-

$$\frac{v_z}{V_o} = \frac{C \tan \varphi}{4\pi \sqrt{x}} \left\{ \left(2 - \frac{3}{4} \frac{z^2 \tan^2 \varphi}{x^2} \right) \log \frac{z \tan \varphi}{4x} + \frac{\pi}{2} \frac{z \tan \varphi}{x} \right\} +$$

$$+ \text{ terms of order } \frac{z^2 \tan^2 \varphi}{x^2}$$

The shape of the wing centre-section is obtained by integrating this downwash. In Fig.52, the result is shown for a wing with $\varphi = 55^\circ$, compared with the shapes required to give triangular and uniform chordwise load distributions with the same sectional lift coefficient. The local incidence required in each case is substantially similar.

APPENDIX 3

CALCULATION OF CENTRE OF PRESSURE AND LIFT-DEPENDENT WAVE DRAG FROM CROSS-LOAD DISTRIBUTIONS

The centre of pressure and lift-dependent wave drag are calculated from the cross-load L(x) given by:-

$$L(x) = 2 \int_{a(x)}^{b(x)} - \Delta C_p(x,y)\, dy \qquad (18)$$

where a(x) and b(x) are the inboard and outboard limits, respectively, of a spanwise cross-section of the half-wing. Load distributions of the form:

$$- \Delta C_p = A - B \frac{x - x_L}{x_L - x_T} \qquad (19)$$

are considered. The equation of the leading-edge is

$$x_L = m_o y \qquad \text{for} \qquad 0 < y < \eta_t s \qquad (20)$$

$$x_L = m_o y + f(\eta)\, c_t \text{ for } \eta_t s < y < 1 \qquad (21)$$

where $$f(\eta) = 1 - 2\sqrt{\frac{1 - \eta}{1 - \eta_t}} + \frac{1 - \eta}{1 - \eta_t}$$

The equation of the trailing-edge is

$$x_T = c_o + m_1 y \qquad (22)$$

The explicit form of (18) gives different formulae in different regions of the wing, depending on the limits a and b, and on whether (20) or (21) is the appropriate expression for x_L. Thus $a = 0$ for $x < c_o$, $a = y_t$ for $x > c_o$ and $b = y_L$. y_L has different forms for $x < h$ and $x > h$ where

$$h = \frac{\eta_t s}{m_o}$$

Further divisions arise from the different equations for ΔC_p (due to the different expressions for x_L) for $x < d$ and $x > d$ where $d = h + c(\eta_t s)$. This leads to a definition of five regions in which L(x) has different forms, four of which occur on any particular wing. Two classes of wings can be distinguished in which $c_o < h$ or $c_o > h$ and the regions may be defined as shown below:-

	Class A	Class B
Region 1	$0 < x < c_o$	$0 < x < h$
Region 2	$c_o < x < h$	$h < x < c_o$
Region 3	$h < x < d$	$c_o < x < d$
Region 4	$d < x < \ell$	$d < x < \ell$

The explicit formulae for L(x) are identical for Class A and Class B in all regions except region 2. Region 2 of Class A and Class B will be referred to as regions 2A and 2B respectively.

Formulae may now be developed for L(x) for the five regions:-

Region 1

$$L(x) = 2\left(\frac{A}{m_o} + \frac{B}{m_o - m_1}\right)x - \frac{2B}{m_o - m_1}\left(x - \frac{m_o c_o}{m_o - m_1}\right)\ell n\left(\frac{m_o c_o - (m_o - m_1)x}{m_o c_o}\right) \tag{23}$$

and for $m_o = m_1$:

$$L(x) = \frac{2Ax}{m_o} + \frac{B}{m_o}\frac{x^2}{c_o} \tag{24}$$

Region 2A

$$L(x) = 2\left(A + \frac{Bm_o}{m_o - m_1}\right)\left(\frac{x}{m_o} - \frac{x - c_o}{m_1}\right) - \frac{2B}{m_o - m_1}\left(x - \frac{m_o c_o}{m_o - m_1}\right)\ell n\frac{m_1}{m_o} \tag{25}$$

and for $m_o = m_1$:

$$L(x) = \frac{(2A + B)\,c_o}{m_o} \tag{26}$$

Region 2B

$$L(x) = 2\left(A + \frac{Bm_o}{m_o - m_1}\right)\eta_t s - \frac{2B}{m_o - m_1}\left(x - \frac{m_o c_o}{m_o - m_1}\right)\ell n\frac{c_o - (m_o - m_1)\eta_t s}{c_o} +$$

$$+ 4sk\left\{\left[\tfrac{1}{2}A - \tfrac{1}{2}B\frac{c_t - m_o sk}{P}\right]\left(1 - u_L^2\right) - \frac{2Bc_t m_1 sk}{P^2}\left(1 - u_L\right) +\right.$$

$$\left. + \left[\frac{4Bc_t^2 m_1 sk}{P^3} - \frac{B(1-x)}{P}\right]\ell n\frac{P + 2c_t}{Pu_L + 2c_t}\right\} \tag{27}$$

For $m_o = m_1$ the first two terms of this expression become:

$$2\left(A + B\frac{x}{c_o}\right)\eta_t s - B\frac{m_o}{c_o}(\eta_t s)^2 \qquad (28)$$

Region 3

$$L(x) = 2\left[\frac{A}{m_1} + \frac{Bm_o}{m_1(m_o-m_1)}\right](\ell - m_1 ks - x) -$$

$$- \frac{2B}{(m_o-m_1)}\left[x - m_o s - \frac{m_o c_t}{m_o-m_1}\right] \ell n \left|\frac{m_1[c_t+(m_o-m_1)ks]}{(m_o-m_1)(x-m_o s)-m_o c_t}\right| +$$

$$+ 4sk\left\{\left[\frac{A}{2} - \frac{B(c_t-m_o sk)}{2P}\right]\left(1-u_L^2\right) - \frac{2Bc_t m_1 sk}{P^2}(1-u_L) +\right.$$

$$\left. + \left[\frac{4Bc_t^2 m_1 sk}{P^3} - \frac{B(1-x)}{P}\right] \ell n \left(\frac{P+2c_t}{Pu_L+2c_t}\right)\right\} \qquad (29)$$

For $m_o = m_1$ the first two terms become:

$$2\left(A + B\frac{x}{c_o}\right)\left(\eta_t s - \frac{x-c_o}{m_o}\right) - B\frac{m_o}{c_o}\left[(\eta_t s)^2 - \left(\frac{x-c_o}{m_o}\right)^2\right] \qquad (30)$$

Region 4

$$L(x) = 4sk\left\{\left[\frac{A}{2} - \frac{B(c_t-m_o sk)}{2P}\right]\left(u_T^2 - u_L^2\right) - \frac{2Bc_t m_1 sk}{P^2}(u_T-u_L) +\right.$$

$$\left. + \left[\frac{4Bc_t^2 m_1 sk}{P^3} - \frac{B(1-x)}{P}\right] \ell n \left(\frac{Pu_T+2c_t}{Pu_L+2c_t}\right)\right\} \qquad (31)$$

where $k = (1-\eta_t)$

$$P = (m_o-m_1)sk - c_t$$

$$u_L = \frac{c_t - \sqrt{c_t^2-(c_t-m_o sk)(\ell-x)}}{c_t - m_o sk}$$

$$u_T = \sqrt{\frac{\ell - x}{m_1 sk}}$$

To calculate L(x) upon DEUCE by means of a tabular interpretive programme[15] it is convenient to write the above expressions in one general form, which may be applied to all regions and both classes:

$$L(x) = 2\left(A + B\frac{m_o}{m_o-m_1}\right)\left\{(G_1+G_{2A})\frac{x}{m_o} - G_{2A}\frac{c_o-x}{m_1} + G_{2B}\,\eta_t s + G_3\left(\frac{\ell-m_1 ks-x}{m_1}\right)\right\}$$

$$- \frac{2B}{m_o-m_1}\left\{\left[x - \frac{m_o c_o}{m_o-m_1}\right]\left[G_1\,\ell n\,\frac{m_o c_o-(m_o-m_1)x}{m_o c_o} + G_{2A}\,\ell n\,\frac{m_1}{m_o} + \right.\right.$$

$$\left. + G_{2B}\,\ell n\,\frac{c_o-(m_o-m_1)\eta_t s}{c_o}\right]$$

$$\left. + G_3\left[x - m_o s - \frac{m_o c_t}{m_o-m_1}\right]\ell n\left|\frac{m_1[c_t+(m_o-m_1)ks]}{(m_o-m_1)(x-m_o s)-m_o c_t}\right|\right\} +$$

$$+ (G_{2B}+G_3+G_4)\,4sk\left\{\left[\frac{A}{2} - \frac{B(c_t-m_o sk)}{2P}\right]\left(u_T^2-u_L^2\right) - \frac{2Bc_t m_1 sk}{P^2}(u_T-u_L) + \right.$$

$$\left. + \left[\frac{4Bc_t^2 m_1 sk}{P^3} - \frac{B(1-x)}{P}\right]\ell n\,\frac{Pu_T+2c_t}{Pu_L+2c_t}\right\} \qquad (32)$$

where $$u_T = G_4\sqrt{\frac{\ell-x}{m_1 sk}} + 1 - G_4$$

When $m_o = m_1$, the first two terms of equation (32) are replaced by:-

$$\frac{2A}{m_o}(G_1 x + G_{2A}c_o) + \frac{B}{m_o c_o}\left[G_1 x^2 + G_{2A}c_o^2 + G_3(x-c_o)^2\right] +$$

$$+ \left(A + B\frac{x}{c_o}\right)\left\{(G_{2A}+G_3)\,2\eta_t s - G_3\left(\frac{x-c_o}{m_o}\right)\right\} - (G_{2A}+G_3)\,B\frac{m_o}{c_o}(\eta_t s)^2$$

(33)

The factors G_1, G_{2A} etc. have been introduced as a means of eliminating those terms which are not required in specific regions. They are equal to zero except in the regions indicated by their respective suffices where they become unity, thus:

G_1	= 1	where	$x < c_o$ and h
G_{2A}	= 1	where	$c_o < x < h$
G_{2B}	= 1	where	$h < x < c_o$
G_3	= 1	where	c_o and $h < x < d$
G_4	= 1	where	$d < x < \ell$

These columns of 0's and 1's can be generated very simply; for example G_3 can be obtained by evaluating the function:

$$G_3 = \left(\frac{(d-x) + |d-x|}{2|d-x|}\right)\left(\frac{(x-h) + |x-h|}{2|x-h|}\right)\left(\frac{(x-c_o) + |x-c_o|}{2|x-c_o|}\right) \qquad (34)$$

In equations (27) to (33) a difficulty occurs when $(m_o-m_1)sk-c_t$ approaches zero, that is when T approaches $\frac{1-\eta_t}{2-\eta_t}$. Consequently it was not possible to calculate L(x) with sufficient accuracy for wings 16 and 21 for a finite value of B.

L(x) was calculated for the 34 wings at $x/\ell = 0(0.01)1$; by using the trapezium rule, both $\int_0^1 L\left(\frac{x}{\ell}\right) d\left(\frac{x}{\ell}\right)$ and $\int_0^1 \frac{x}{\ell}.L\left(\frac{x}{\ell}\right) d\left(\frac{x}{\ell}\right)$ were found, and hence the centre of pressure position.

The lift-dependent wave drag is given by

$$\frac{D_W}{\frac{1}{2}\rho V_o^2} = -\frac{(M_o^2-1)}{16\pi}\int_0^\ell\int_0^\ell \frac{L'(x)}{\frac{1}{2}\rho V_o^2}\,\frac{L'(x_1)}{\frac{1}{2}\rho V_o^2}\,\ell n|x-x_1|\,dx\,dx_1 \qquad (35)$$

Double integrals of similar form occur in the calculation of the zero-lift wave drag of bodies and a method of evaluating them on a digital computer has been developed by Eminton[9]. The formula in Ref.9 corresponding to (35) is

$$\mathcal{J} = -\frac{1}{2\pi}\int_0^1\int_0^1 S''(x)\,S''(x_1)\,\ell n|x-x_1|\,dx\,dx_1 \qquad (36)$$

and the numerical method evaluates this from a table of values of S(x) at equally spaced points. To evaluate (35) the same method is used, replacing s(x) by $\int_0^{x/\ell} L\left(\frac{x}{\ell}\right) d\left(\frac{x}{\ell}\right)$ at $\frac{x}{\ell} = 0(0.05)1.0$. Thus

$$\frac{D_W}{\frac{1}{2}\rho V_o^2} = \frac{M_o^2-1}{8}\,\mathcal{J} \qquad (37)$$

LIST OF PRINCIPAL SYMBOLS

A	Aspect ratio
$c(y)$	Local chord
c_o	Root chord
$\bar{c}$	Geometric mean chord
c_t	Projected tip chord (see Fig.1)
$C_L(y)$	Local sectional lift coefficient
$\overline{C_L}$	Overall wing lift coefficient
C_{DV}, C_{DW}	Lift-dependent vortex and wave drag coefficients
D_V, D_W	Total lift-dependent vortex and wave drag
K	$= \dfrac{C_{DV} + C_{DW}}{C_L^2/\pi A}$ Total lift-dependent drag factor
K_V	Lift-dependent vortex drag factor, see equation (8)
K_W	Lift-dependent wave drag factor, see equation (12)
ℓ	Overall length of wing
$L(x)$	Cross-load $= \frac{1}{2}\rho V_o^2 \int_{-o}^{\sigma} (-\Delta C_p)\, dy$
M_o	Free-stream Mach number
s	Wing semispan
S	Wing area
T	"Taper ratio" c_t/c_o
x,y,z	Cartesian coordinates: x streamwise y spanwise z vertical
$x_L(y)$ $x_T(y)$	Leading- and trailing-edge
$z_c(\xi)$	Wing camber-line ordinates
$z_t(\xi)$	Wing thickness ordinates
$\Delta C_p(x,y)$	Local load coefficient, equal to pressure difference across wing divided by dynamic pressure of free stream

LIST OF PRINCIPAL SYMBOLS (Contd.)

$\alpha(y)$	Local incidence
α_o	Incidence of wing centre-line
α_J	Incidence of wing-fuselage junction section
β	$= \sqrt{M_o^2 - 1}$
η	$= y/s$
ξ	$= \dfrac{x - x_L}{x_T - x_L}$
$\sigma(x)$	Local semispan
φ_o, φ_1	Leading- and trailing-edge sweep angles

TABLE 1

Some characteristics of the wings considered

Wing No.	A	φ_o	φ_1	T	c_o/s	s/ℓ	Centre of pressure		Low-speed aero-dynamic centre x_{ac}/ℓ
							Triangular load x_{cp}/ℓ	Uniform load x_{cp}/ℓ	
1	3.5	55°	35°	0.24	0.954	0.604	0.469	0.535	0.474
2	"	"	45°	0.48	0.818	0.550	0.449	0.508	0.445
3	"	"	55°	1.00	0.623	0.487	0.435	0.483	0.412
4	"	60°	35°	0.06	1.092	0.558	0.471	0.541	0.491
5	"	"	45°	0.23	0.956	0.511	0.454	0.512	0.470
6	"	"	55°	0.60	0.762	0.457	0.442	0.489	0.441
7	2.75	55°	35°	0.35	1.124	0.548	0.469	0.542	0.463
8	"	"	45°	0.57	0.988	0.503	0.449	0.516	0.436
9	"	"	55°	1.00	0.793	0.450	0.430	0.487	0.403
10	"	60°	35°	0.18	1.262	0.510	0.479	0.553	0.489
11	"	"	45°	0.35	1.126	0.470	0.460	0.525	0.463
12	"	"	55°	0.67	0.932	0.424	0.441	0.496	0.432
13	2.0	55°	35°	0.49	1.422	0.471	0.465	0.549	0.440
14	"	"	45°	0.67	1.286	0.438	0.444	0.521	0.413
15	"	"	55°	1.00	1.091	0.397	0.423	0.490	0.383
16	"	60°	35°	0.34	1.560	0.442	-	0.561	0.467
17	"	"	45°	0.49	1.424	0.413	0.459	0.534	0.444
18	"	"	55°	0.75	1.229	0.376	0.438	0.504	0.413
19	3.5	65°	55°	0.25	0.949	0.421	0.441	0.487	0.461
20	"	"	65°	1.00	0.623	0.361	0.442	0.477	0.435
21	"	70°	65°	0.33	0.897	0.329	-	0.465	0.454
22	2.75	65°	35°	0.00	1.450	0.465	0.483	0.556	0.509
23	"	"	45°	0.13	0.314	0.432	0.465	0.531	0.487
24	"	"	55°	0.36	1.119	0.393	0.453	0.501	0.462
25	"	"	65°	1.00	0.793	0.340	0.438	0.480	0.427
26	"	70°	55°	0.05	1.393	0.354	0.447	0.502	0.480
27	"	"	65°	0.44	1.067	0.311	0.439	0.479	0.457
28	2.0	65°	35°	0.17	1.747	0.409	0.492	0.574	0.501
29	"	"	45°	0.29	1.611	0.383	0.473	0.547	0.477
30	"	"	55°	0.49	1.417	0.352	0.452	0.515	0.448
31	"	"	65°	1.00	1.091	0.309	0.432	0.484	0.410
32	"	70°	45°	0.07	1.885	0.347	0.480	0.554	0.507
33	"	"	55°	0.22	1.691	0.321	0.462	0.524	0.483
34	"	"	65°	0.56	1.365	0.285	0.444	0.494	0.451

WT.2078.C.P.512.K3 - Printed in England

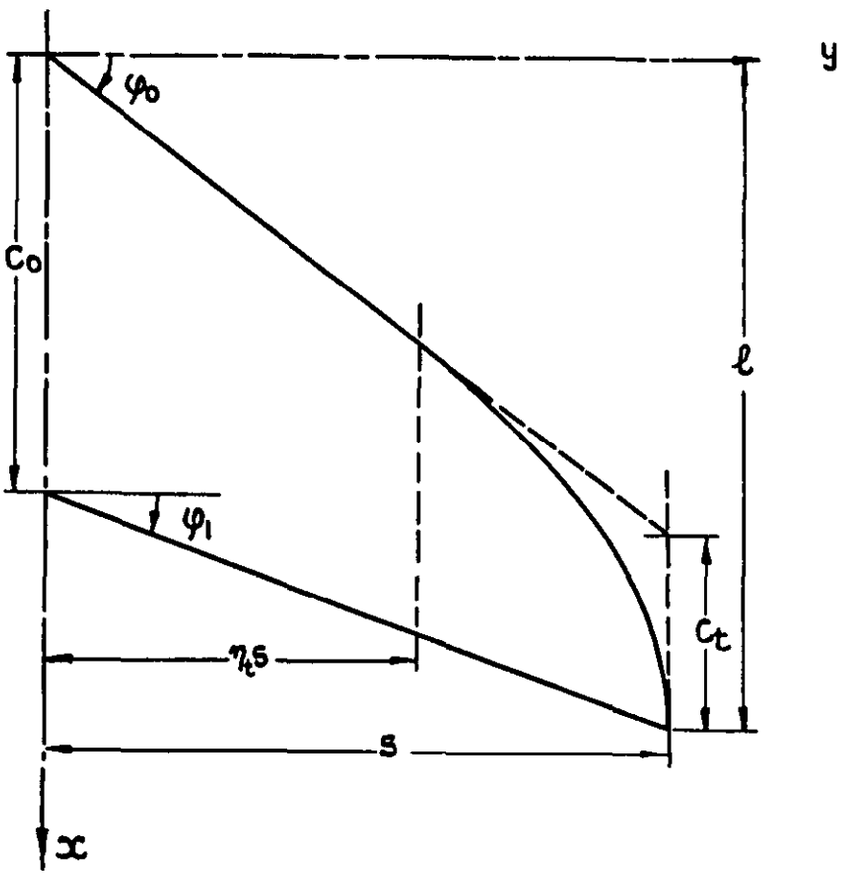

$m_0 = \tan \varphi_0$; $m_1 = \tan \varphi_1$

$\eta_t = \frac{1}{2}$ FOR ALL WINGS CONSIDERED HERE.

$T = C_t / C_0$

FIG. 1 GENERAL SHAPE AND NOMENCLATURE OF SWEPT BACK WINGS WITH CURVED TIPS.

FIG. 2. PLANFORMS OF 34 SWEPT BACK WINGS WITH CURVED TIPS.

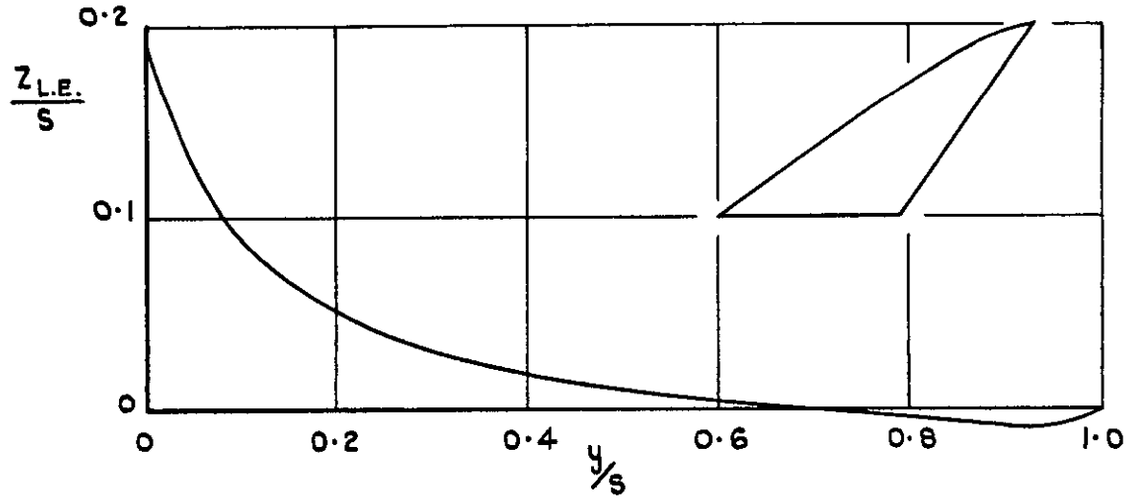

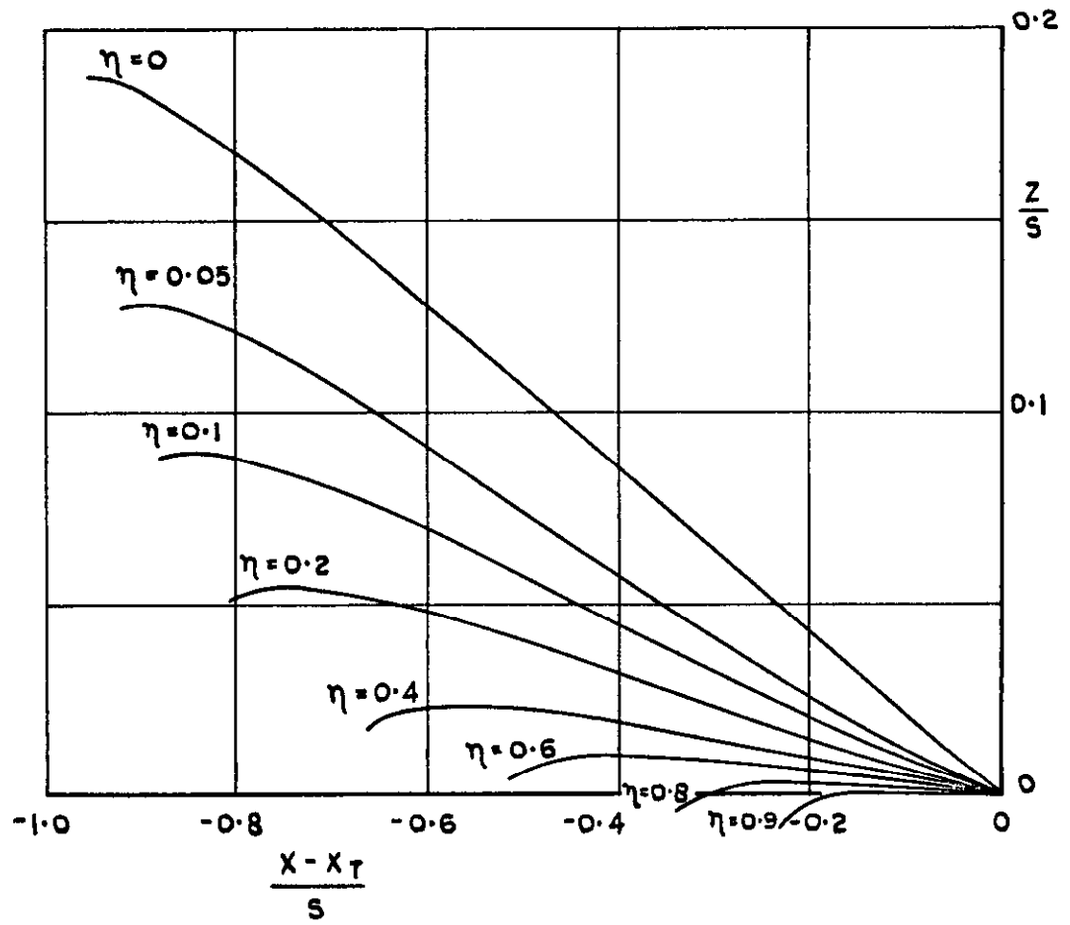

FIG.3. WING 1. $A = 3{\cdot}5$, $\varphi_0 = 55^\circ$, $\varphi_1 = 35^\circ$;

$-\Delta C_p = 0{\cdot}5 - 0{\cdot}5\,\xi$; $M_0 = 1{\cdot}2$.

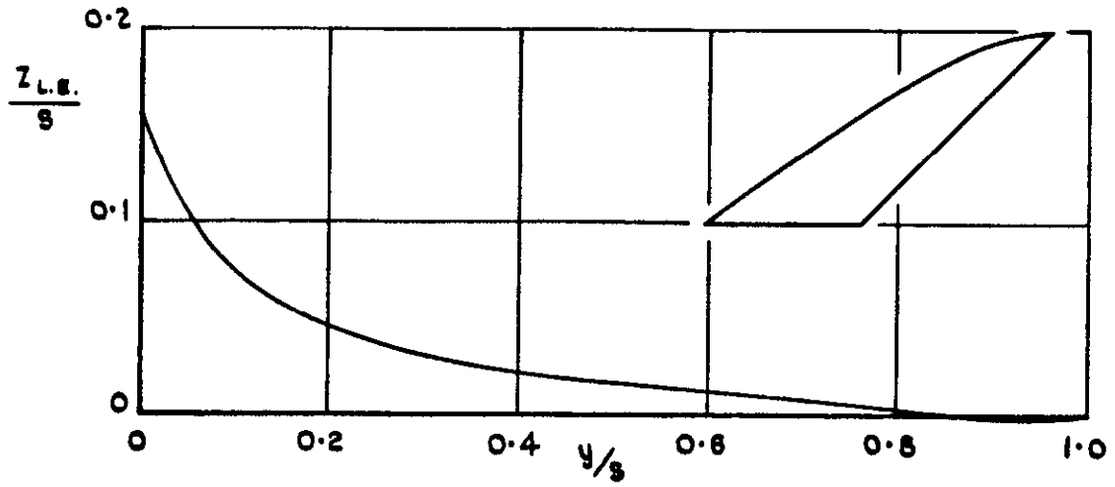

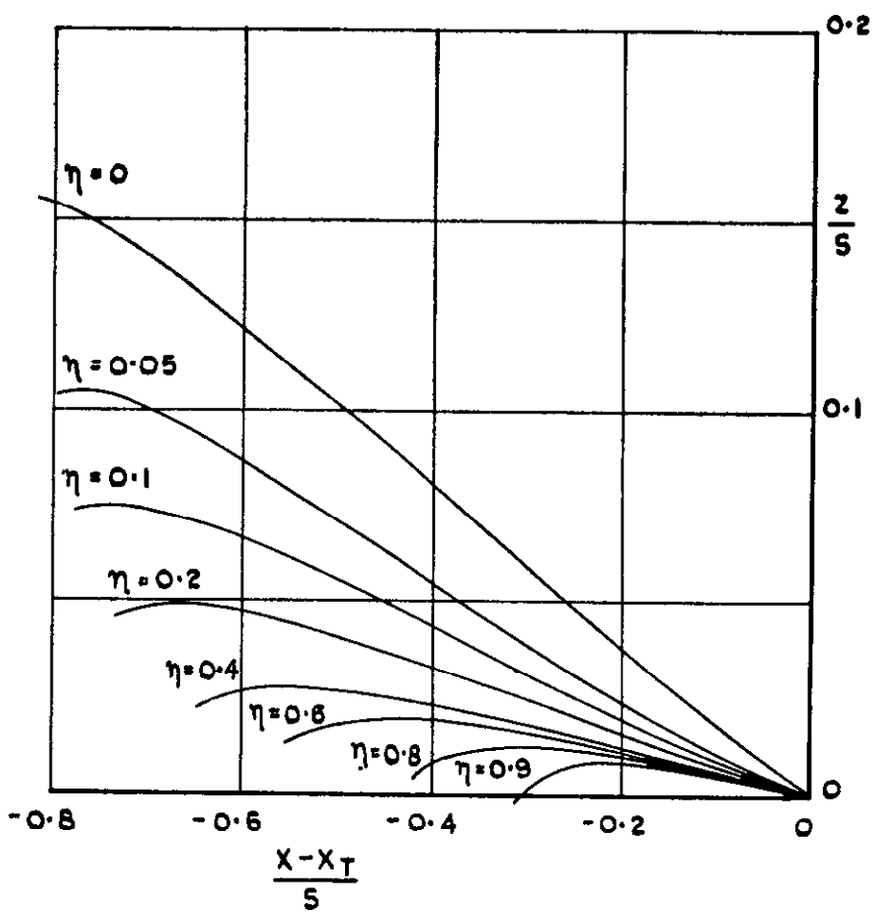

FIG. 4. WING 2. $A = 3·5$, $\varphi_0 = 55°$, $\varphi_1 = 45°$;
$-\Delta C_p = 0·5 - 0·5\,\xi$; $M_0 = 1·2$.

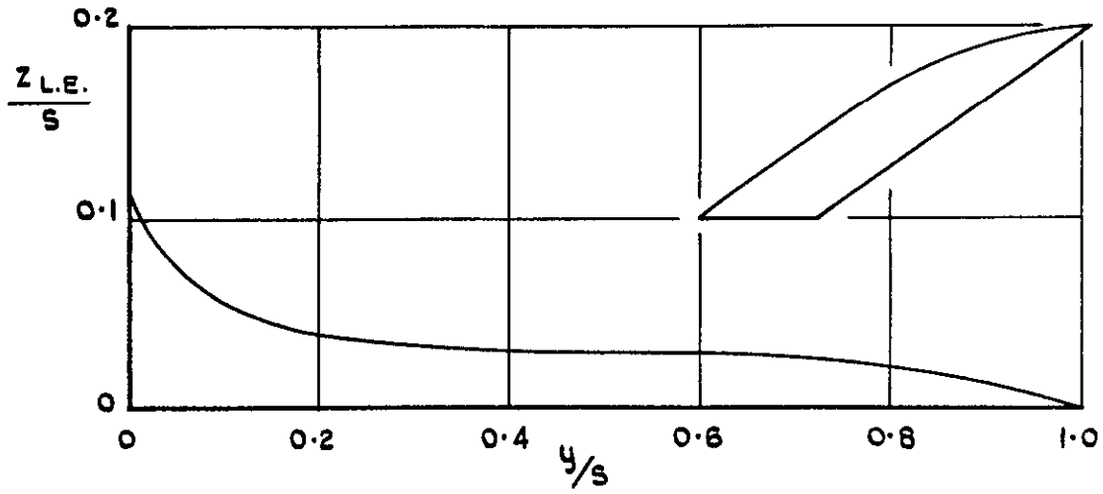

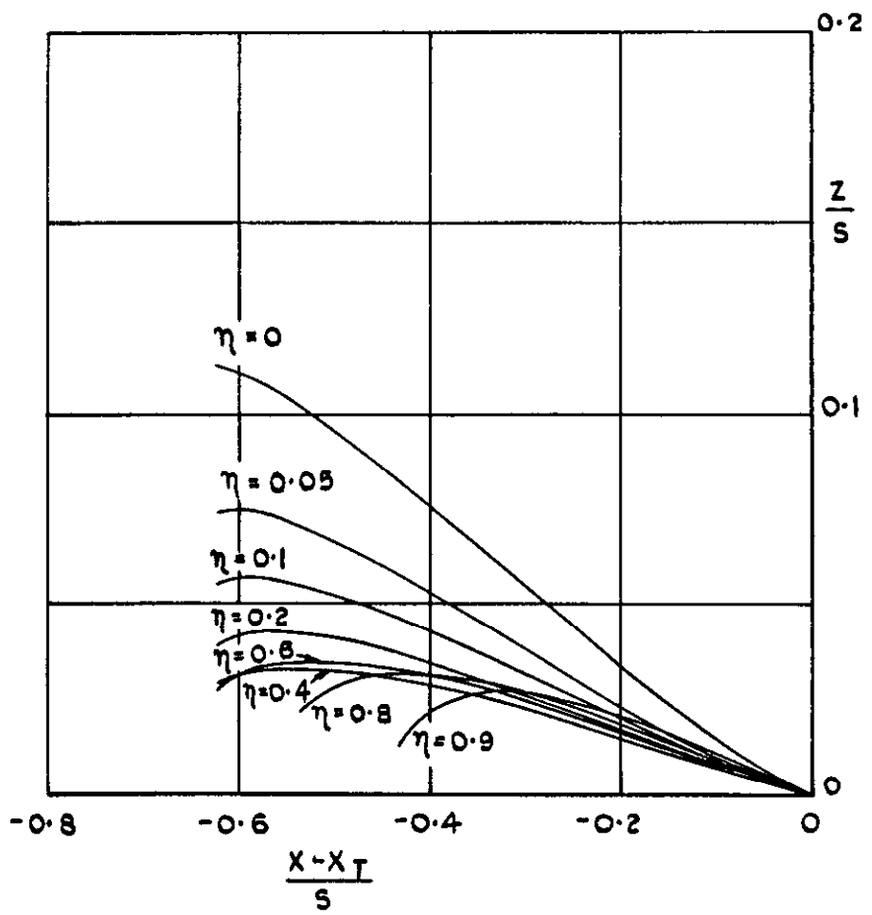

FIG.5. WING 3. $A = 3·5$, $\varphi_0 = 55°$, $\varphi_1 = 55°$;
$-\Delta C_p = 0·5 - 0·5\,\xi$; $M_0 = 1·2$.

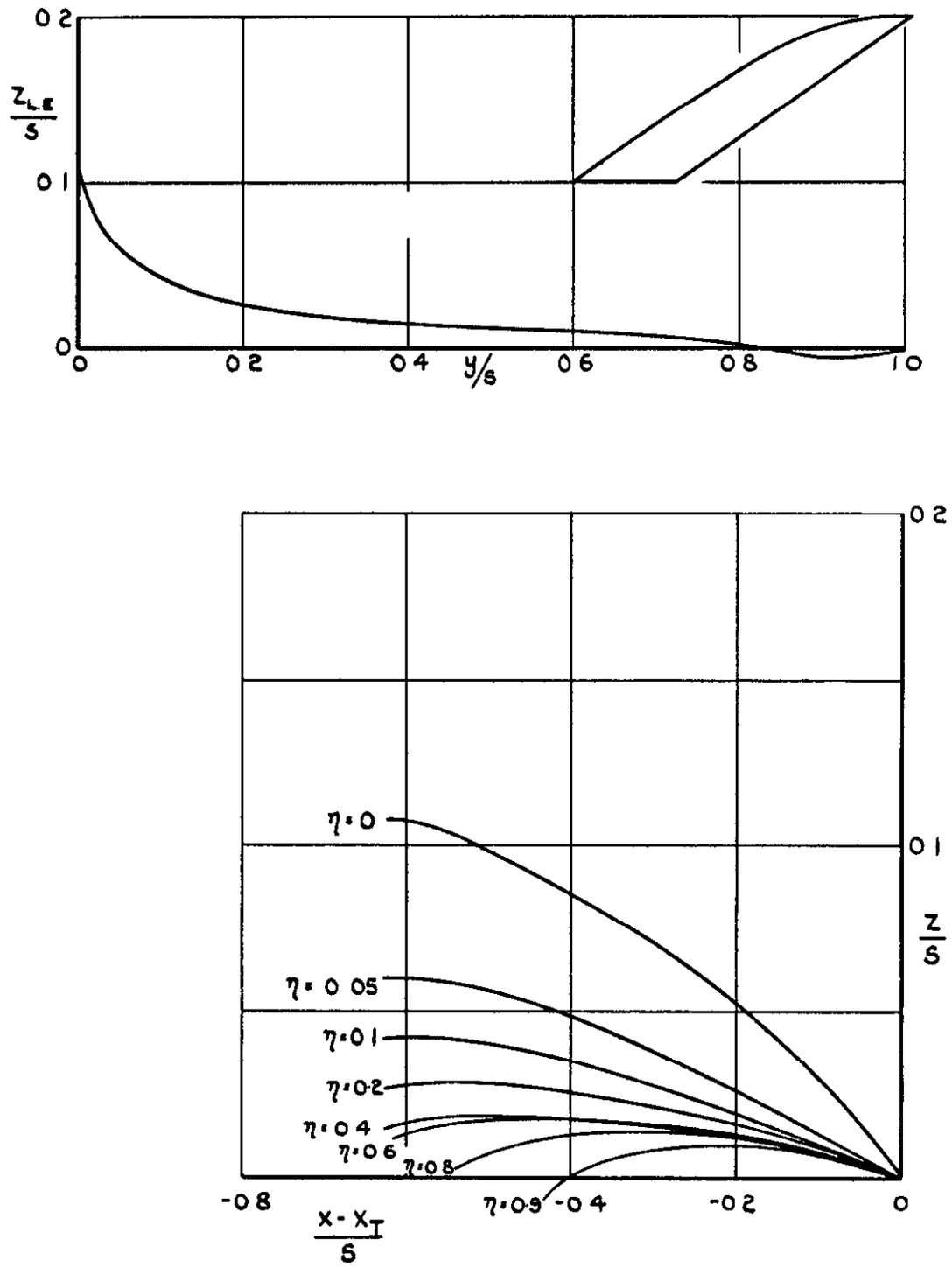

FIG. 6. WING 3. $A=3{\cdot}5$, $\varphi_0 = 55°$, $\varphi_1 = 55°$; $-\Delta C_p = 0{\cdot}25$; $M_0 = 1{\cdot}2$.

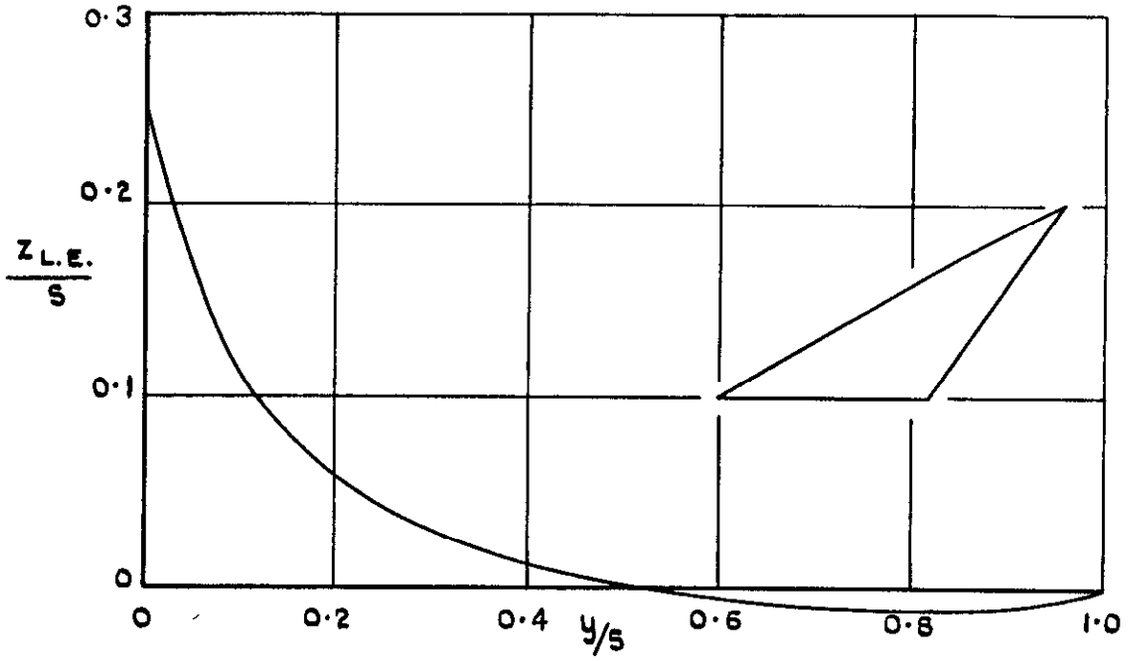

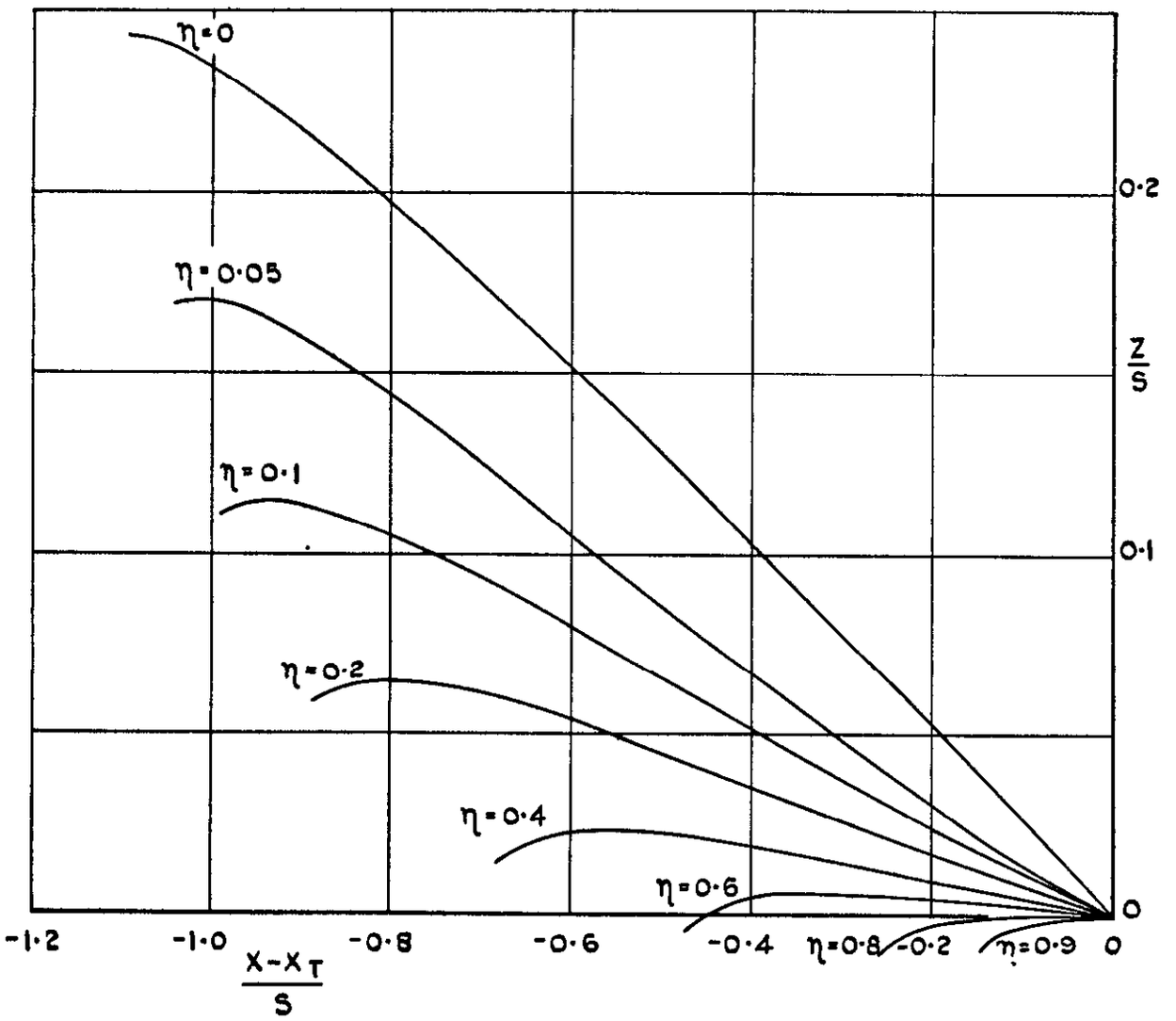

FIG.7. WING 4. $A = 3{\cdot}5$, $\varphi_0 = 60^\circ$, $\varphi_1 = 35^\circ$; $-\Delta C_p = 0{\cdot}5 - 0{\cdot}5\xi$; $M_0 = 1{\cdot}2$.

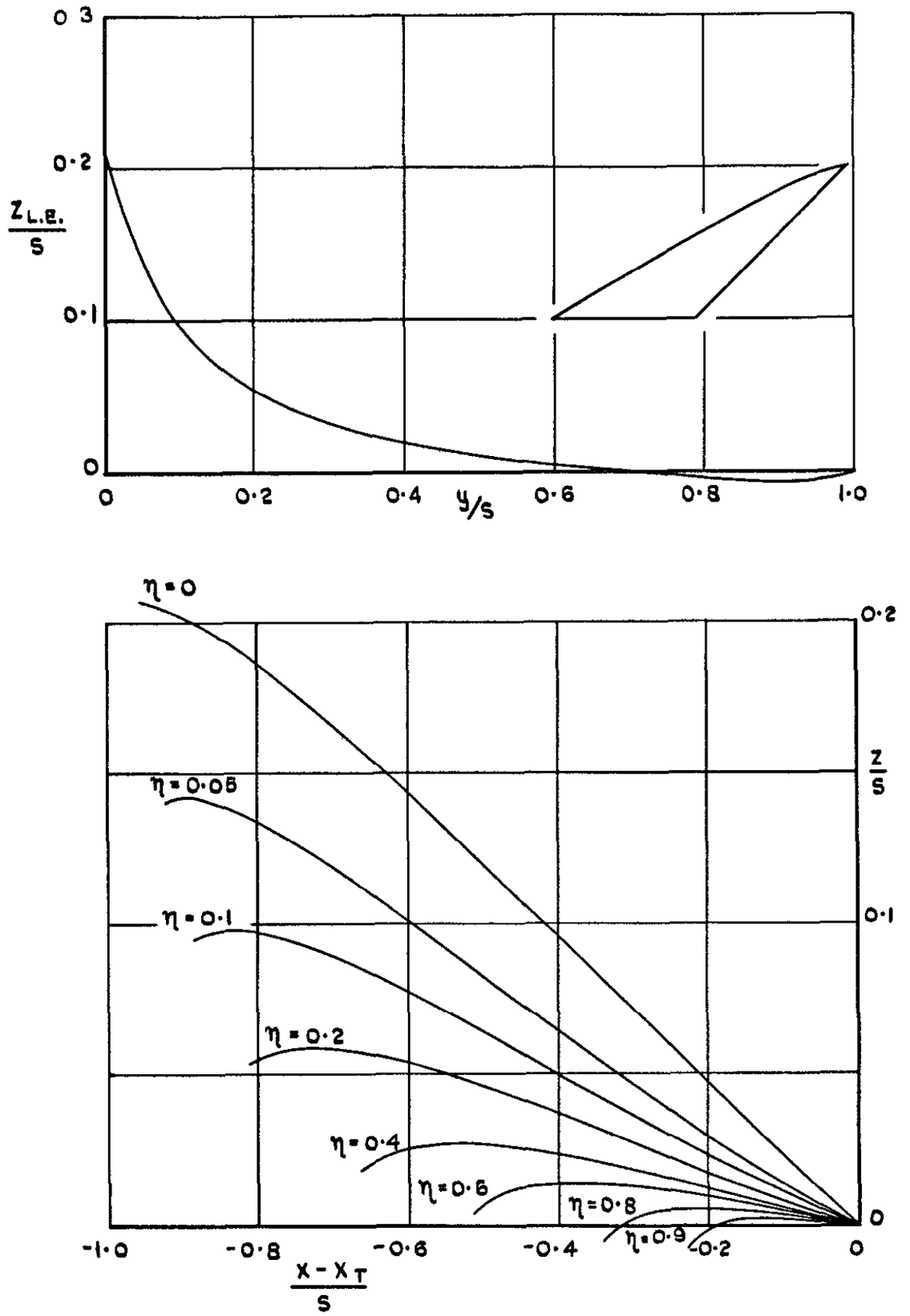

FIG. 8. WING 5. $A = 3{\cdot}5$, $\varphi_0 = 60^\circ$, $\varphi_1 = 45^\circ$;
$-\Delta C_p = 0{\cdot}5 - 0{\cdot}5\xi$; $M_0 = 1{\cdot}2$.

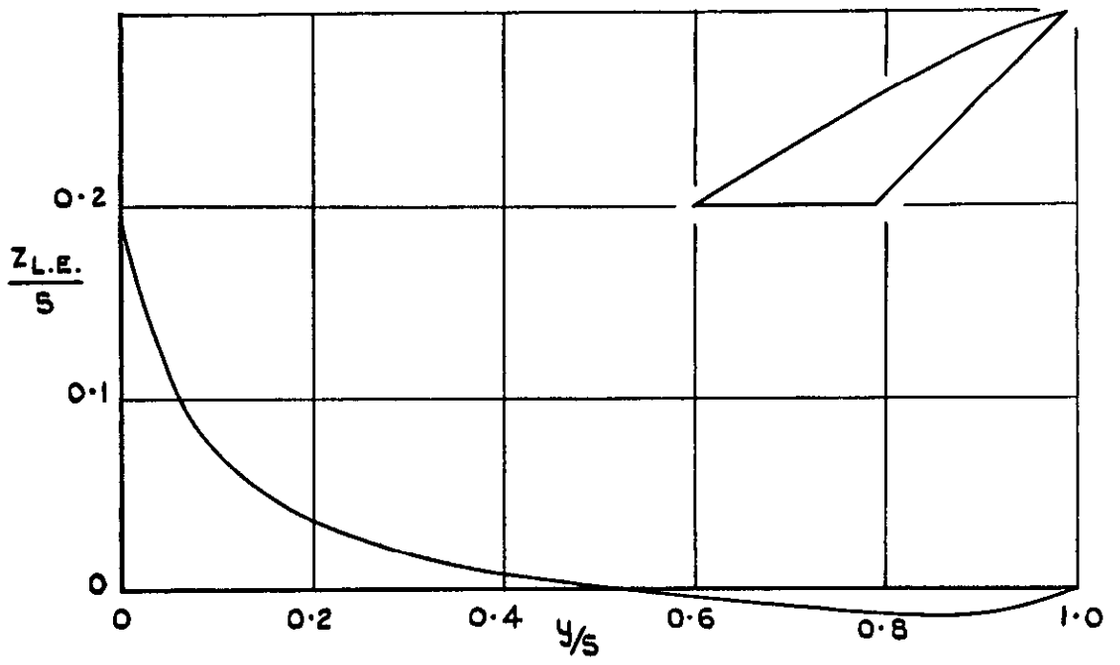

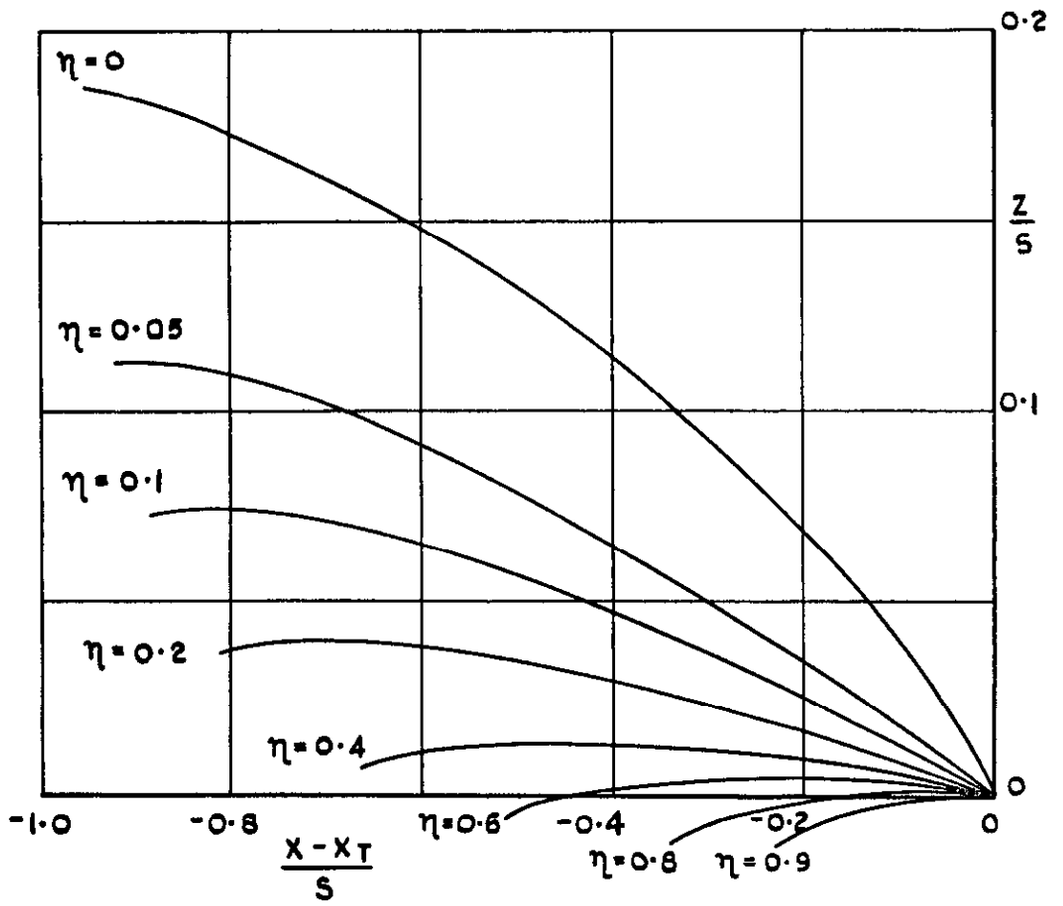

FIG.9. WING 5. $A = 3{\cdot}5$, $\varphi_0 = 60^\circ$, $\varphi_1 = 45^\circ$;
$-\Delta C_p = 0{\cdot}25$; $M_0 = 1{\cdot}2$.

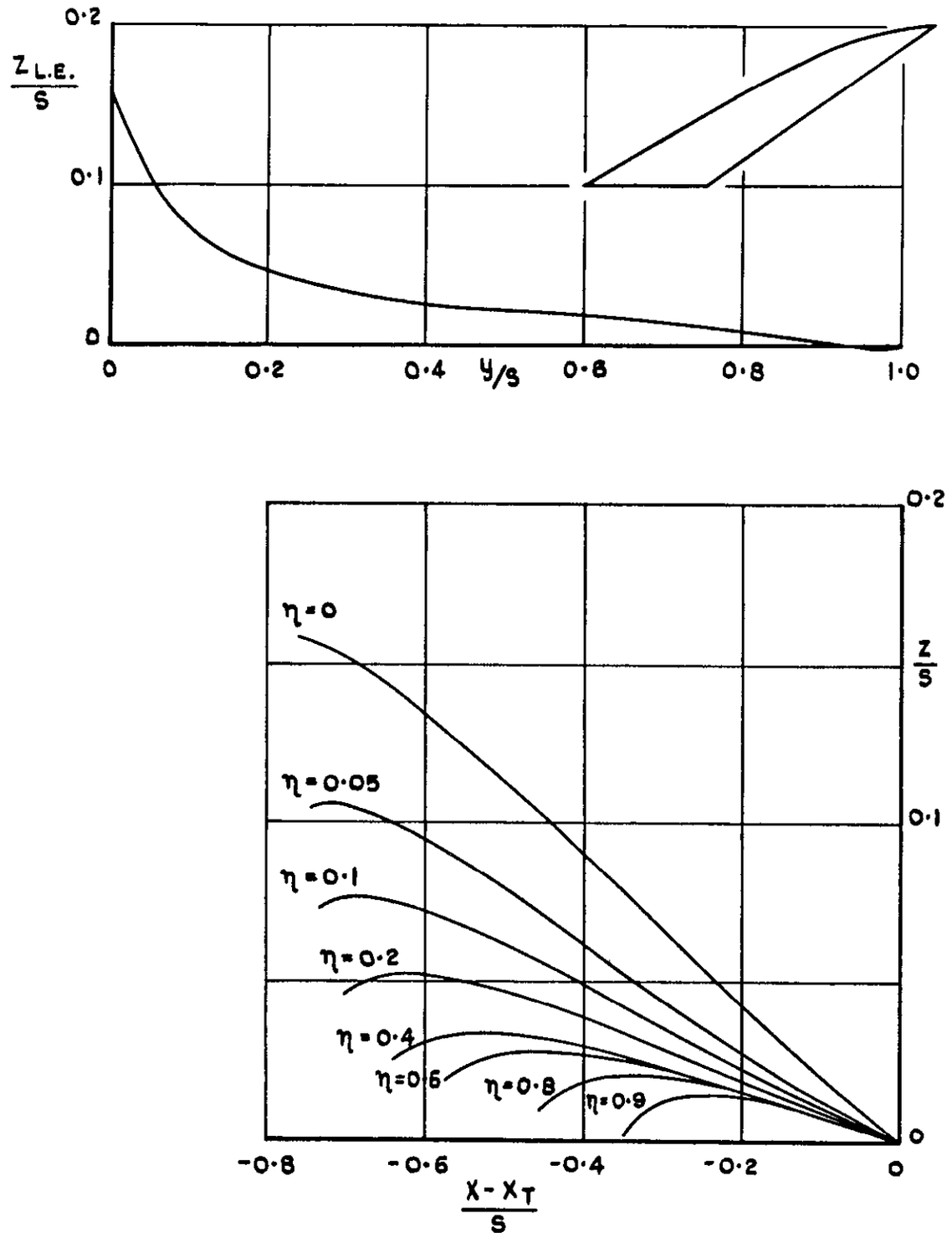

FIG.10. WING 6. $A = 3{\cdot}5$, $\varphi_0 = 60^\circ$, $\varphi_1 = 55^\circ$;
$-\Delta C_p = 0{\cdot}5 - 0{\cdot}5\,\xi$; $M_0 = 1{\cdot}2$.

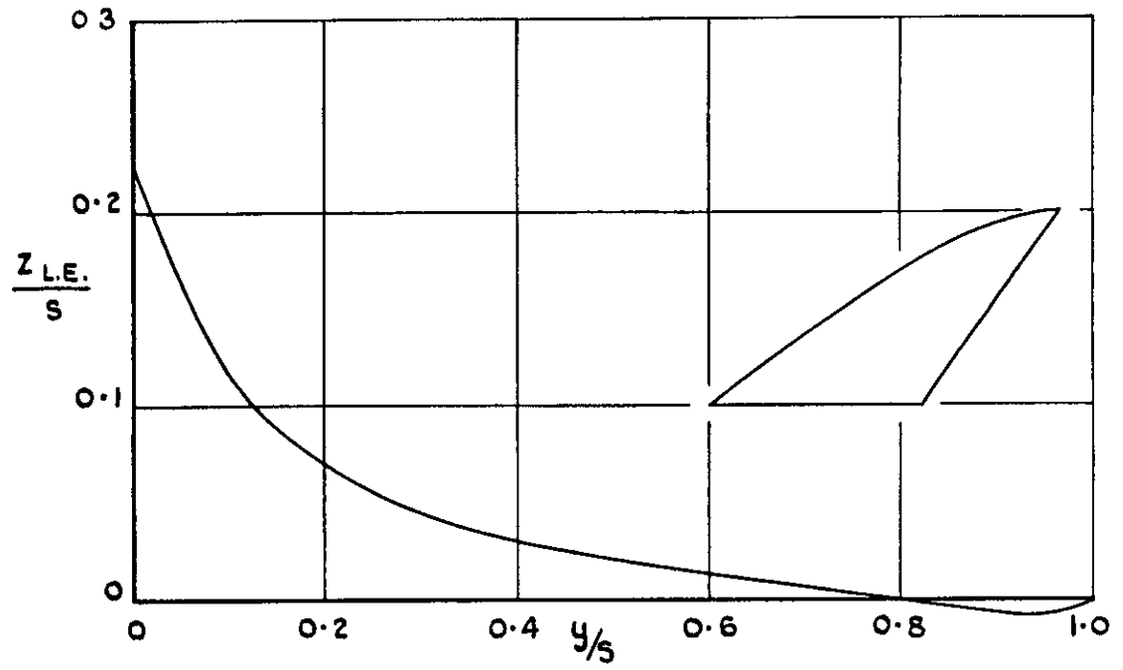

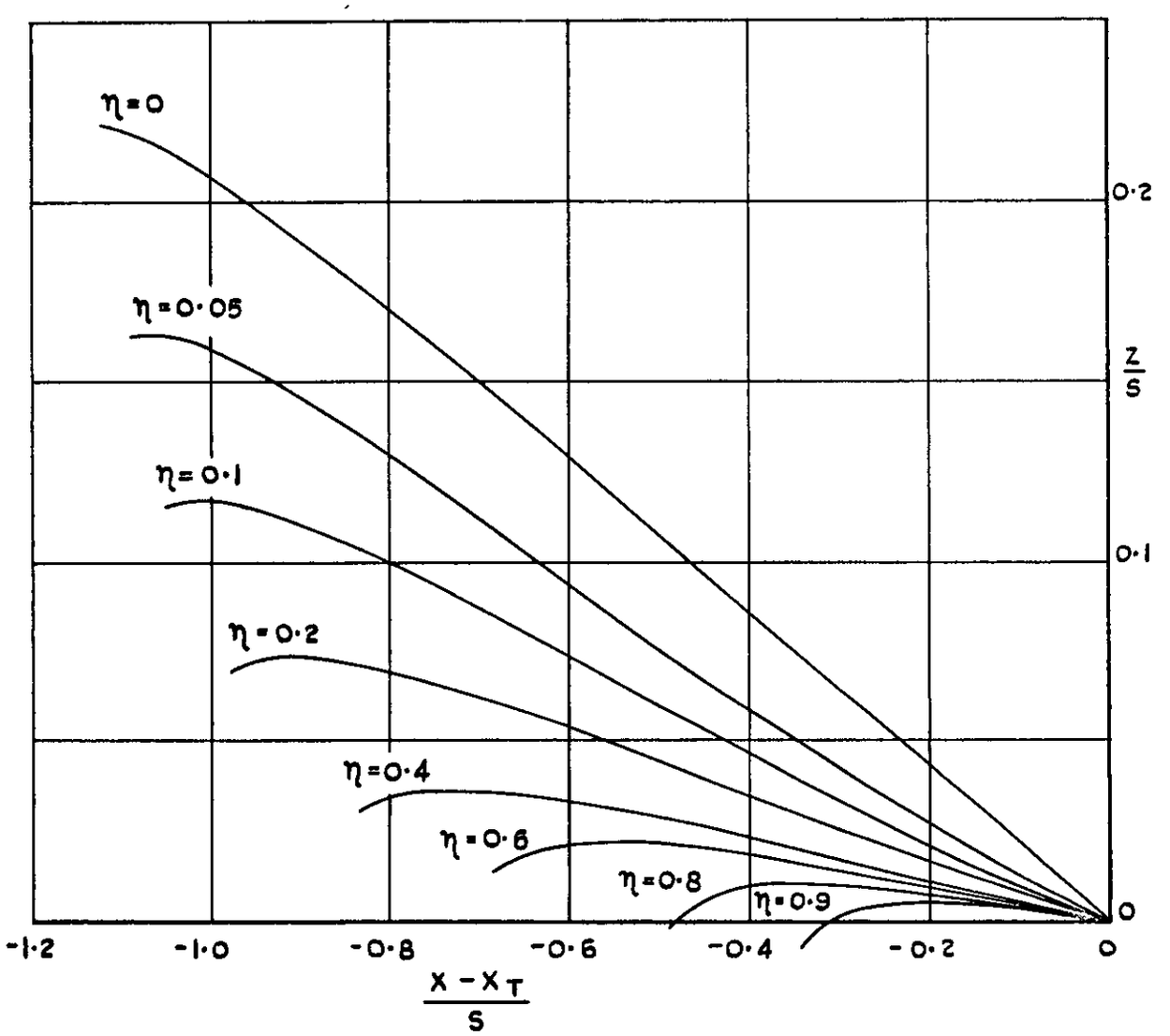

FIG.11. WING 7. $A = 2{\cdot}75$, $\varphi_0 = 55°$, $\varphi_1 = 35°$; $-\Delta C_p = 0{\cdot}5 - 0{\cdot}5\,\xi$; $M_0 = 1{\cdot}2$.

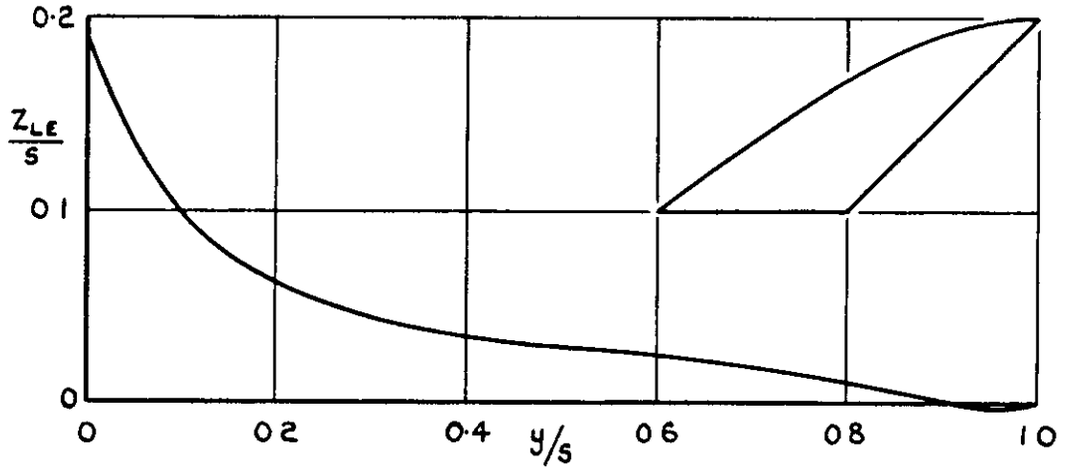

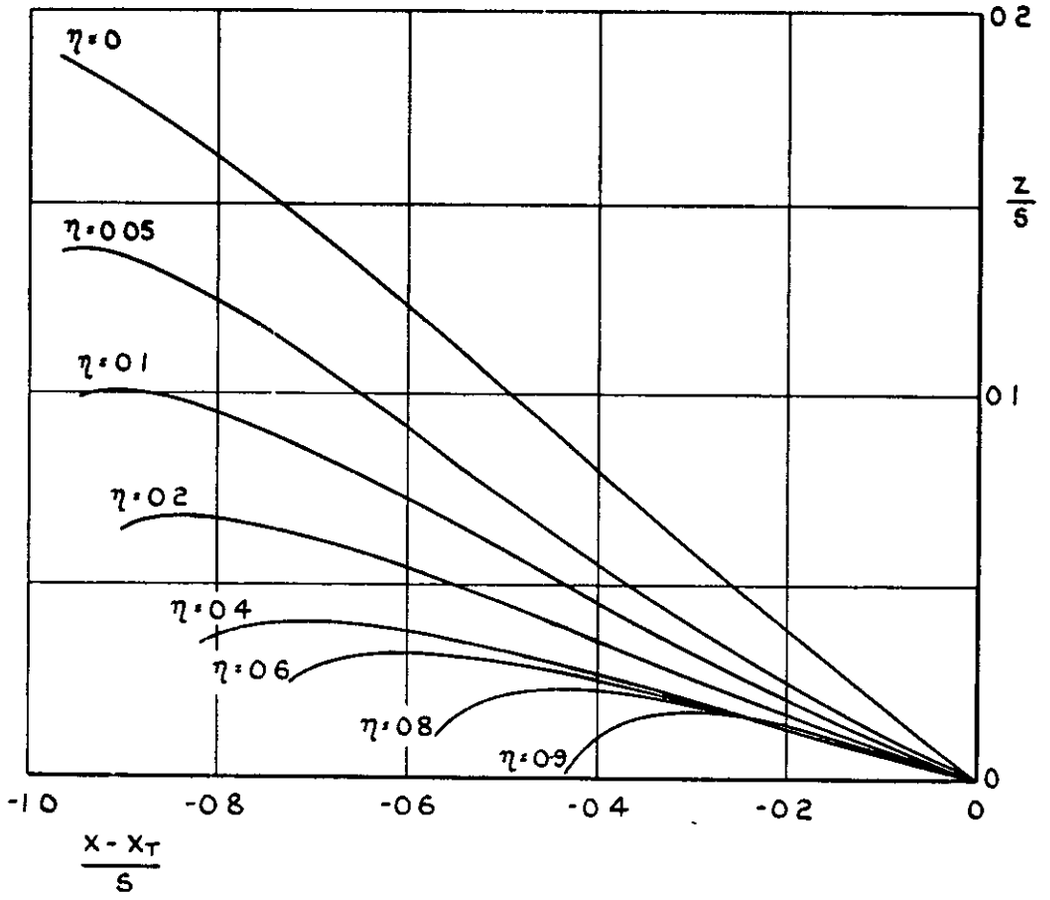

FIG.12. WING 8. $A = 2{\cdot}75$, $\varphi_0 = 55°$, $\varphi_1 = 45°$; $-\Delta C_p = 0{\cdot}5 - 0{\cdot}5\,\xi$; $M_0 = 1{\cdot}2$.

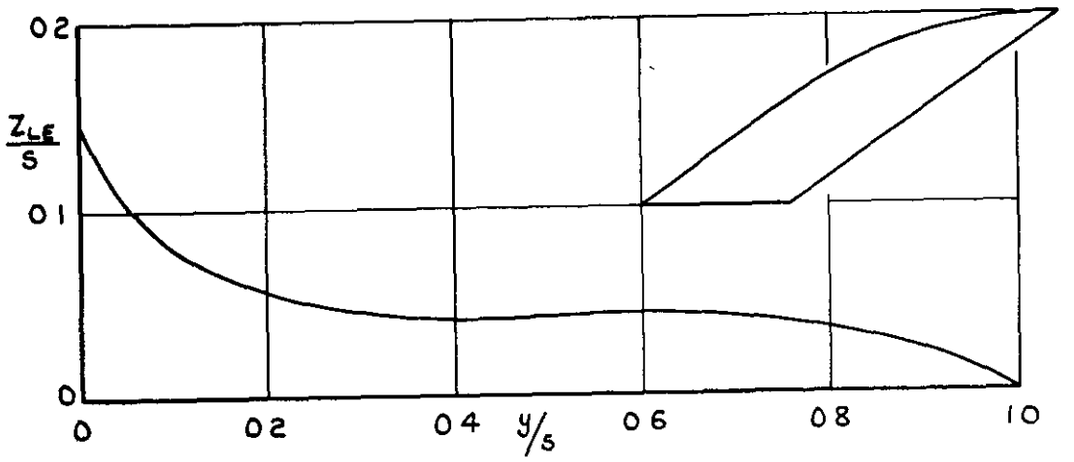

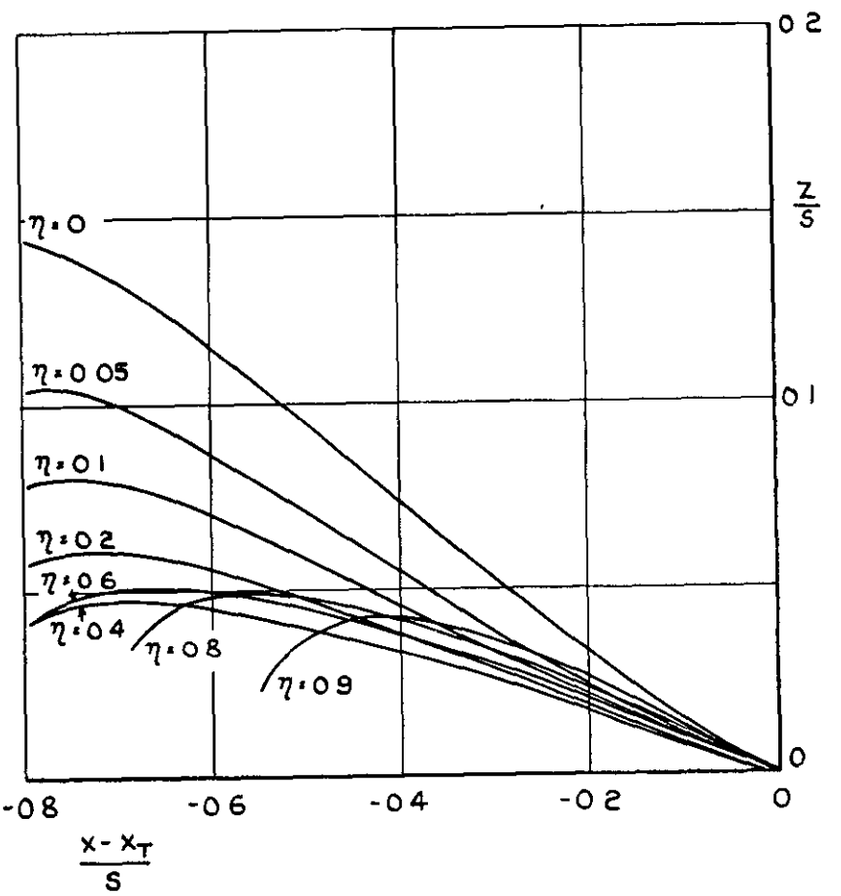

FIG. 13. WING 9. $A = 2{\cdot}75$, $\varphi_0 = 55^\circ$, $\varphi_1 = 55^\circ$; $-\Delta C_p = 0{\cdot}5 - 0{\cdot}5\,\xi$; $M_0 = 1{\cdot}2$.

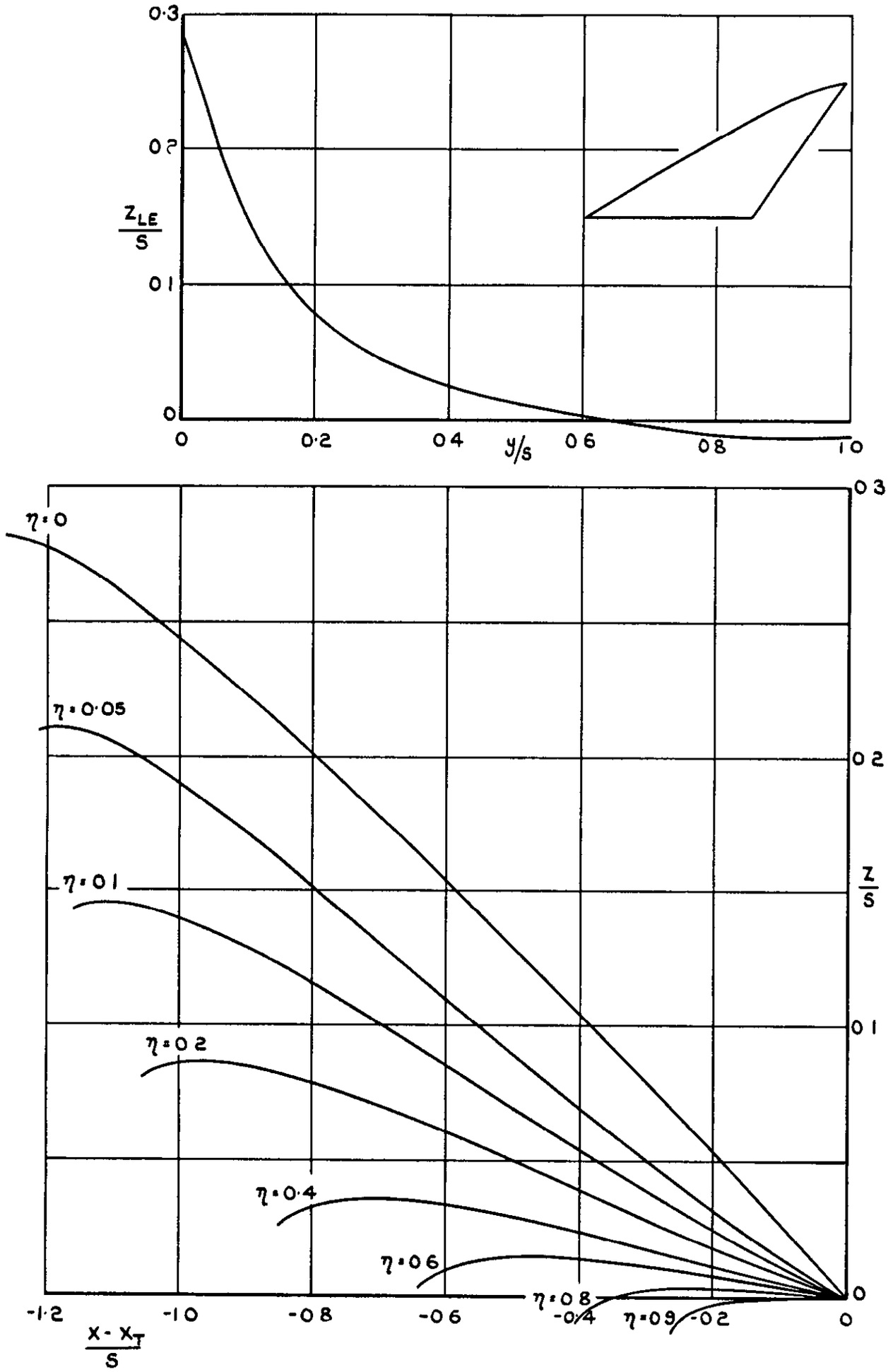

FIG.14. WING 10. A=2·75, $\varphi_0 = 60°$, $\varphi_1 = 35°$; $-\Delta C_p = 0·5 - 0·5$ }; $M_0 = 1·2$.

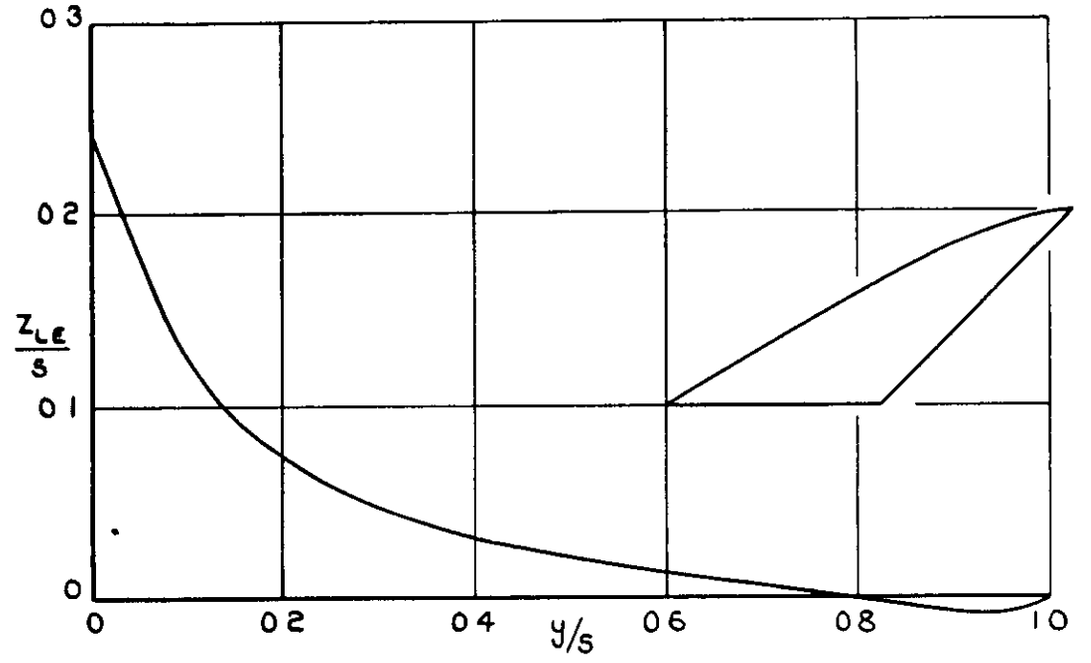

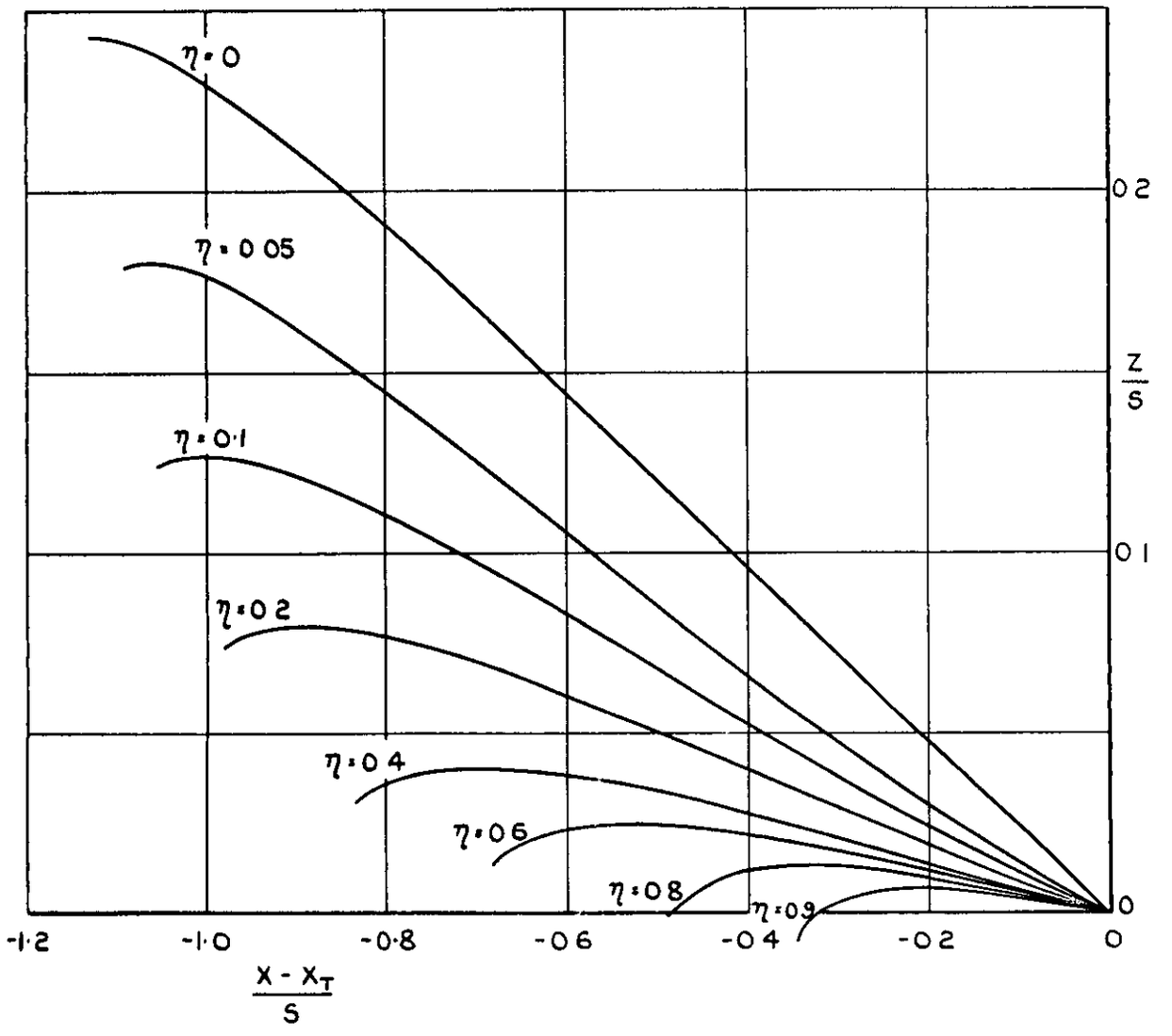

FIG. 15. WING 11. $A = 2{\cdot}75$, $\varphi_0 = 60°$, $\varphi_1 = 45°$; $-\Delta C_p = 0{\cdot}5 - 0{\cdot}5\,\xi$; $M_0 = 1{\cdot}2$.

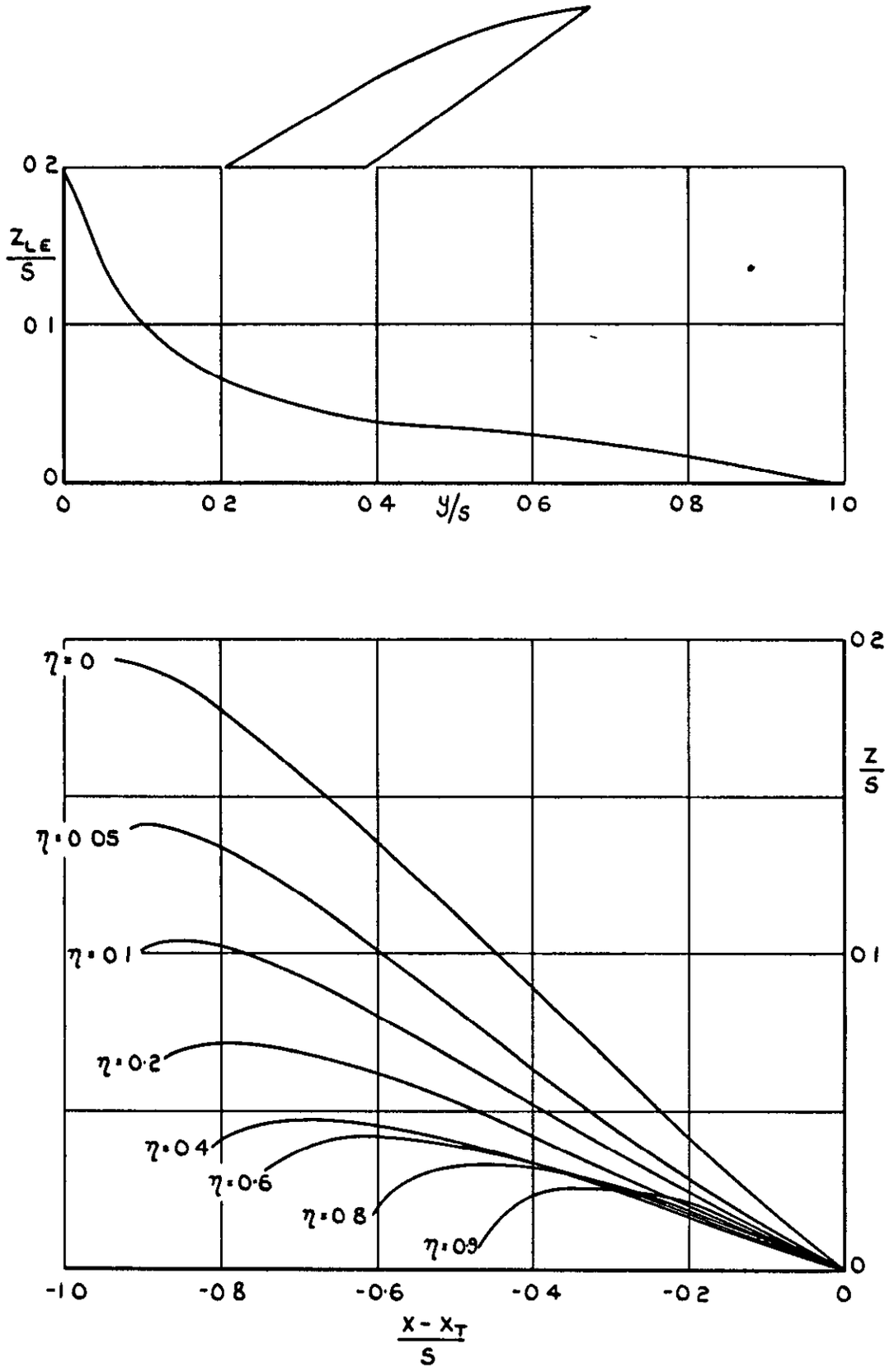

FIG.16. WING 12. $A = 2\cdot75$, $\varphi_0 = 60°$, $\varphi_1 = 55°$; $-\Delta C_p = 0\cdot5 - 0\cdot5\,\zeta$; $M_0 = 1\cdot2$.

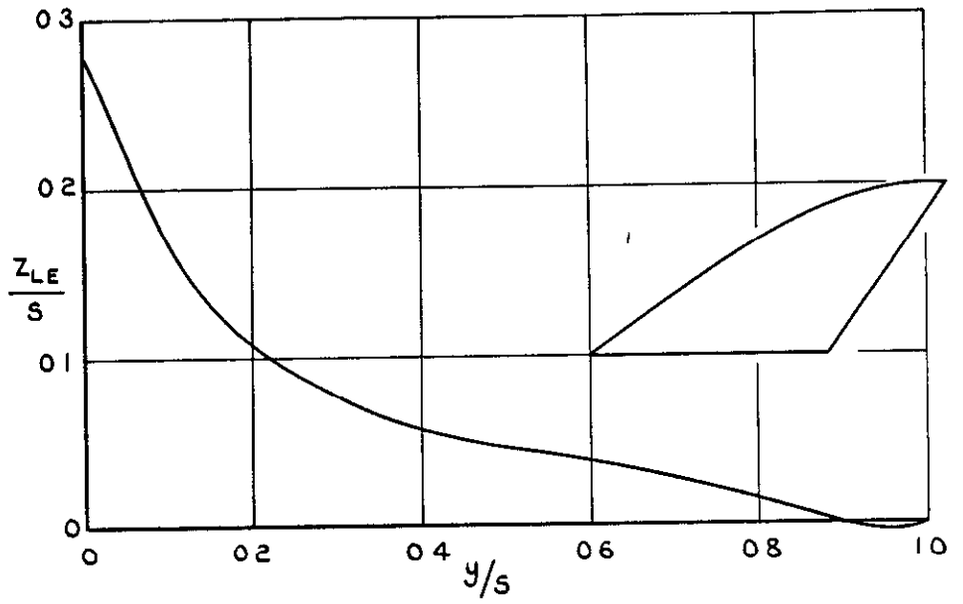

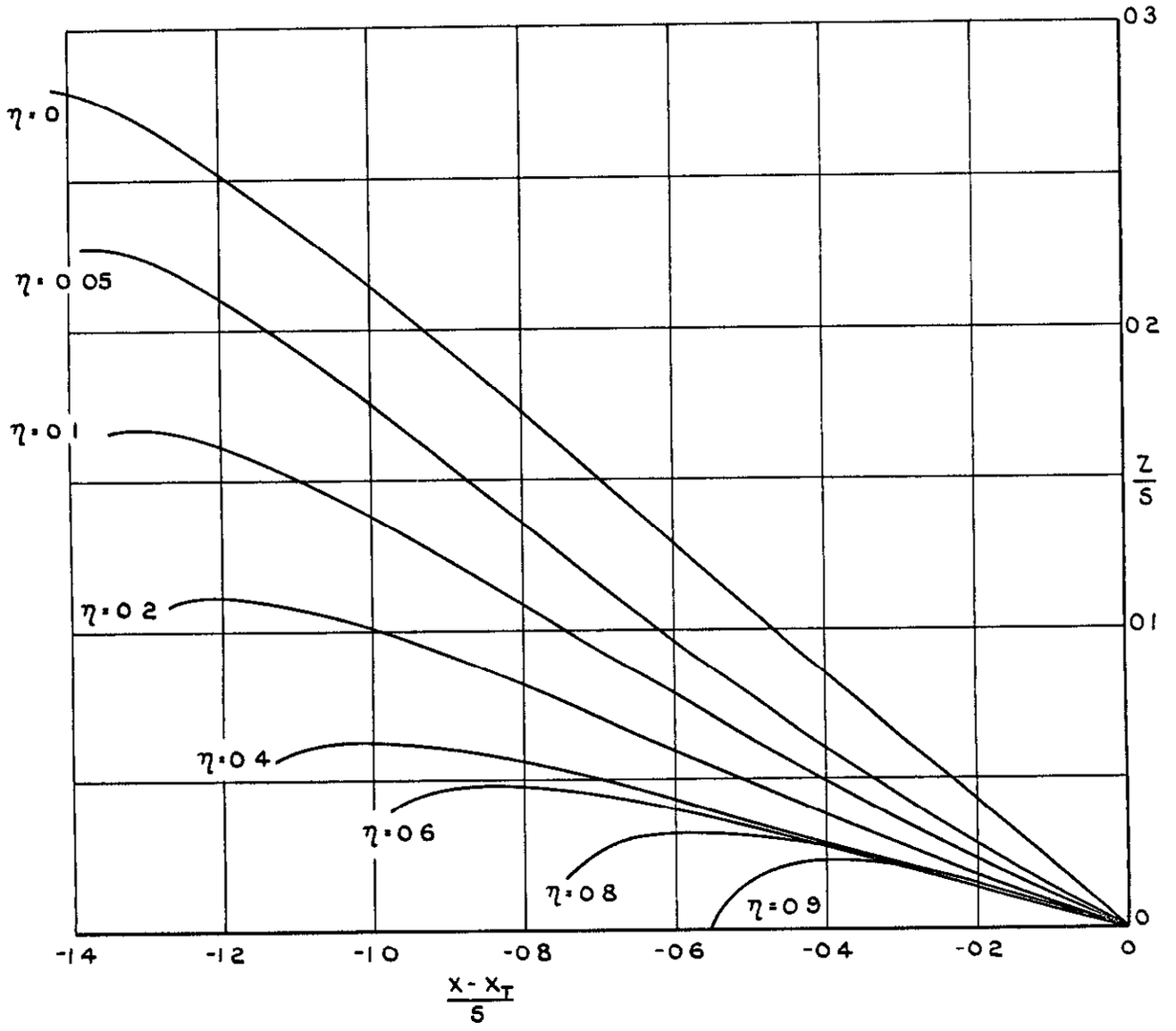

FIG. 17. WING 13. A=2·0, $\varphi_0 = 55°$, $\varphi_1 = 35°$; $-\Delta C_p = 0·5 - 0·5\,\xi$; $M_0 = 1·2$.

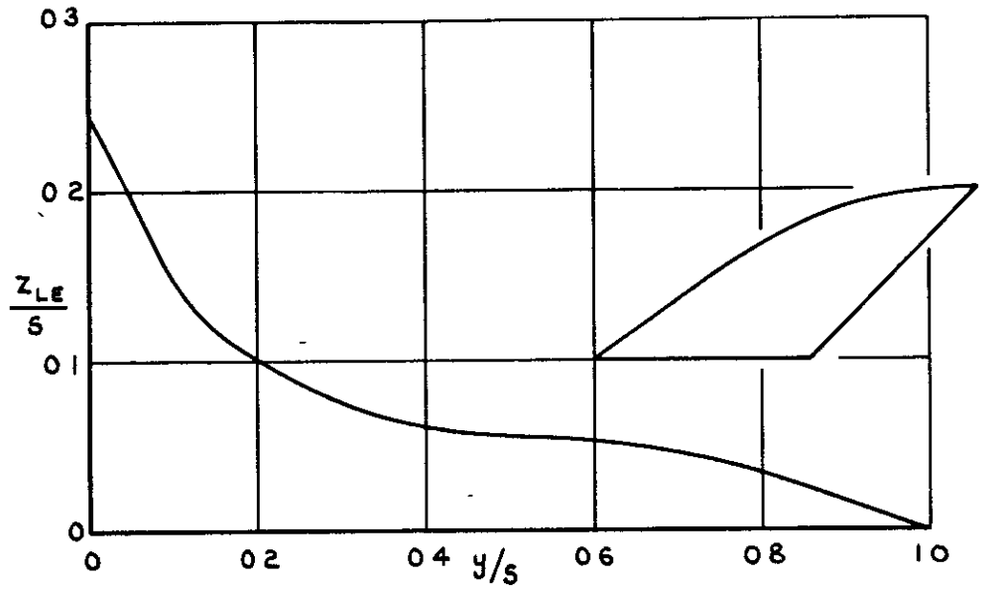

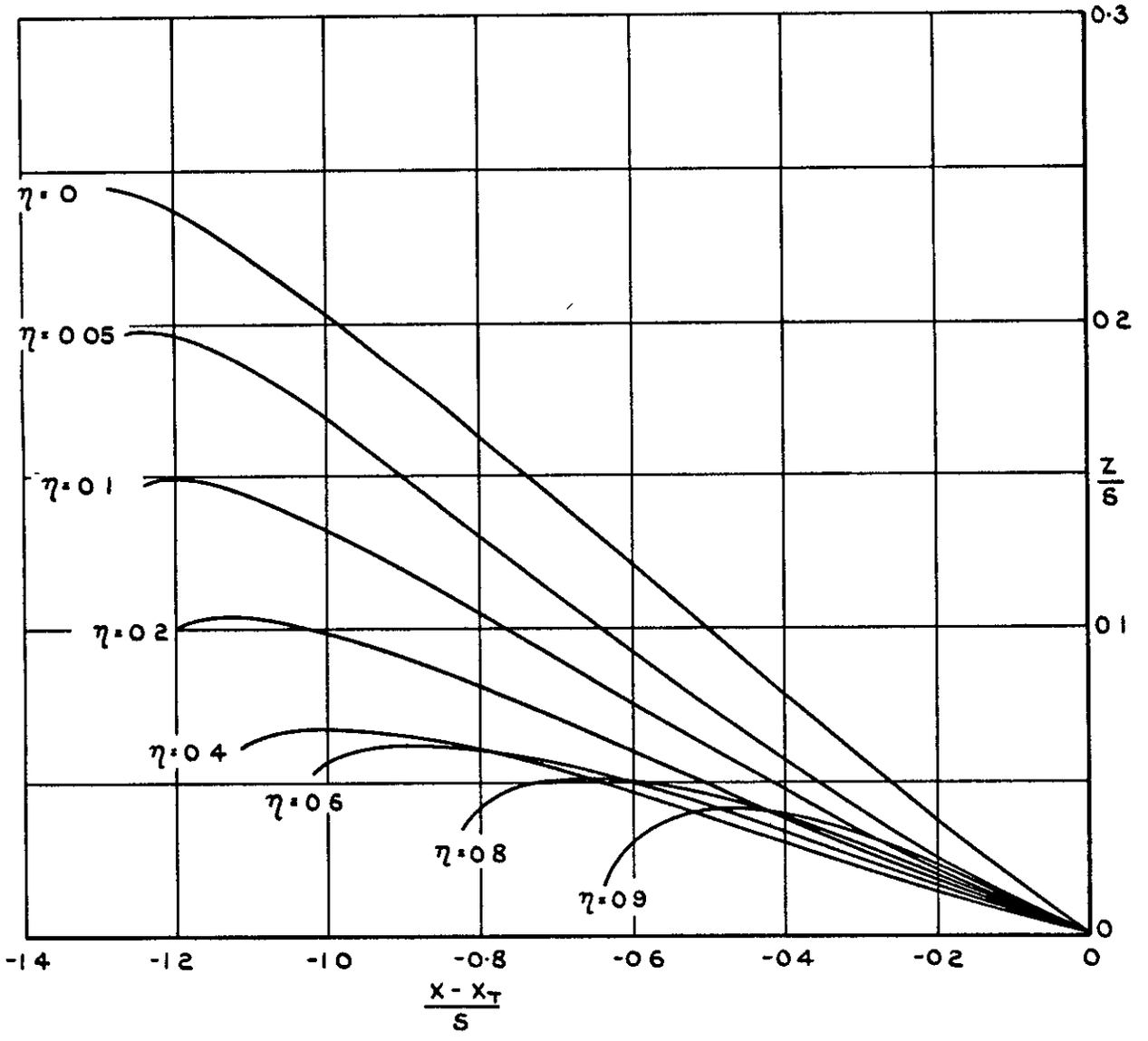

FIG. 18. WING 14. A=2, $\varphi_0 = 55^\circ$, $\varphi_1 = 45^\circ$;
$-\Delta C_p = 0{\cdot}5 - 0{\cdot}5\,\xi$; $M_0 = 1{\cdot}2$.

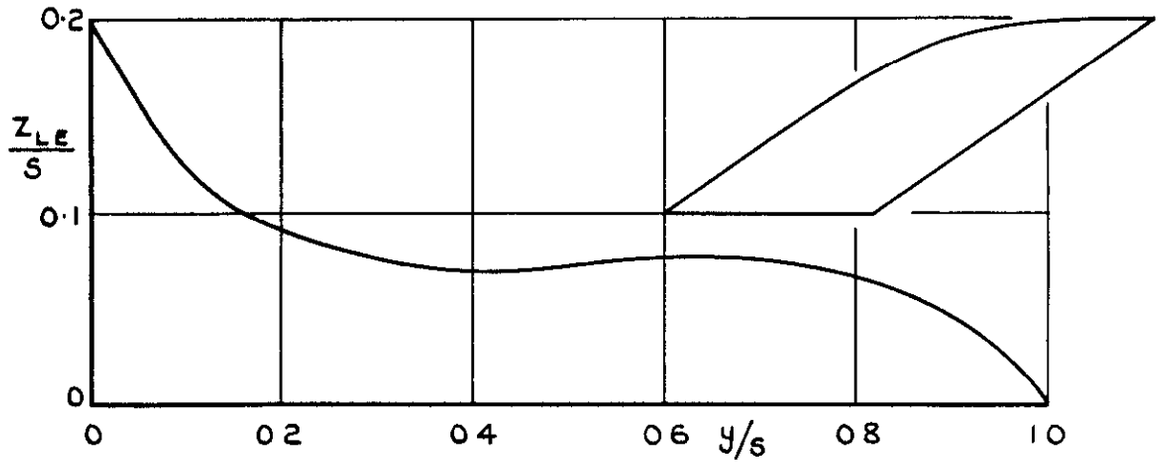

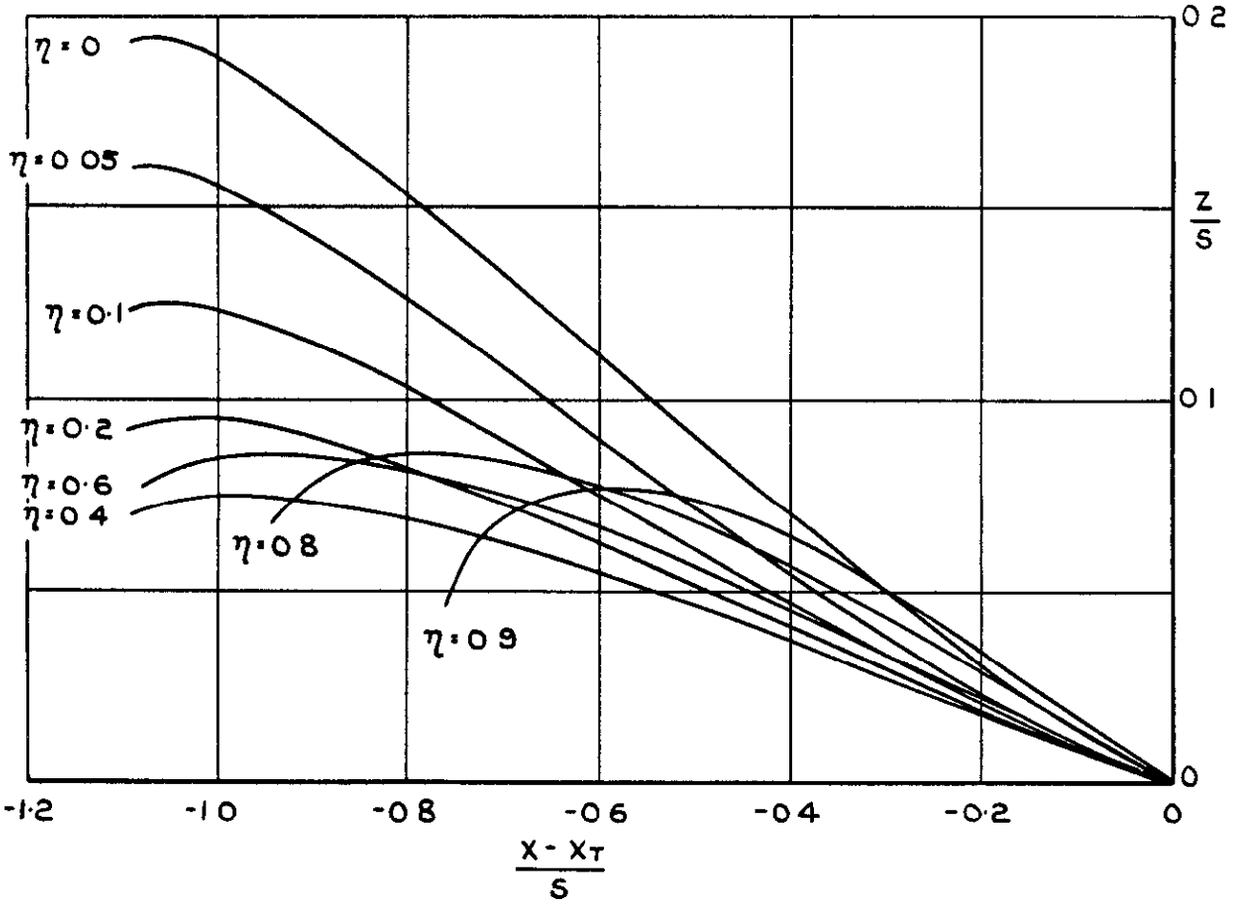

FIG. 19. WING 15. A=2, $\varphi_0 = 55°$, $\varphi_1 = 55°$; $-\Delta C_p = 0{\cdot}5 - 0{\cdot}5\,\zeta$; $M_0 = 1{\cdot}2$.

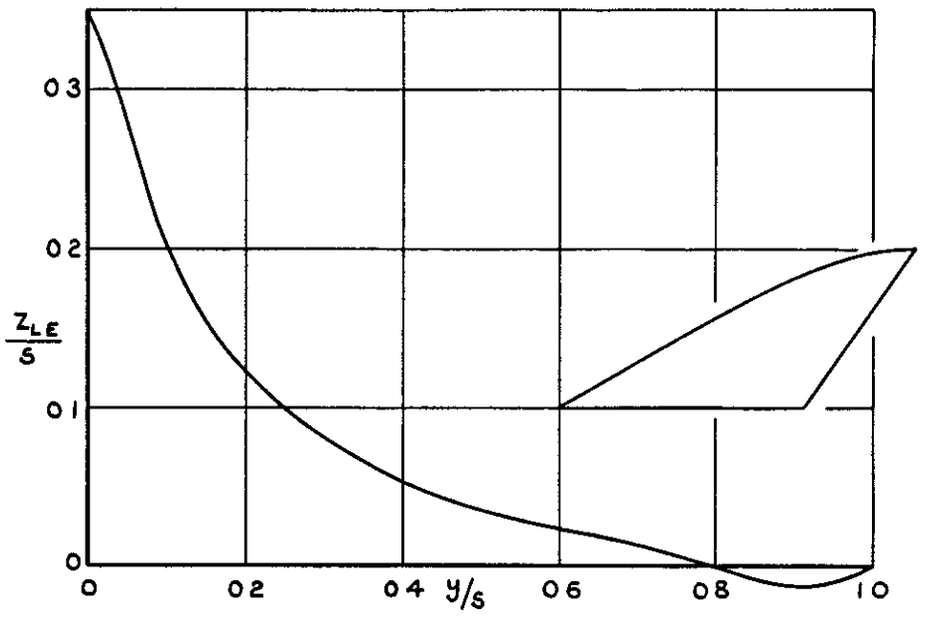

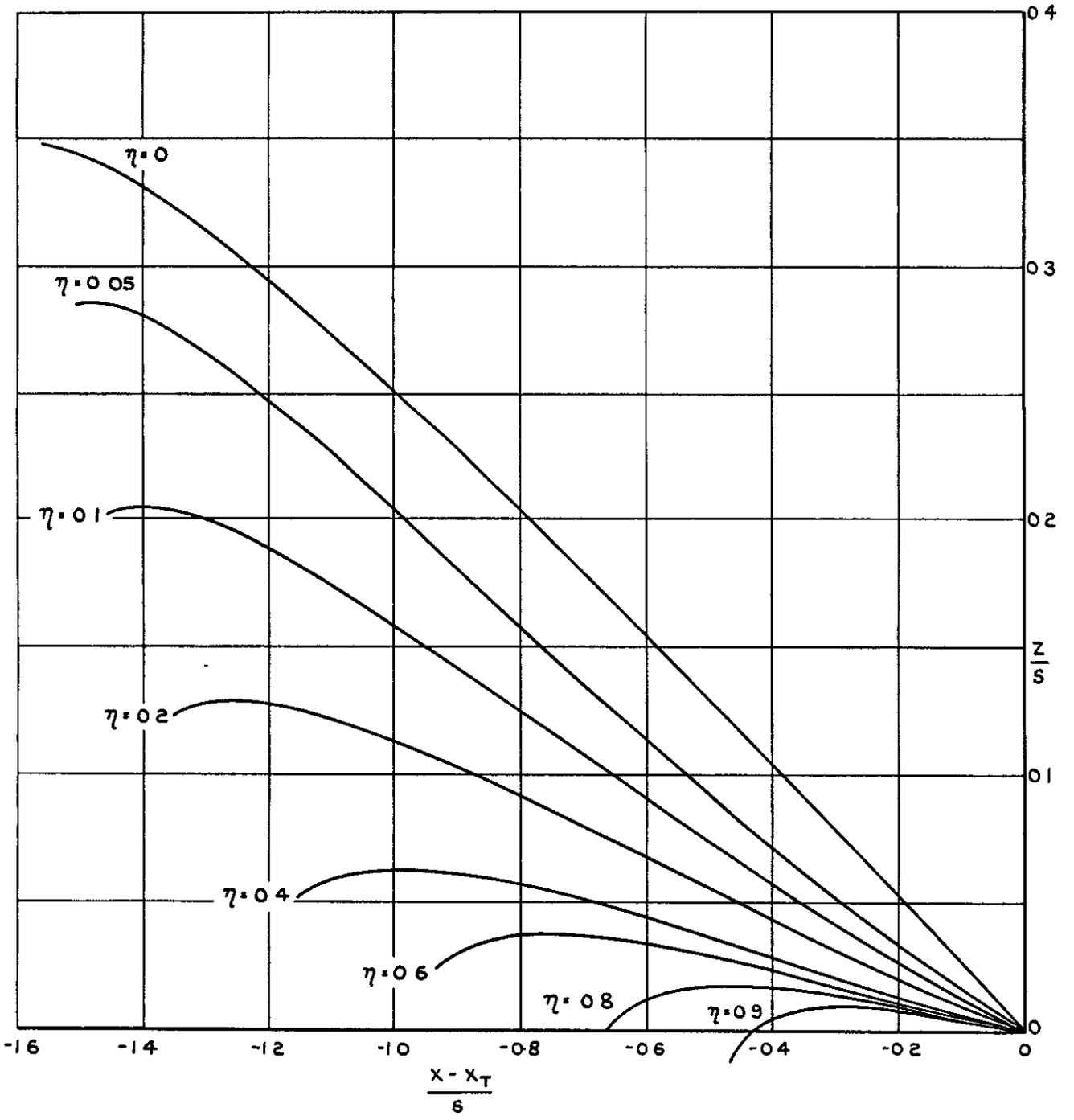

FIG. 20. WING 16. $A = 2$, $\varphi_0 = 60°$, $\varphi_1 = 35°$;
$-\Delta C_p = 0{\cdot}5 - 0{\cdot}5\,\xi$; $M_0 = 1{\cdot}2$.

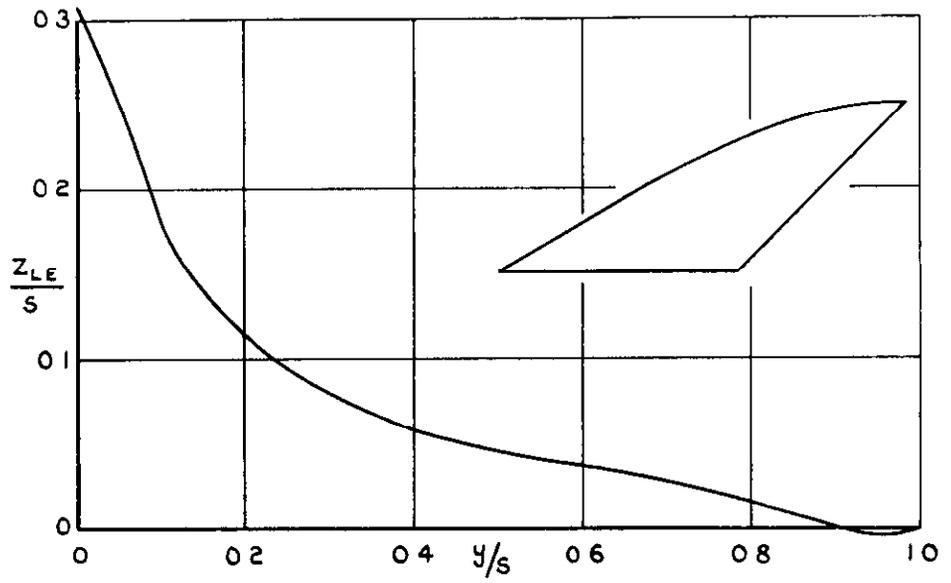

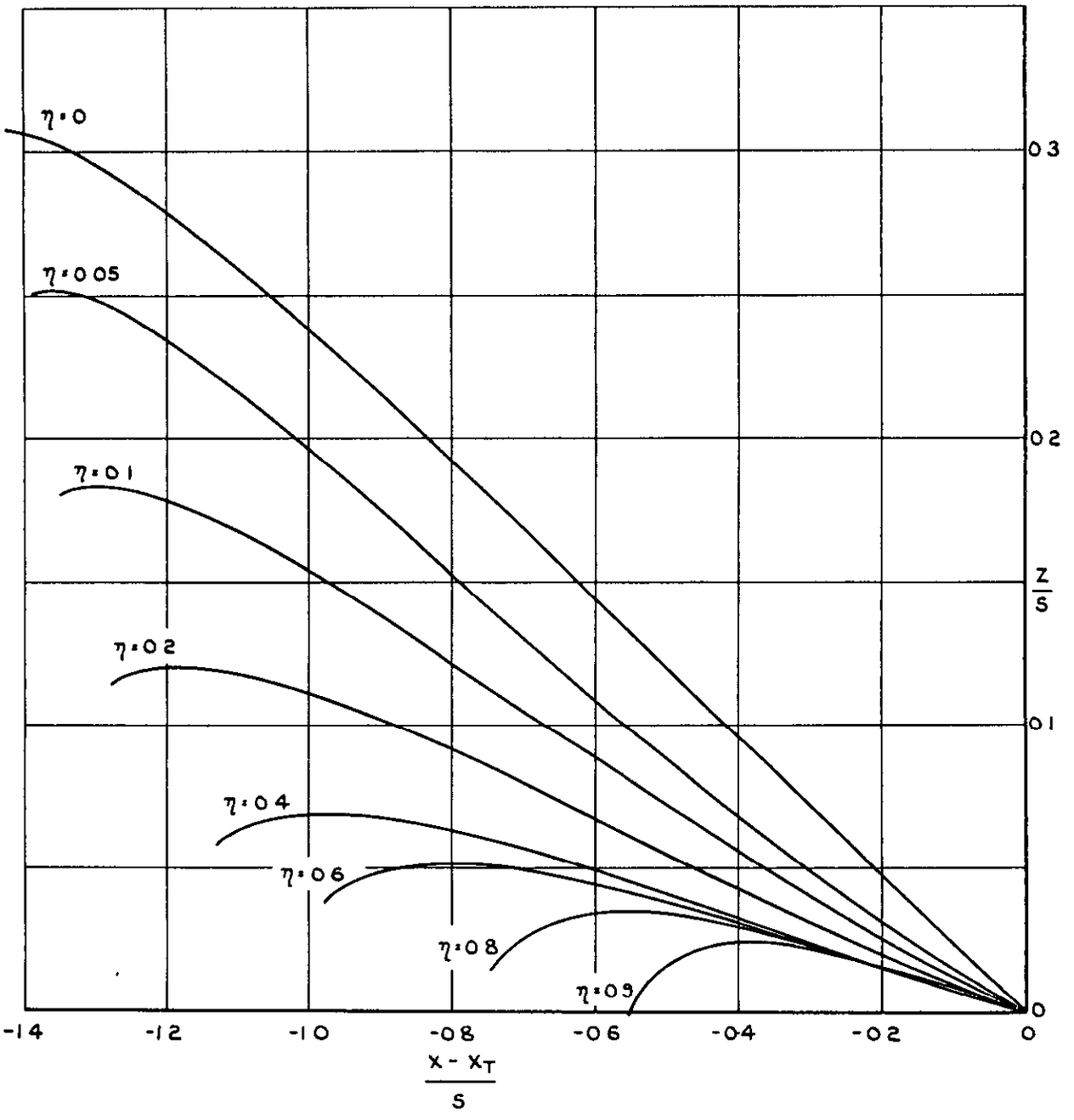

FIG. 21. WING 17. $A = 2{\cdot}0$, $\varphi_0 = 60°$, $\varphi_1 = 45°$;
$-\Delta C_p = 0{\cdot}5 - 0{\cdot}5\,\xi$, $M_0 = 1{\cdot}2$.

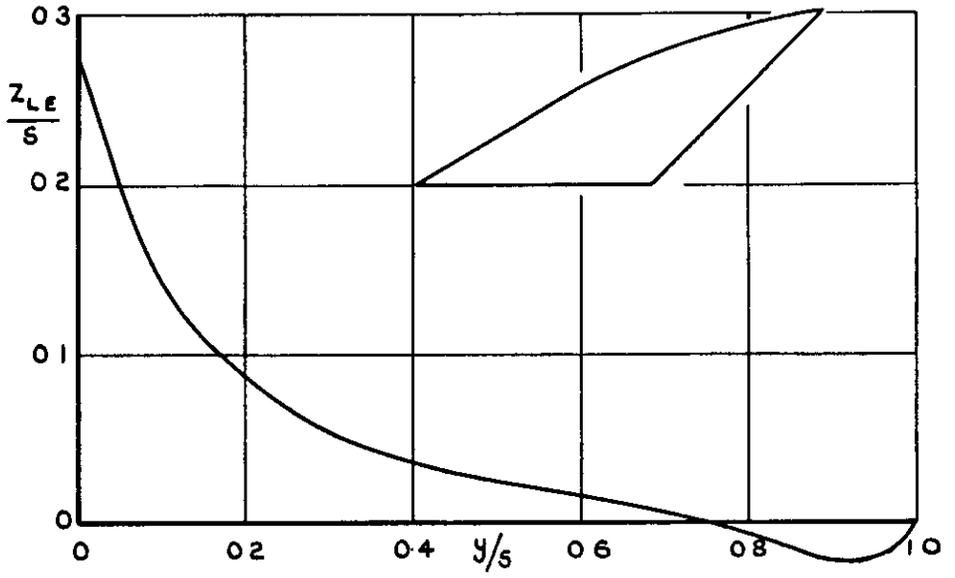

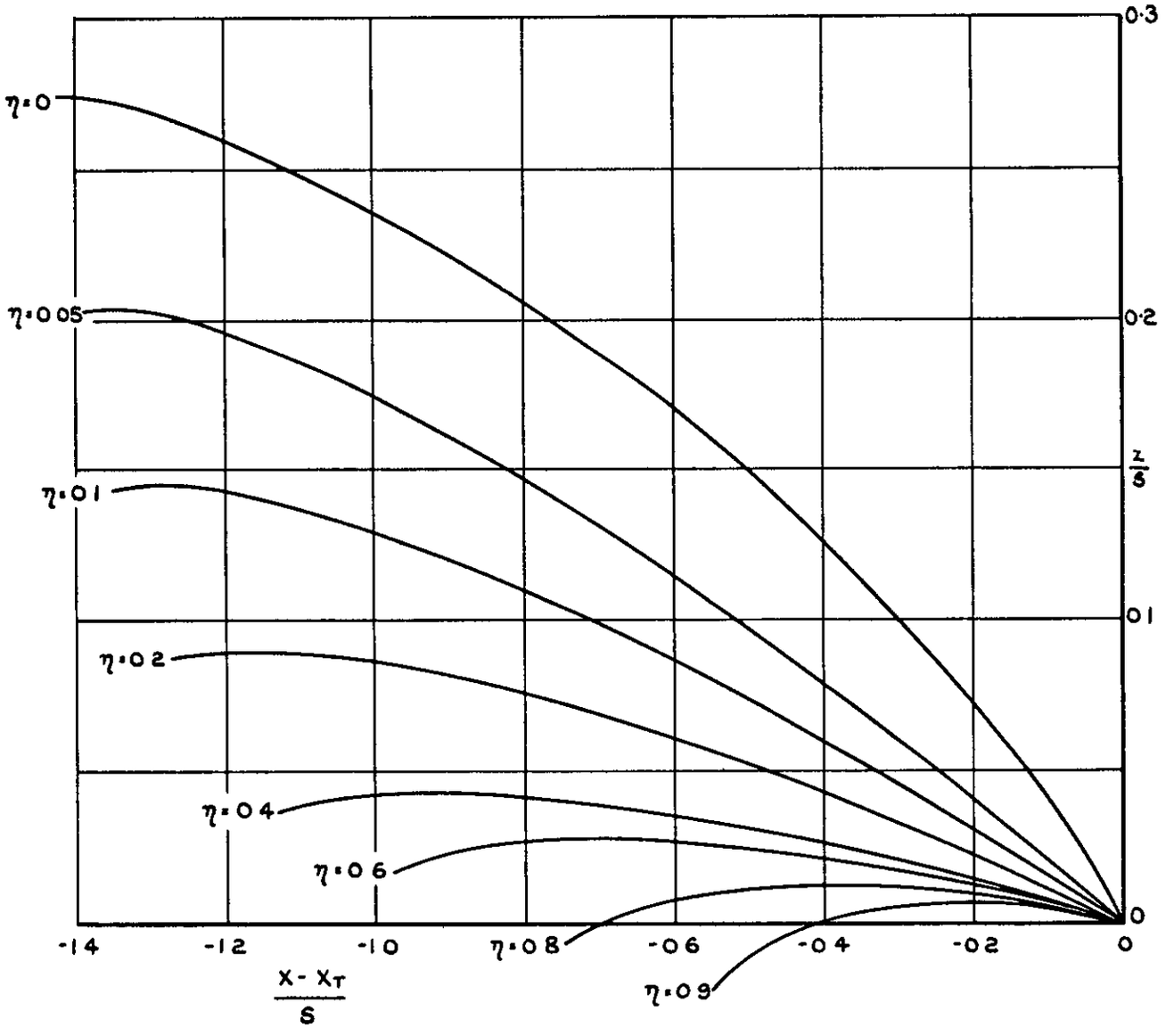

FIG. 22. WING 17. $A=2{\cdot}0$, $\varphi_0=60°$, $\varphi_1=45°$; $-\Delta C_p=0{\cdot}25$; $M_0=1{\cdot}2$.

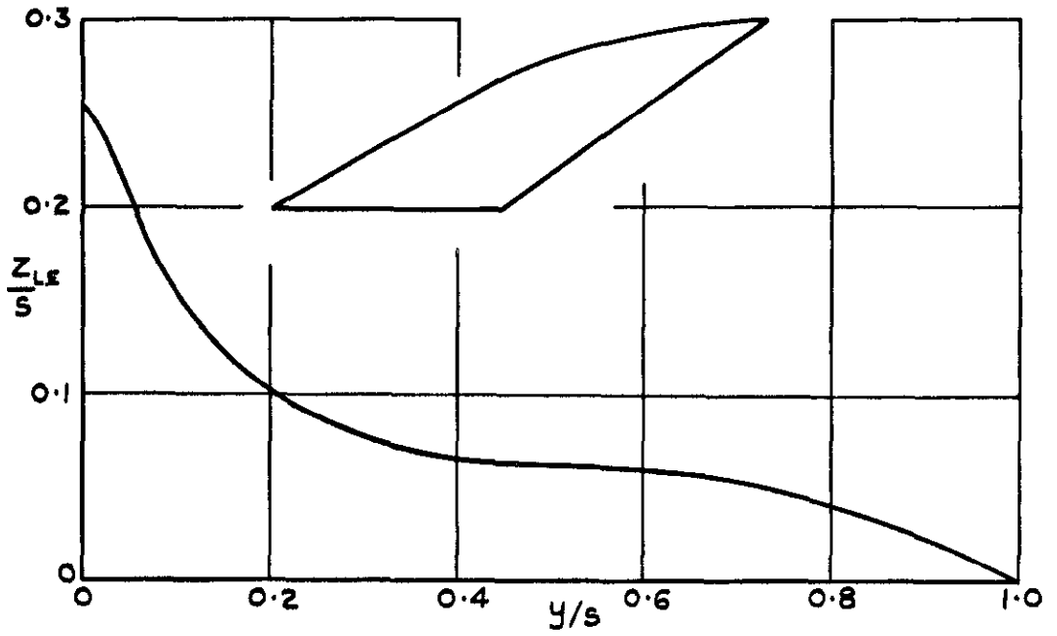

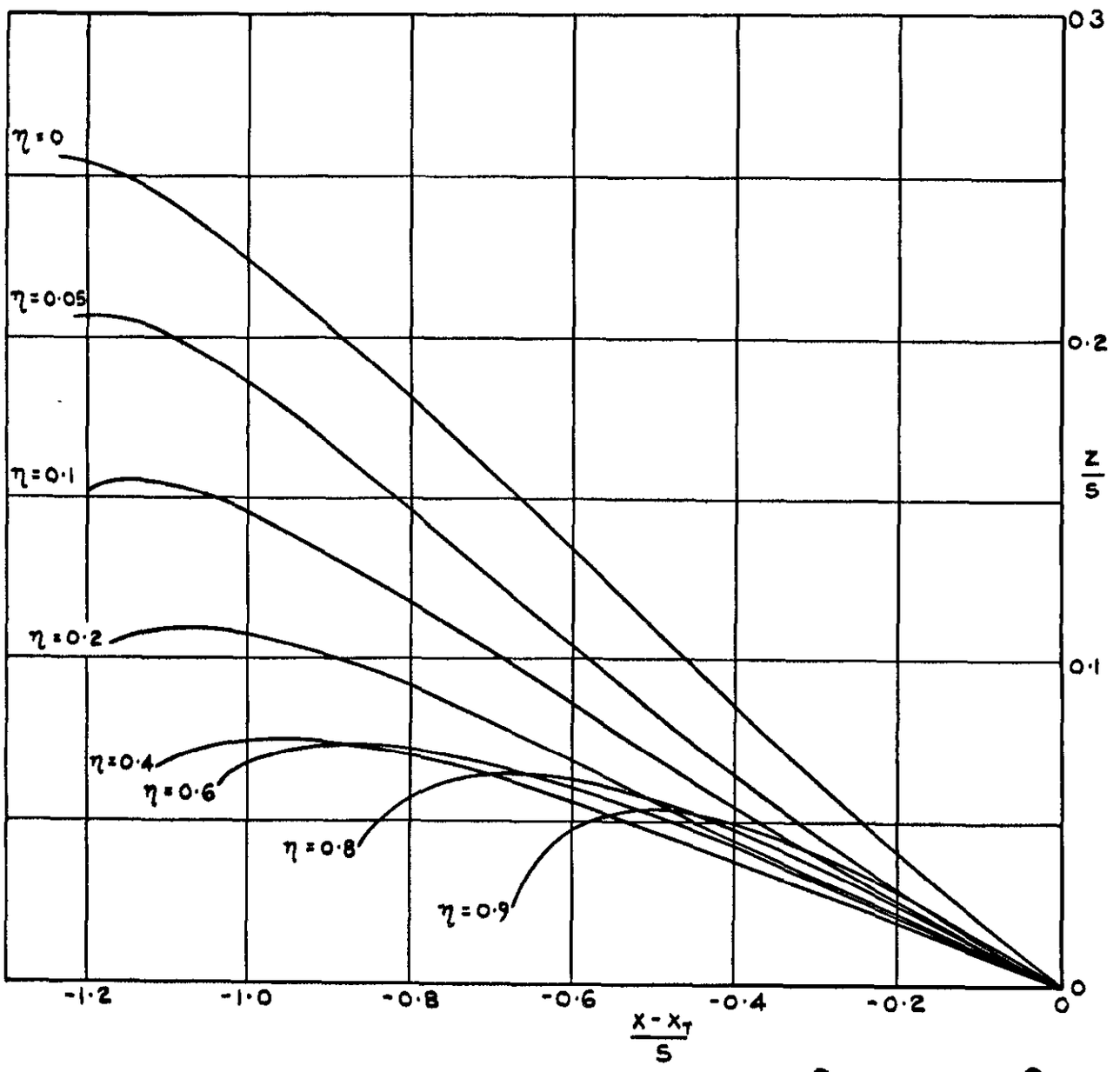

FIG. 23. WING 18. $A = 2{\cdot}0$, $\varphi_0 = 60^\circ$, $\varphi_1 = 55^\circ$; $-\Delta C_p = 0{\cdot}5 - 0{\cdot}5\xi$; $M_0 = 1{\cdot}2$.

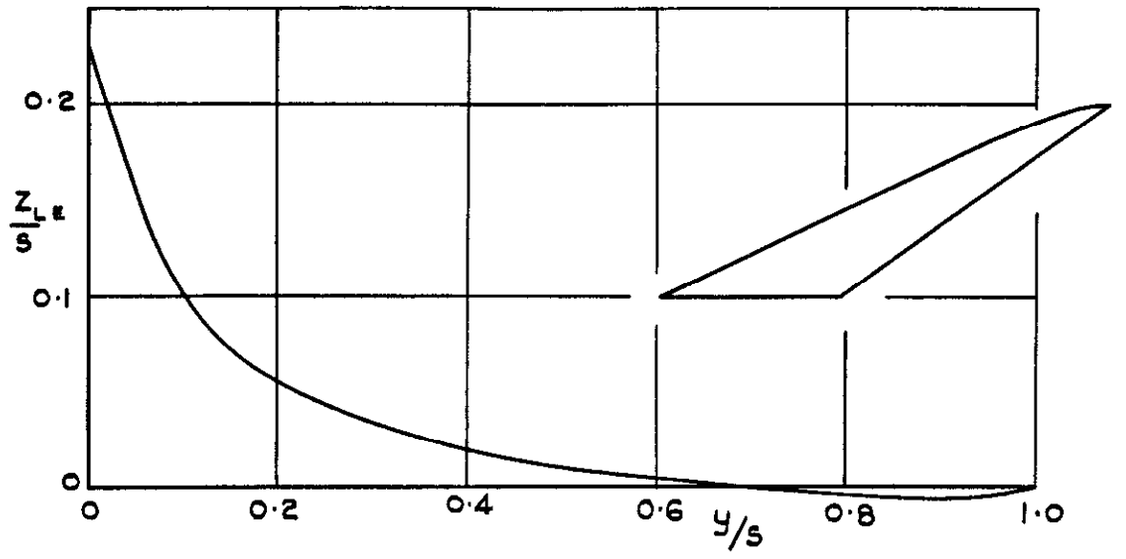

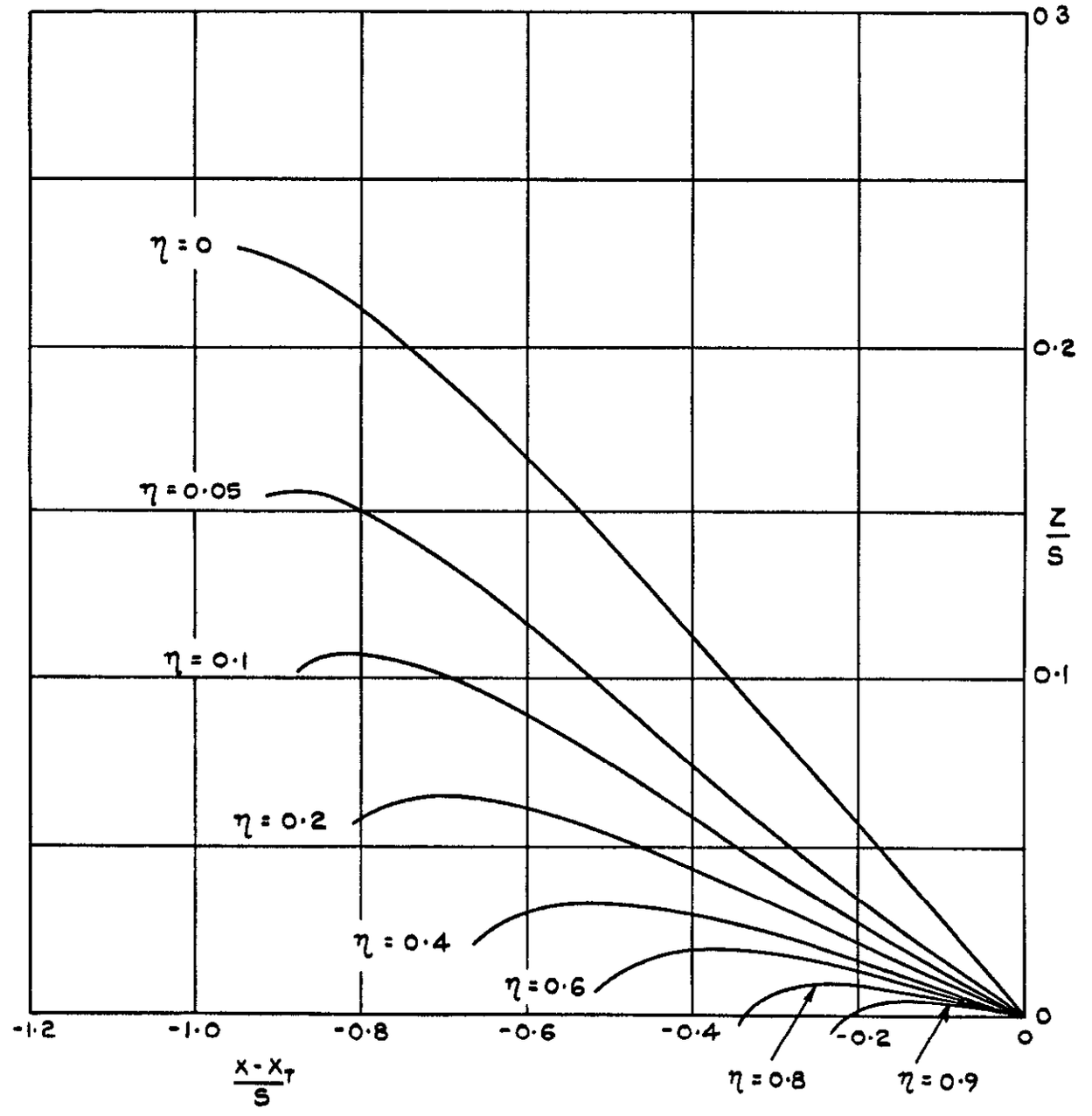

FIG. 24. WING 19. $A = 3 \cdot 5$, $\varphi_0 = 65^\circ$, $\varphi_1 = 55^\circ$; $-\Delta C_p = 0 \cdot 5 - 0 \cdot 5\,\xi$; $M_0 = 1 \cdot 2$.

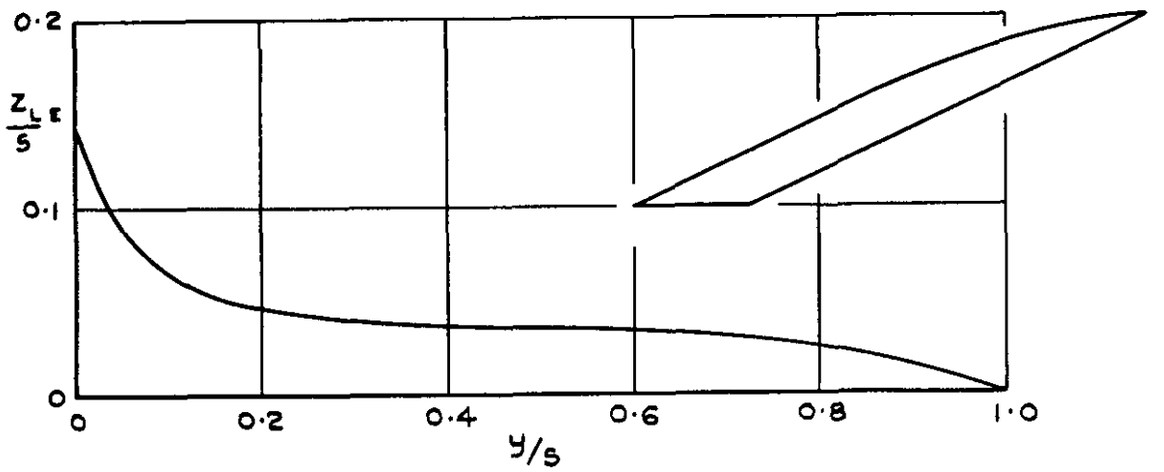

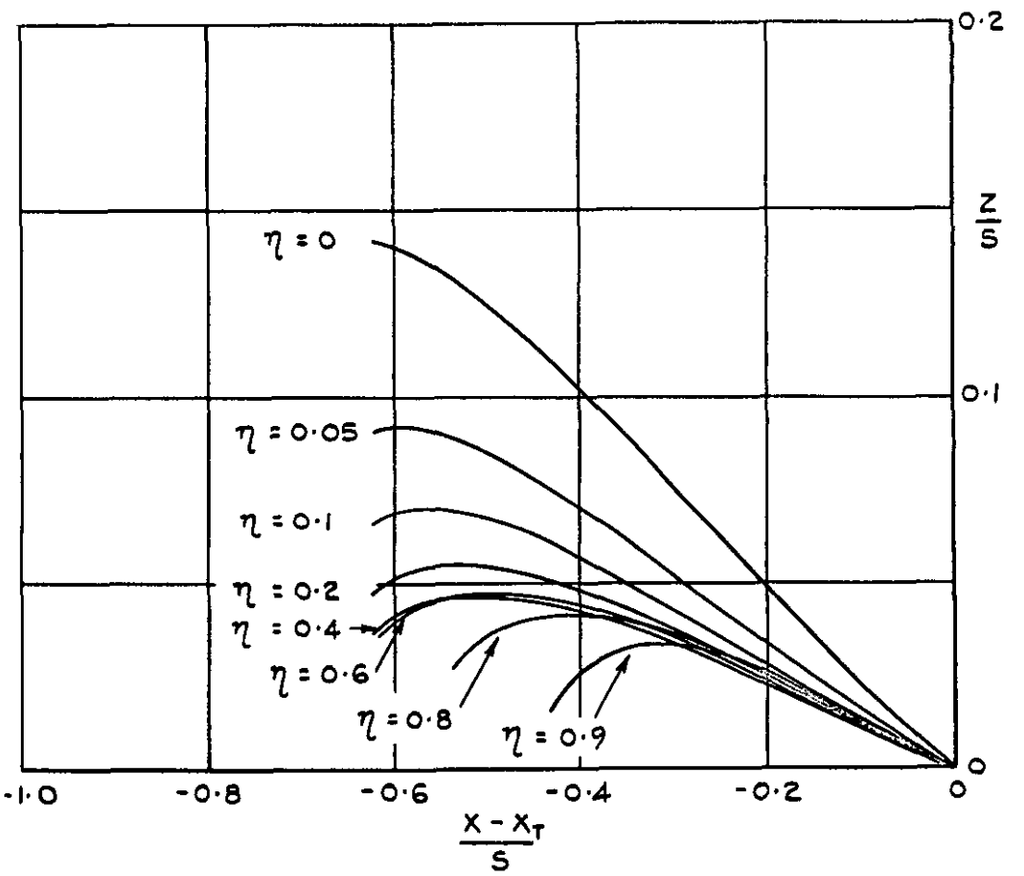

FIG. 25. WING 20. $A = 3 \cdot 5$, $\varphi_0 = 65^\circ$, $\varphi_1 = 65^\circ$; $-\Delta C_p = 0 \cdot 5 - 0 \cdot 5\,\xi$; $M_0 = 1 \cdot 2$.

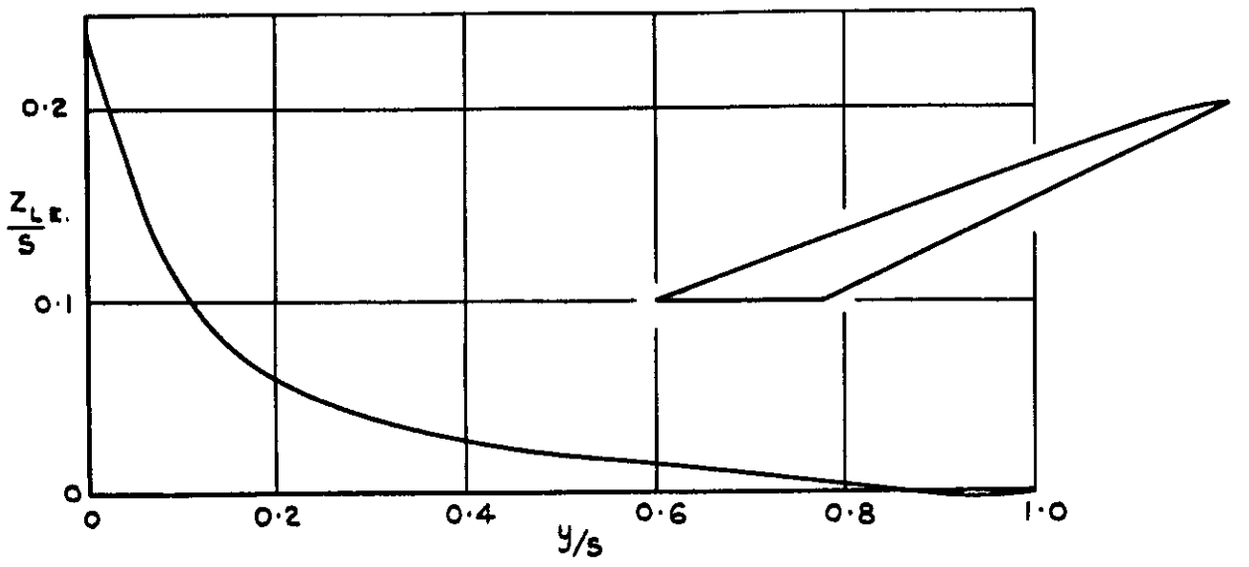

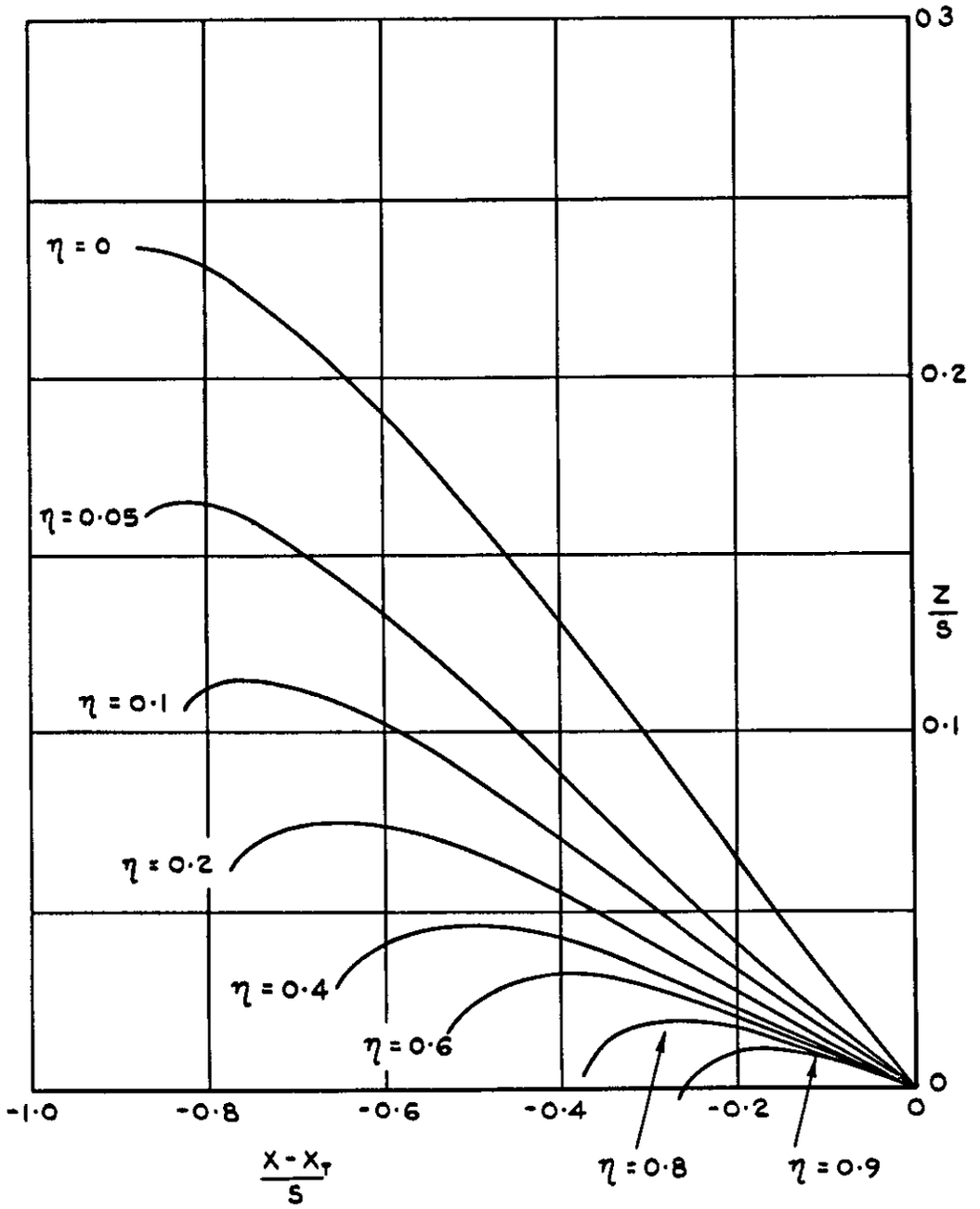

FIG. 26. WING 21. $A = 3 \cdot 5$, $\varphi_0 = 70^\circ$, $\varphi_1 = 65^\circ$; $-\Delta C_p = 0 \cdot 5 - 0 \cdot 5\,\xi$; $M_0 = 1 \cdot 2$.

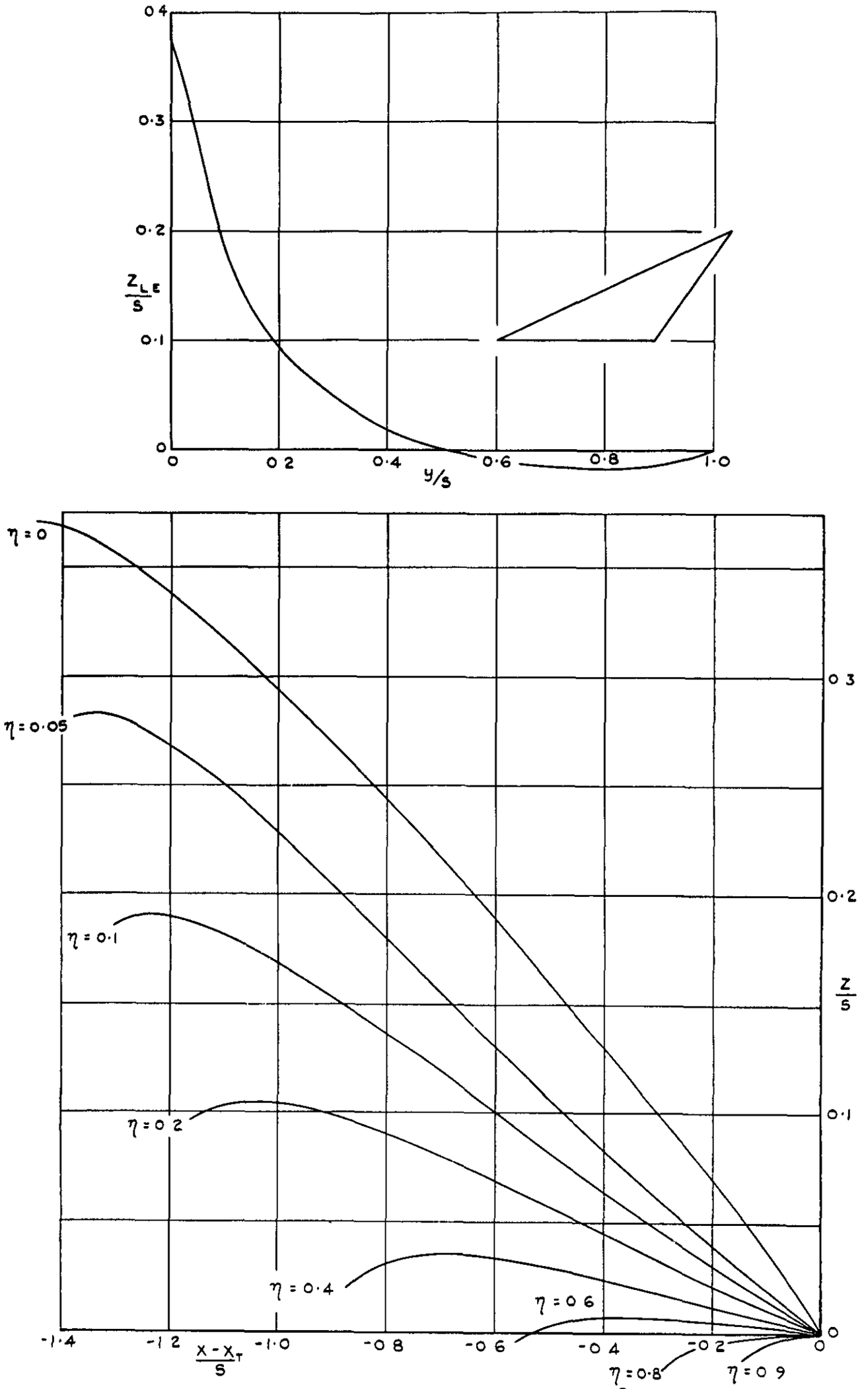

FIG. 27. WING 22. $A = 2 \cdot 75$, $\varphi_0 = 65^\circ$, $\varphi_1 = 35^\circ$;
$-\Delta C_p = 0 \cdot 5 - 0 \cdot 5\,\xi$; $M_0 = 1 \cdot 2$.

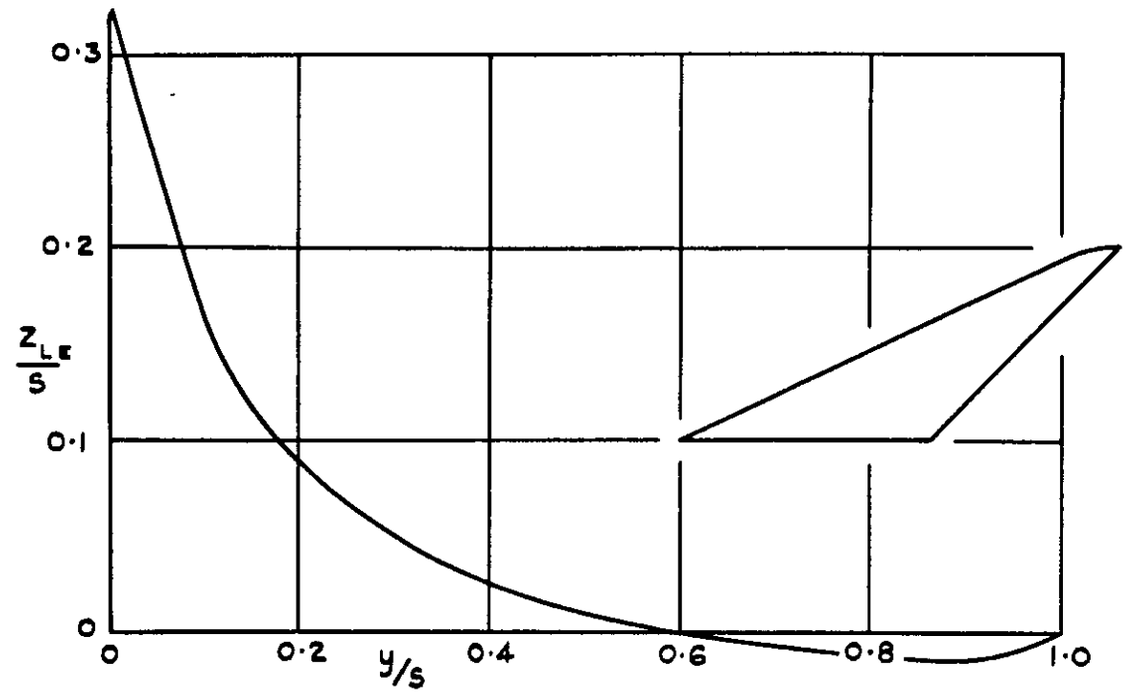

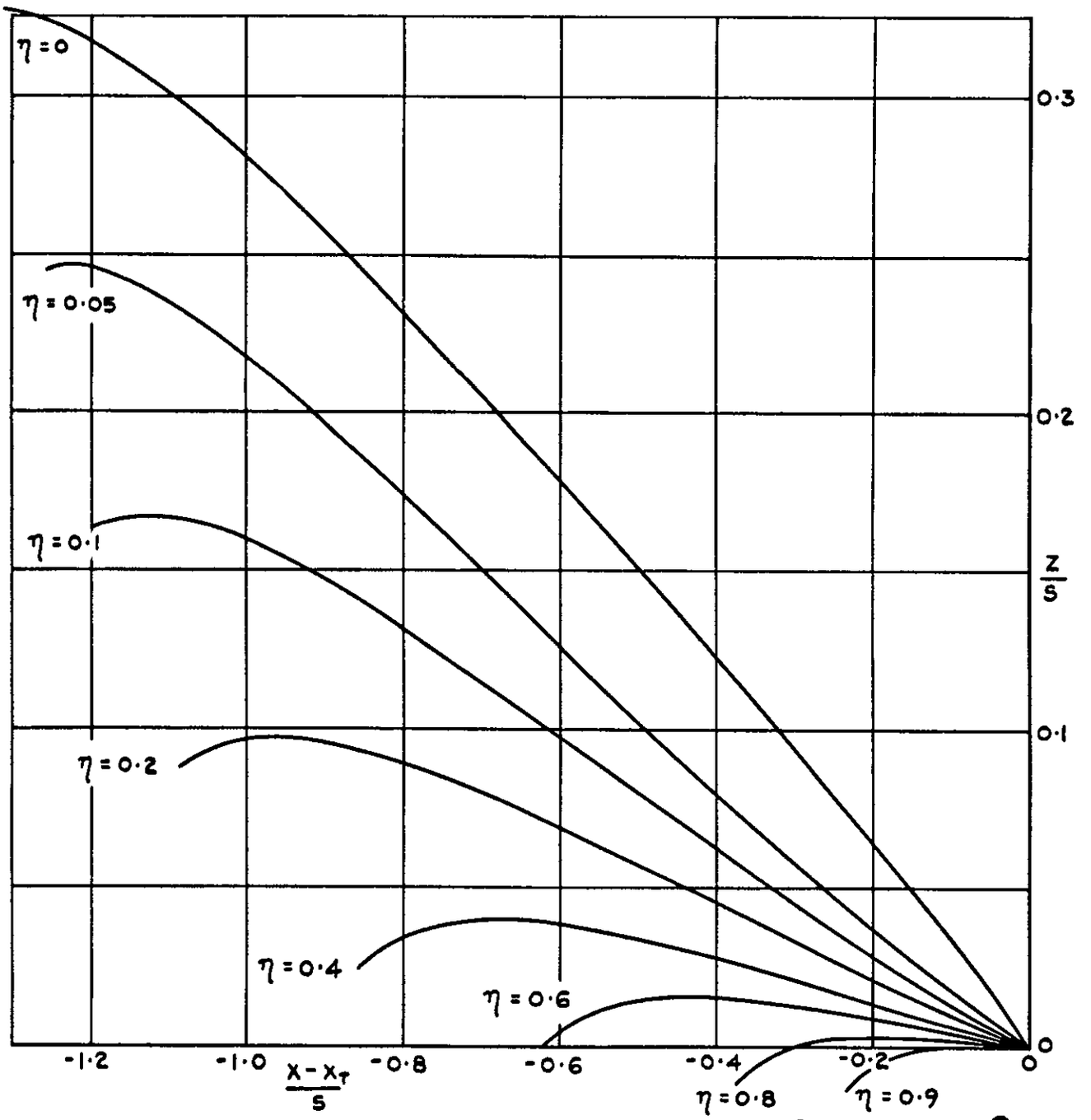

FIG. 28. WING 23. $A = 2{\cdot}75$, $\varphi_0 = 65^\circ$, $\varphi_1 = 45^\circ$; $-\Delta C_p = 0{\cdot}5 - 0{\cdot}5\,\xi$; $M_0 = 1{\cdot}2$.

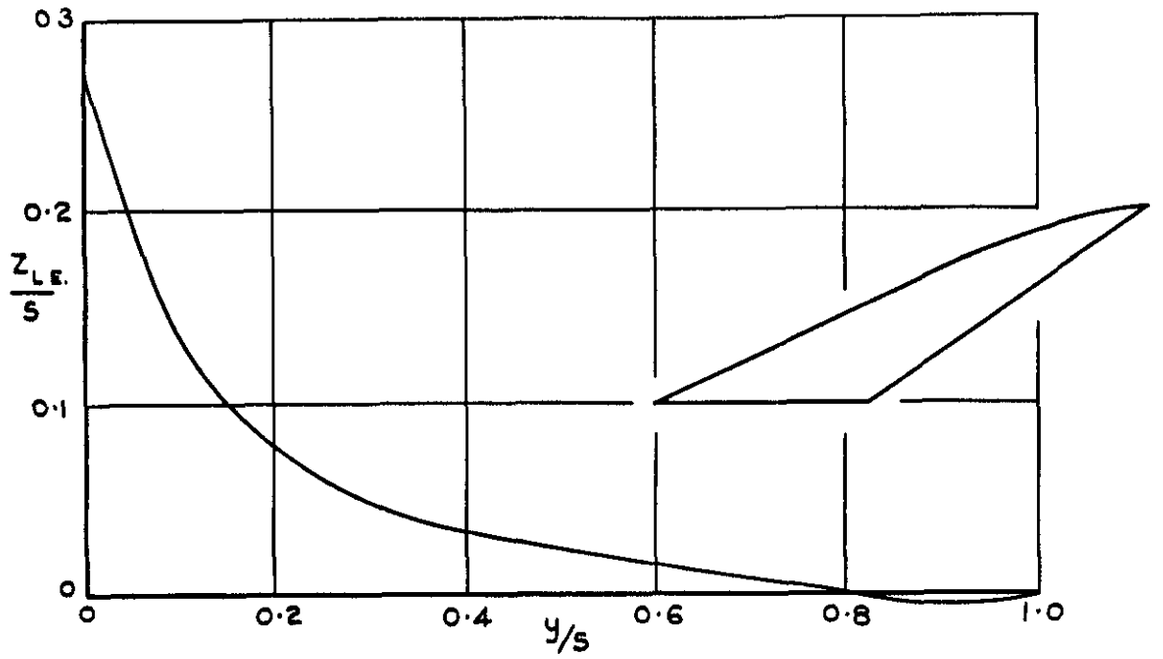

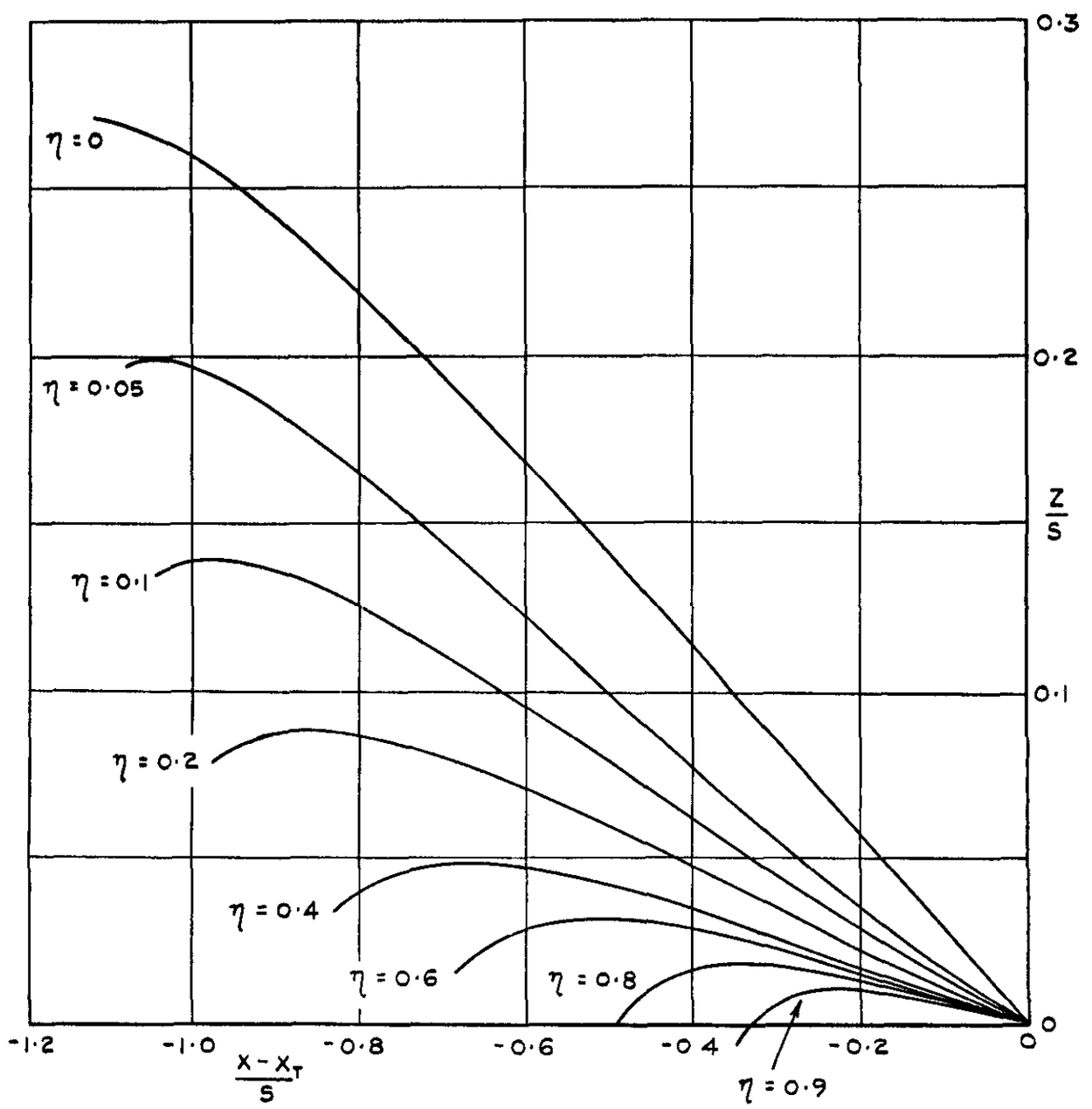

FIG. 29. WING 24. $A = 2{\cdot}75$, $\varphi_0 = 65^\circ$, $\varphi_1 = 55^\circ$; $-\Delta C_p = 0{\cdot}5 - 0{\cdot}5\,\xi$; $M_0 = 1{\cdot}2$.

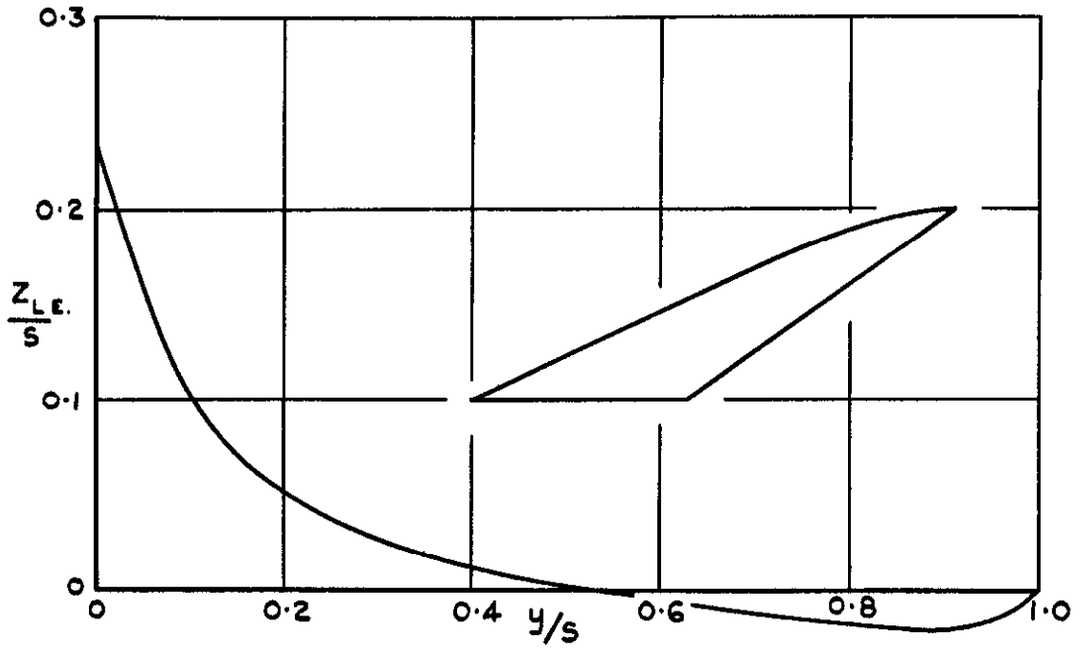

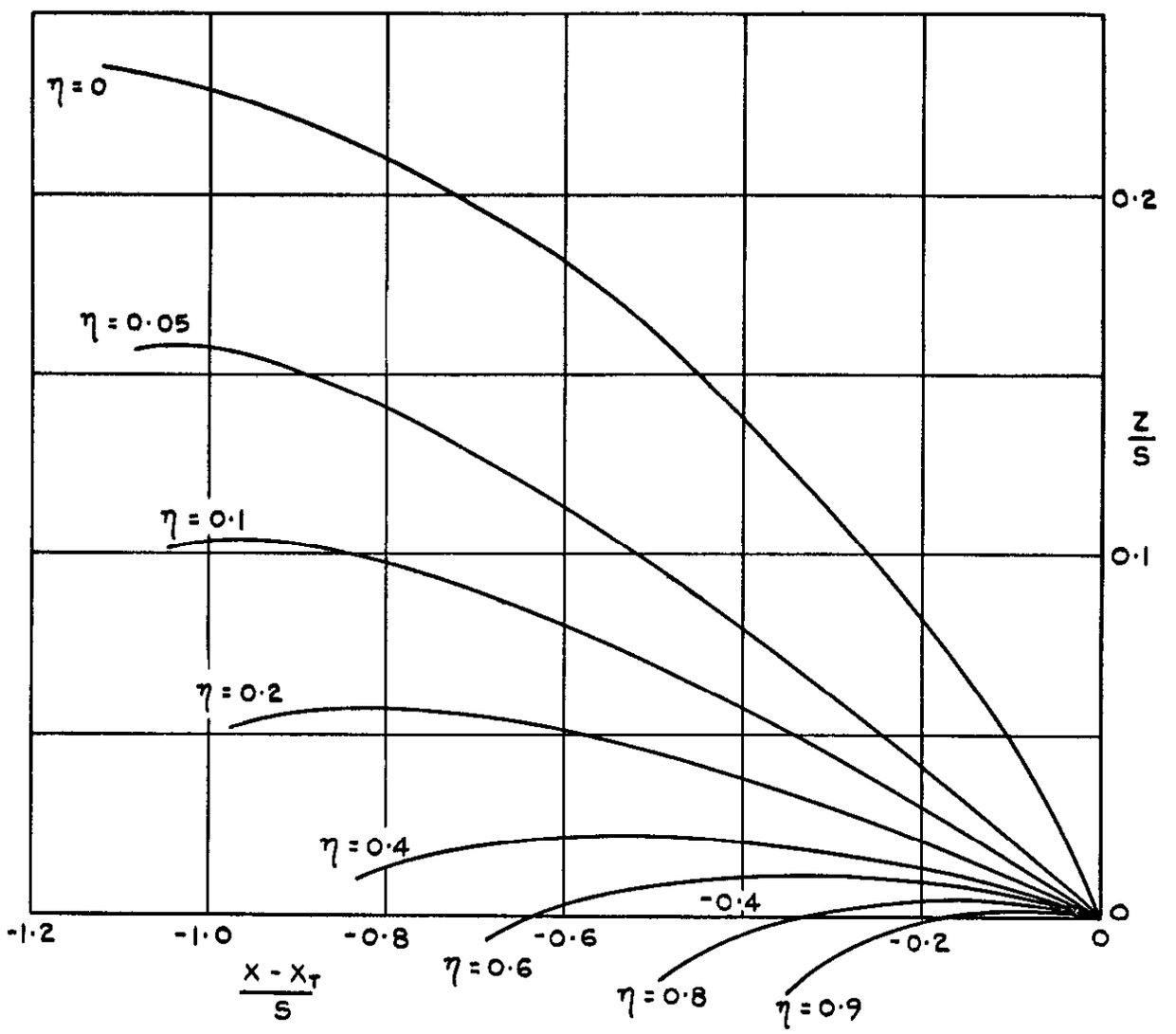

FIG. 30. WING 24. $A = 2 \cdot 75$, $\varphi_0 = 65^\circ$, $\varphi_1 = 55^\circ$; $-\Delta C_p = 0 \cdot 25$; $M_0 = 1 \cdot 2$.

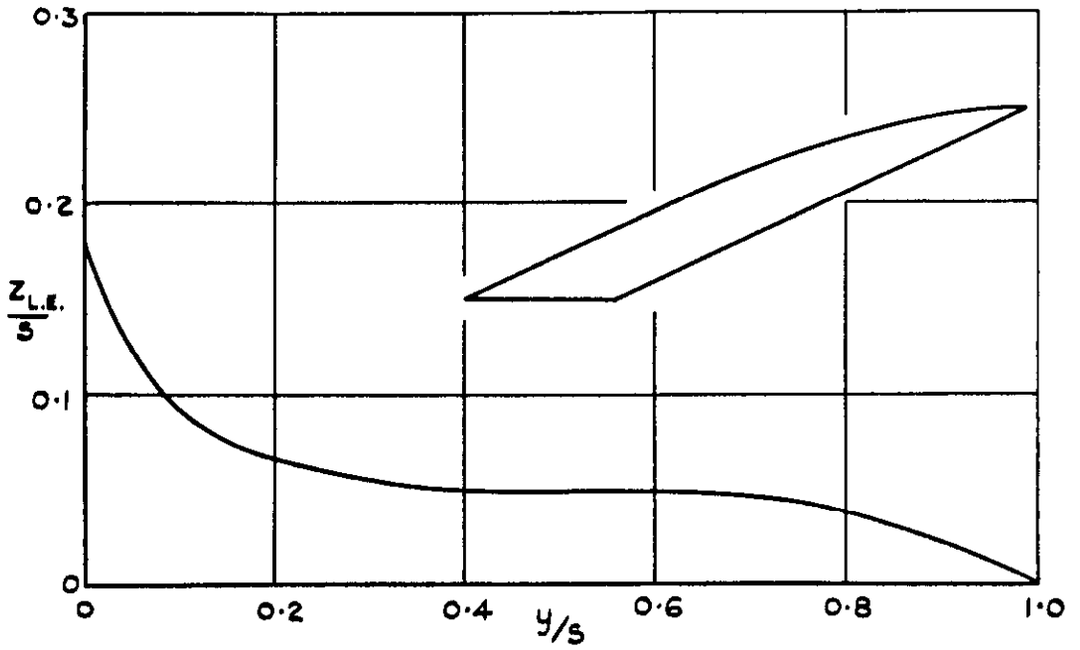

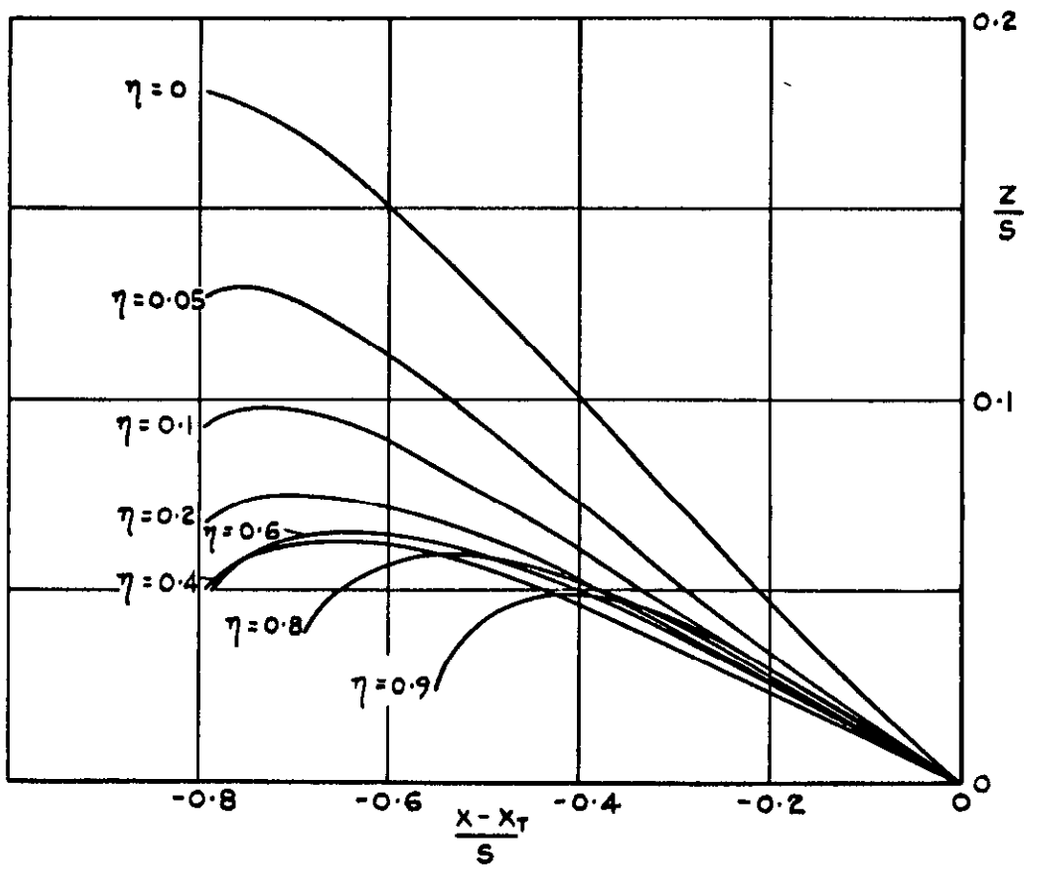

FIG. 31. WING 25. $A = 2{\cdot}75$, $\varphi_0 = 65^\circ$, $\varphi_1 = 65^\circ$; $-\Delta C_p = 0{\cdot}5 - 0{\cdot}5\,\xi$; $M_0 = 1{\cdot}2$.

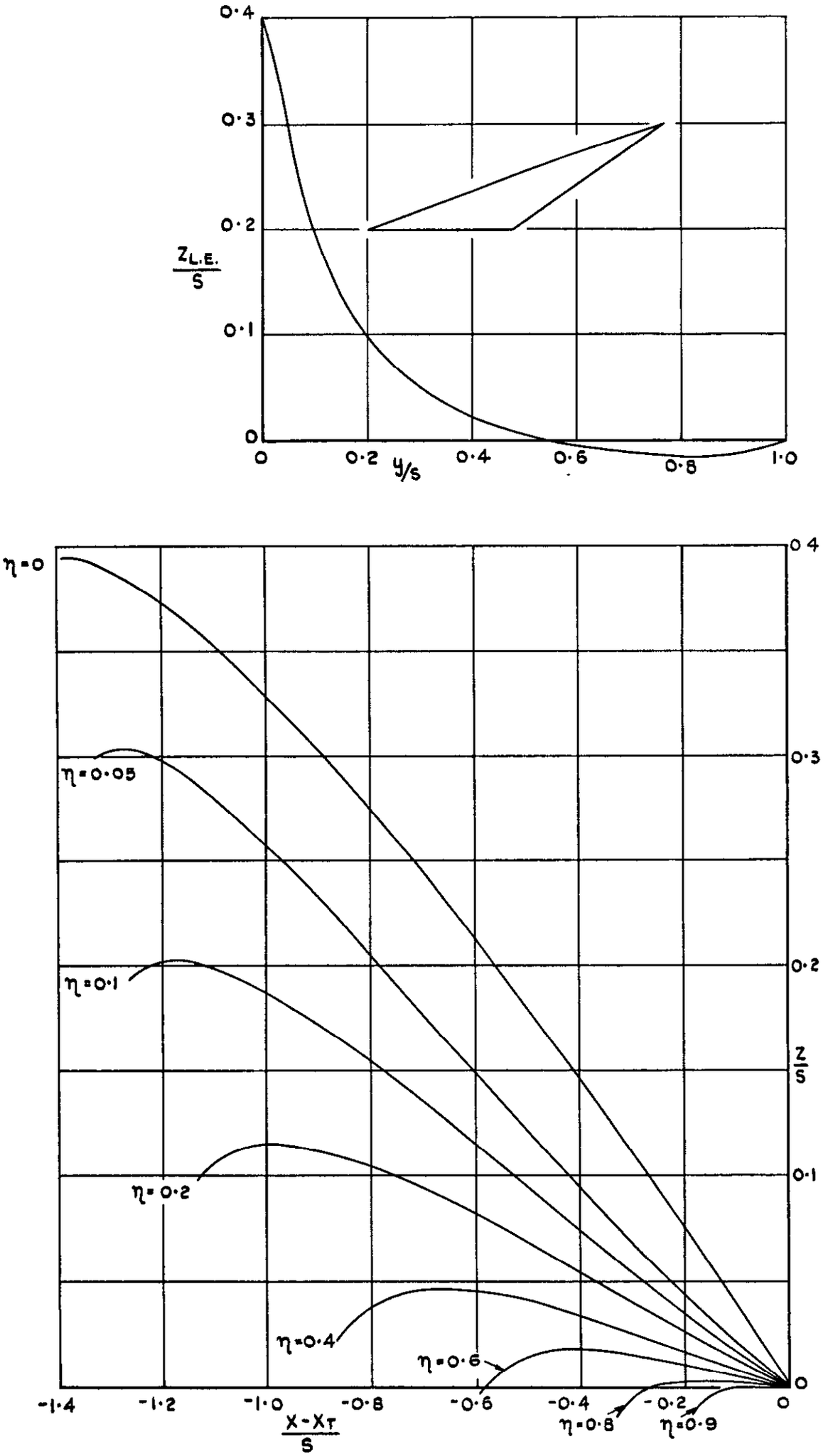

FIG.32. WING 26. $A = 2{\cdot}75$, $\varphi_0 = 70^\circ$, $\varphi_1 = 55^\circ$;
$-\Delta C_p = 0{\cdot}5 - 0{\cdot}5\,\xi$; $M_0 = 1{\cdot}2$.

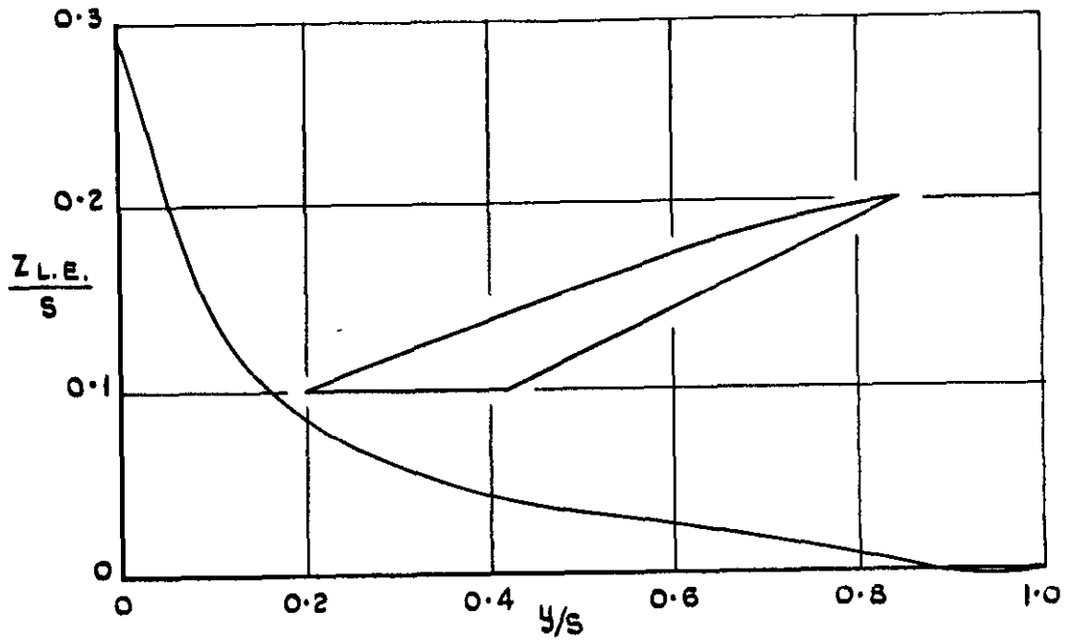

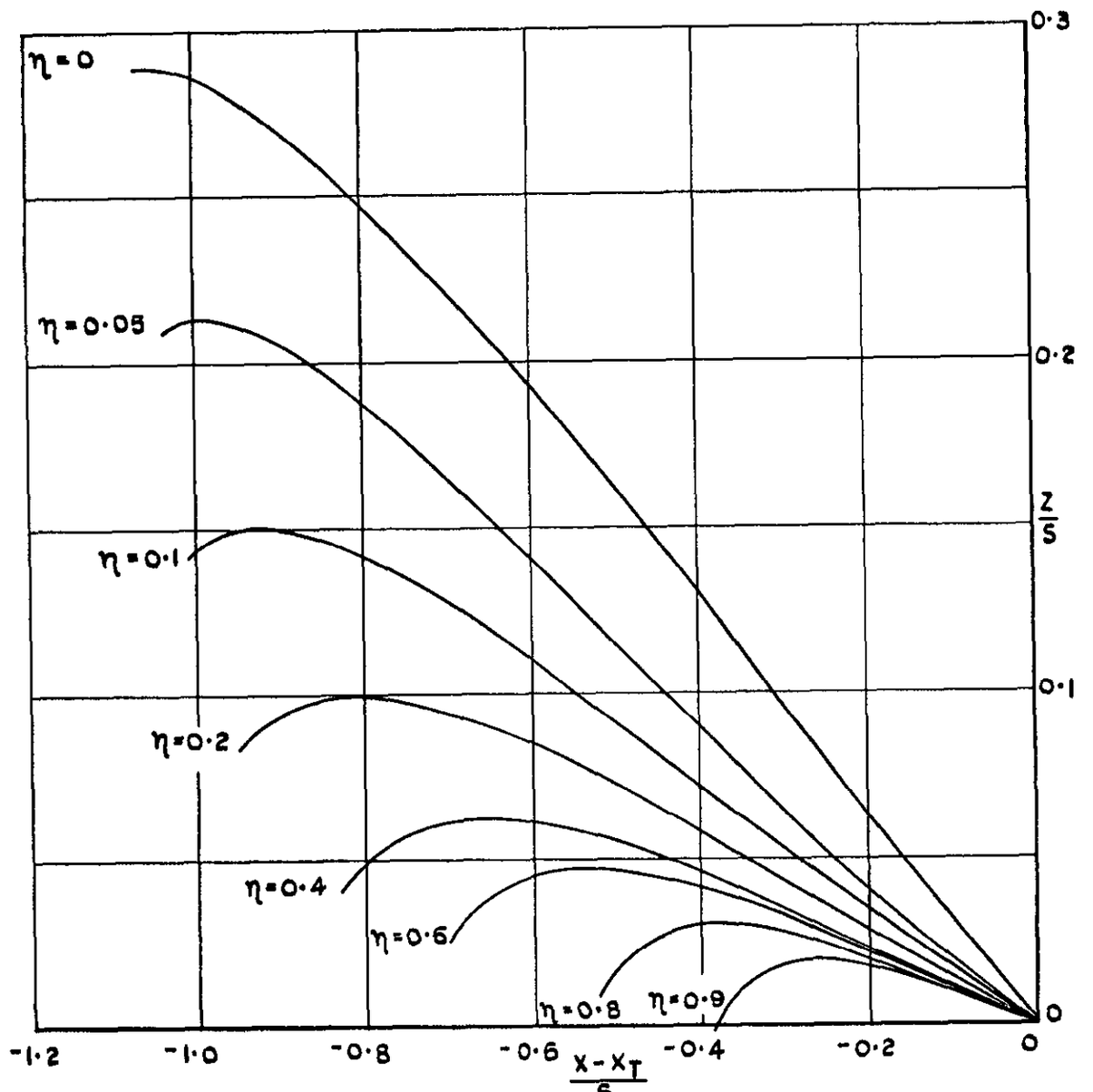

FIG.33. WING 27. $A=2{\cdot}75$, $\varphi_0=70°$, $\varphi_1=65°$;
$-\Delta C_p = 0{\cdot}5 - 0{\cdot}5\xi$; $M_0 = 1{\cdot}2$.

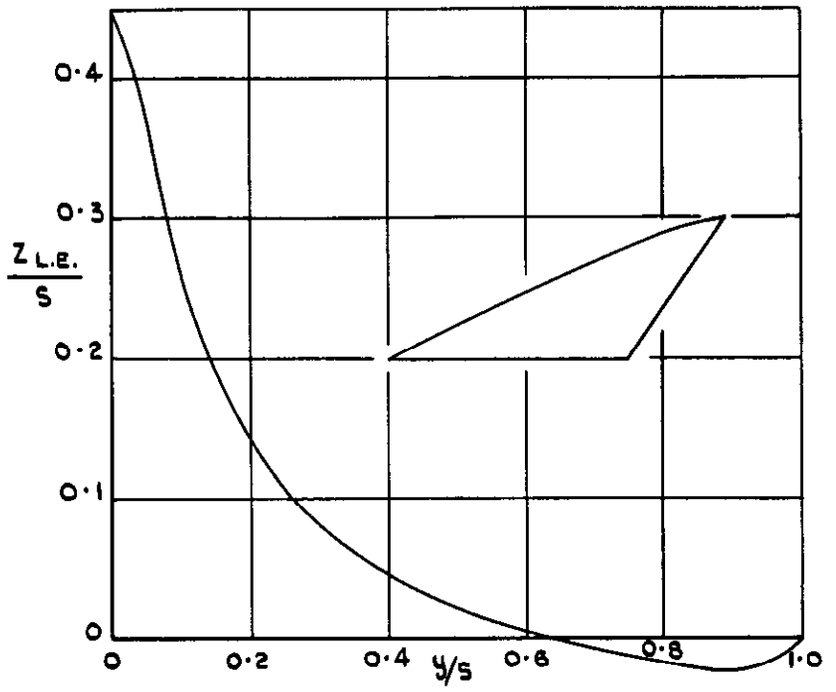

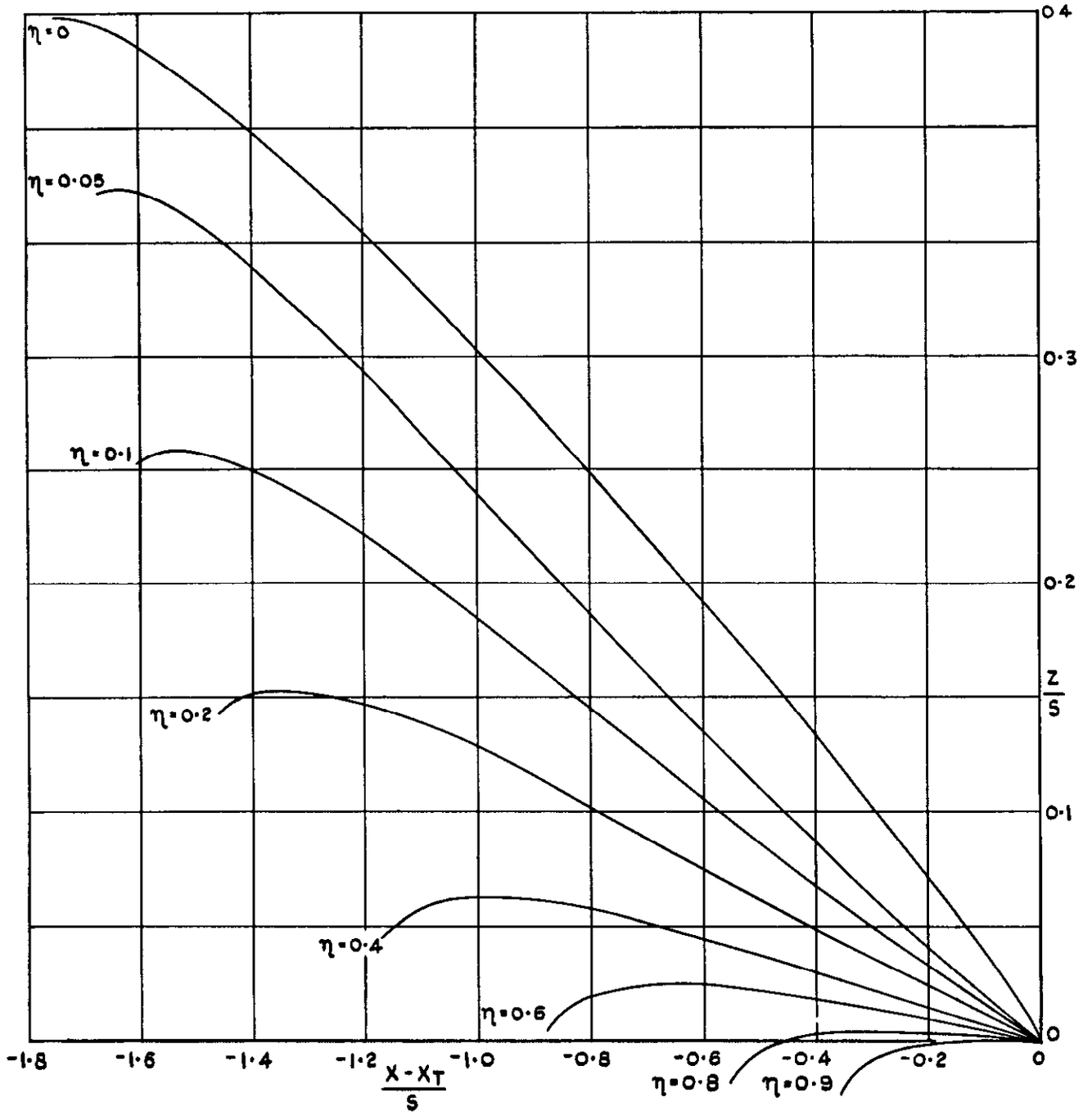

FIG. 34. WING 28. $A = 2{\cdot}0$, $\varphi_0 = 65^\circ$, $\varphi_1 = 35^\circ$; $-\Delta C_p = 0{\cdot}5 - 0{\cdot}5\,\xi$; $M_0 = 1{\cdot}2$.

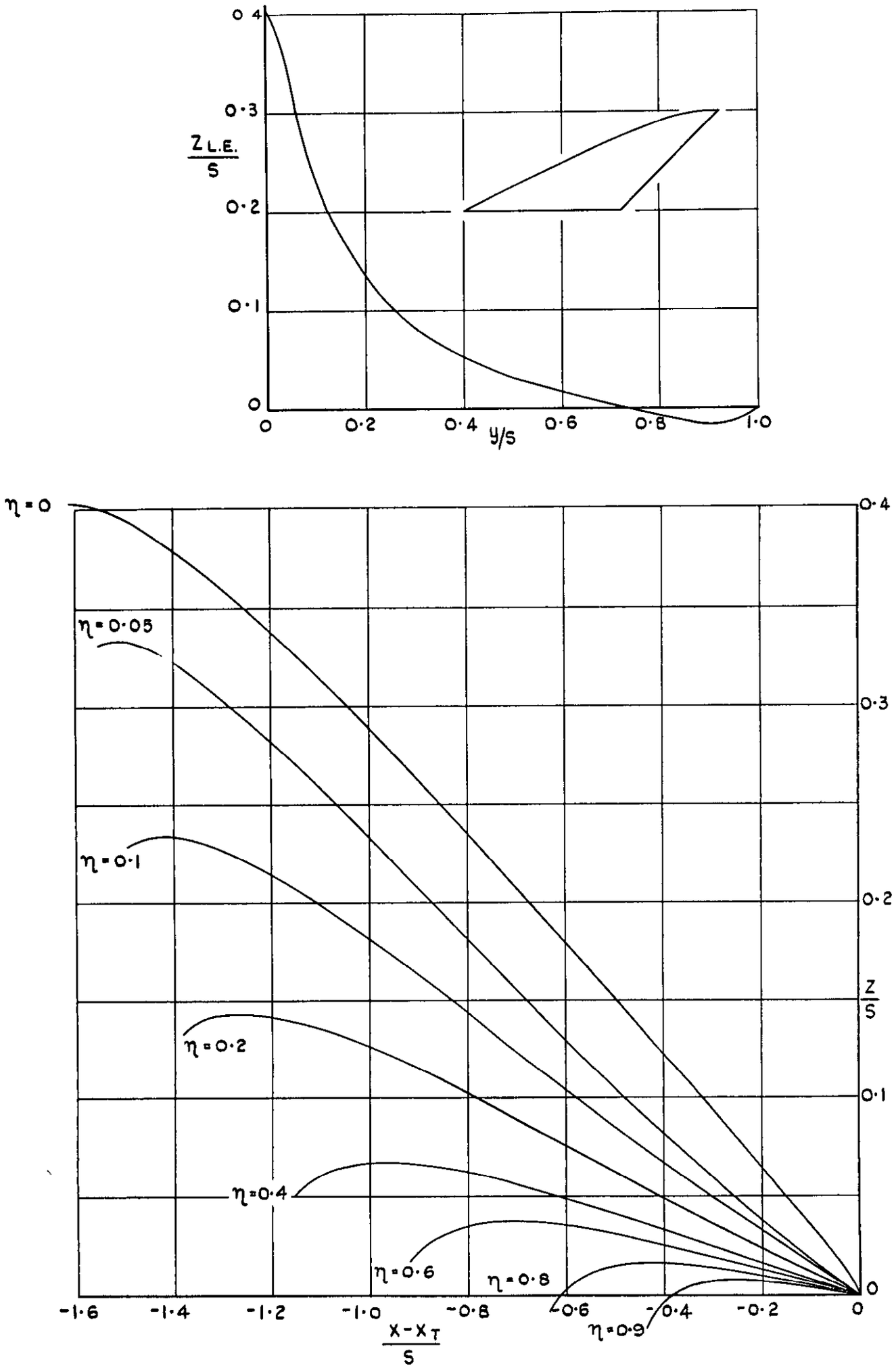

FIG.35. WING 29. $A = 2$, $\varphi_0 = 65^\circ$, $\varphi_1 = 45^\circ$;
$-\Delta C_p = 0{\cdot}5 - 0{\cdot}5\,\xi$; $M_0 = 1{\cdot}2$.

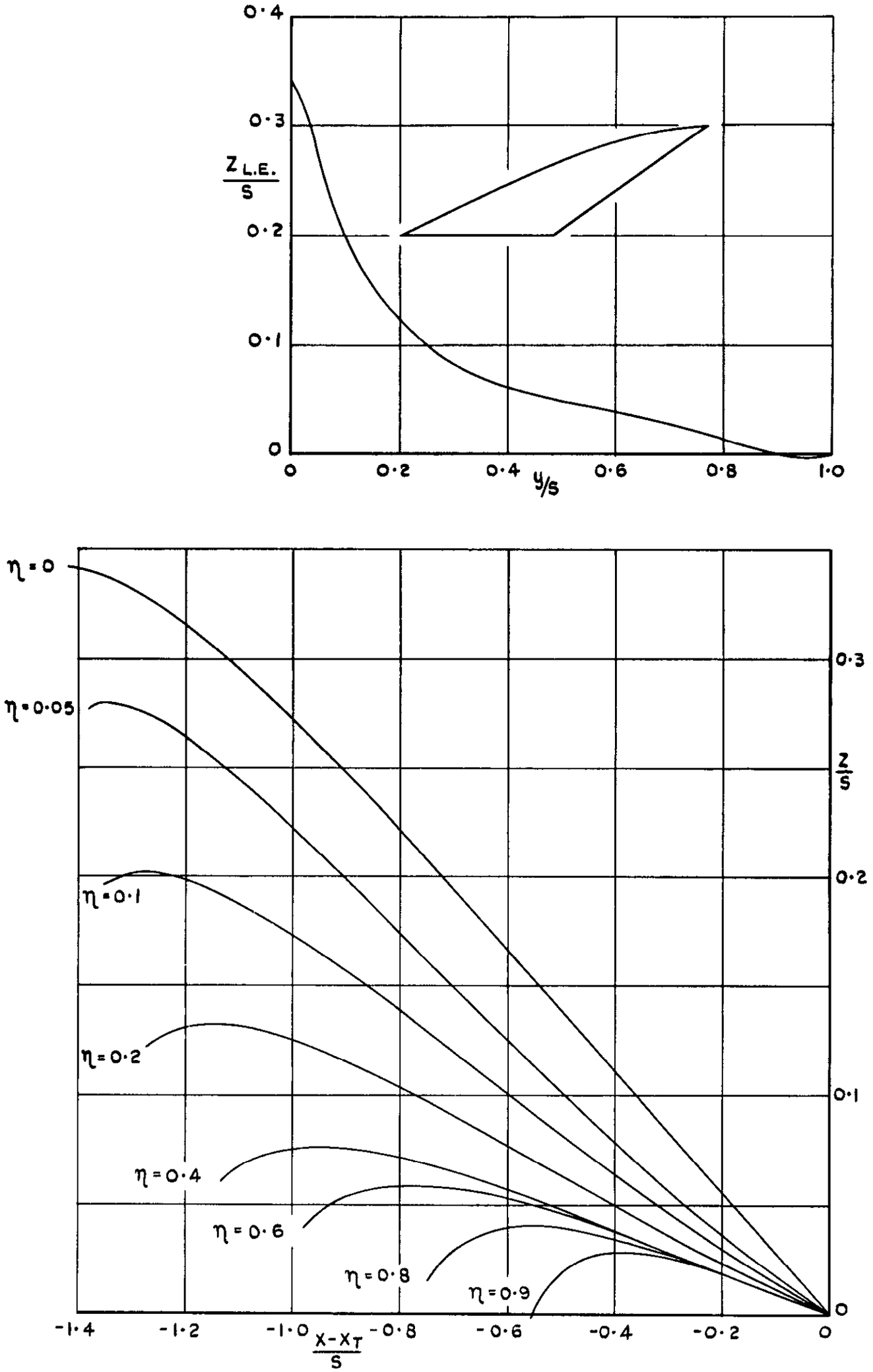

FIG.36. WING 30. $A = 2·0$, $\varphi_0 = 65°$, $\varphi_1 = 55°$;
$-\Delta C_p = 0·5 - 0·5\xi$; $M_0 = 1·2$.

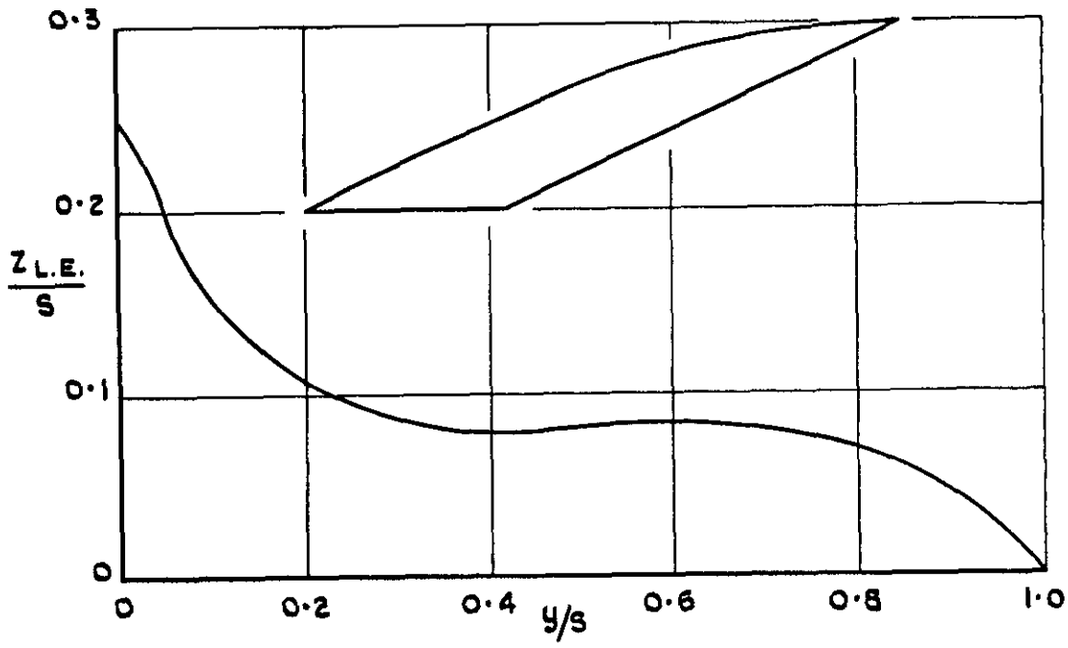

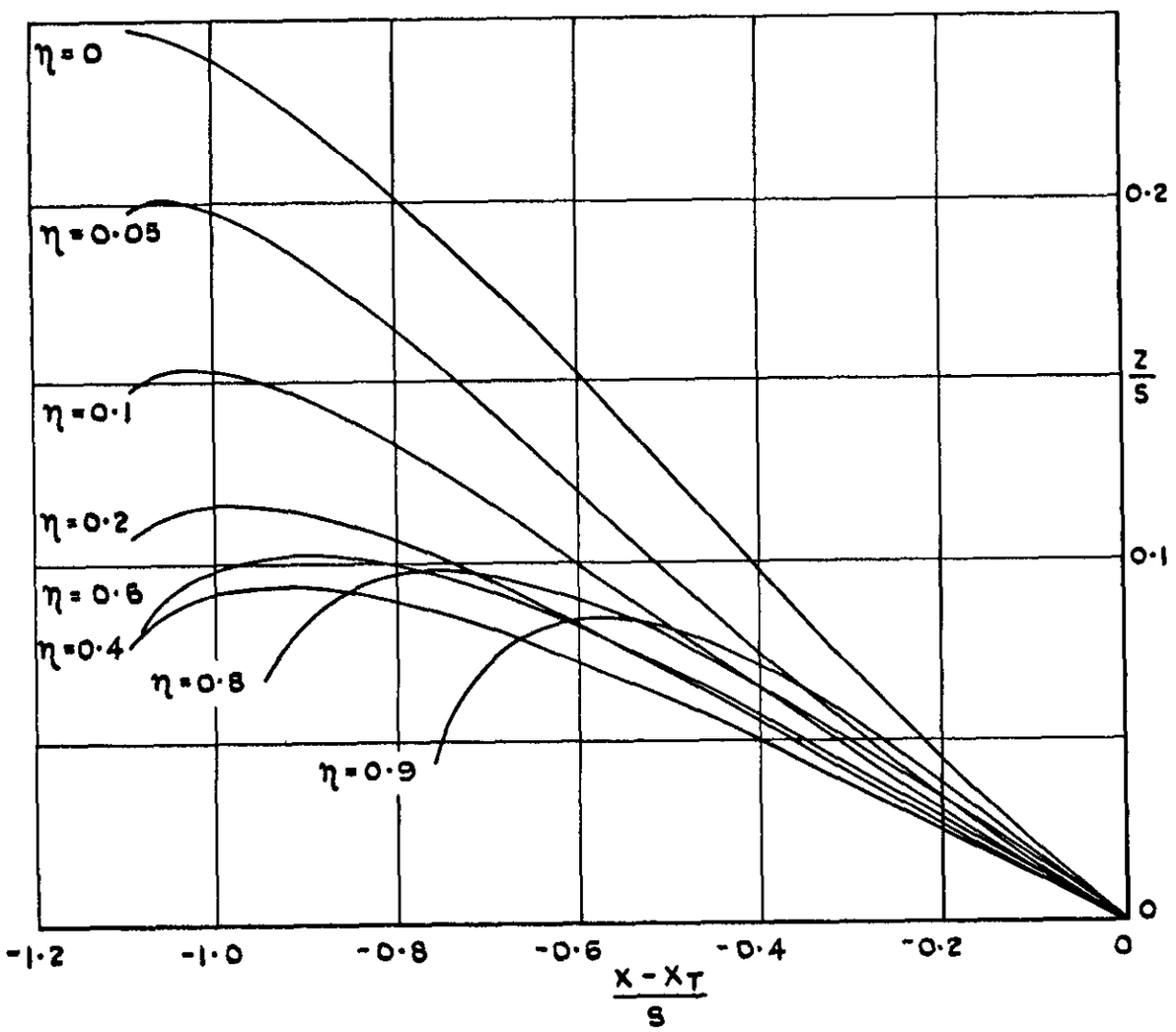

FIG.37. WING 31. $A = 2{\cdot}0$, $\varphi_0 = 65^\circ$, $\varphi_1 = 65^\circ$; $-\Delta C_p = 0{\cdot}5 - 0{\cdot}5\xi$; $M_0 = 1{\cdot}2$.

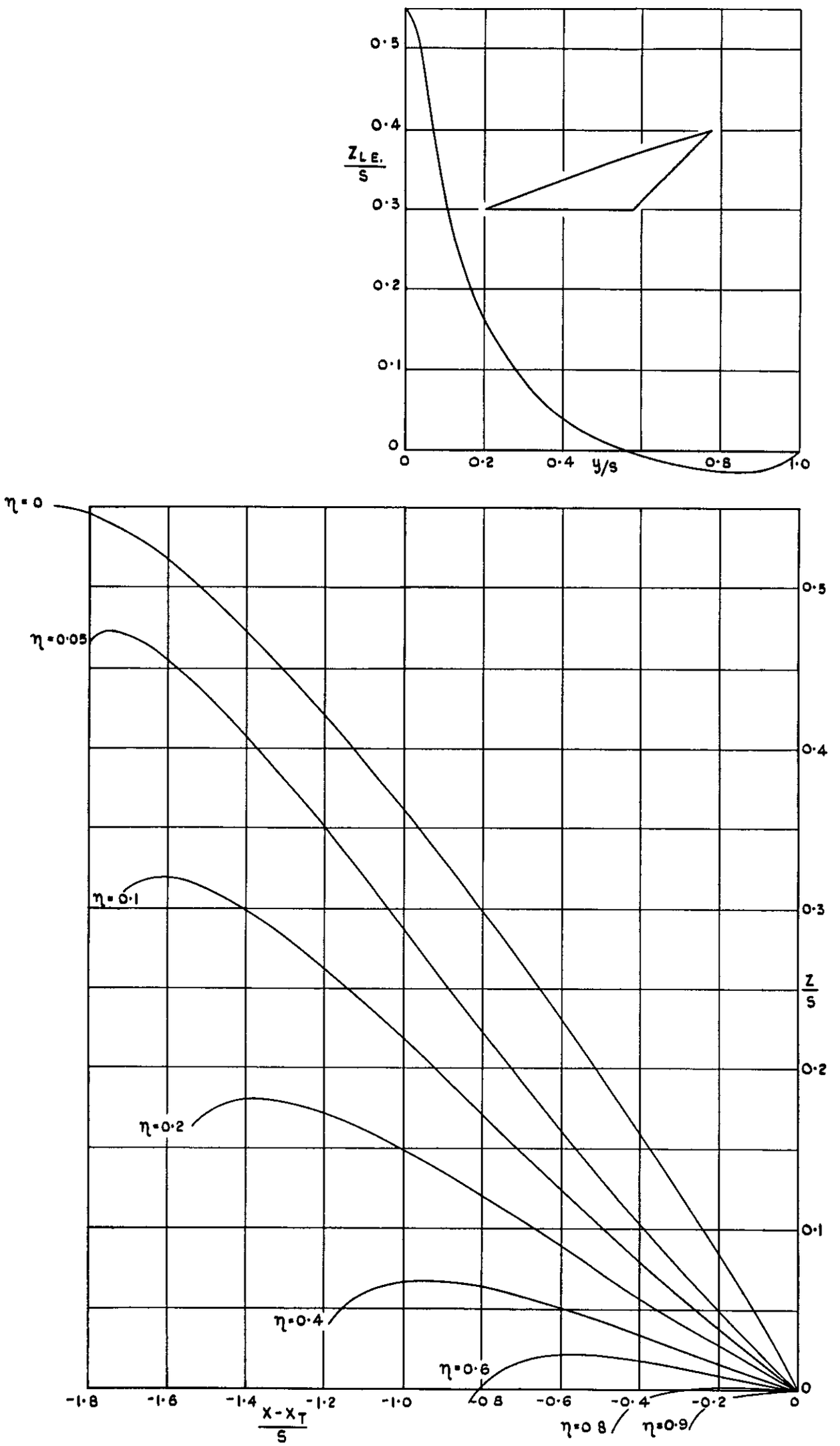

FIG. 38. WING 32. $A = 2{\cdot}0$, $\varphi_0 = 70°$, $\varphi_1 = 45°$;
$-\Delta C_p = 0{\cdot}5 - 0{\cdot}5\xi$; $M_0 = 1{\cdot}2$.

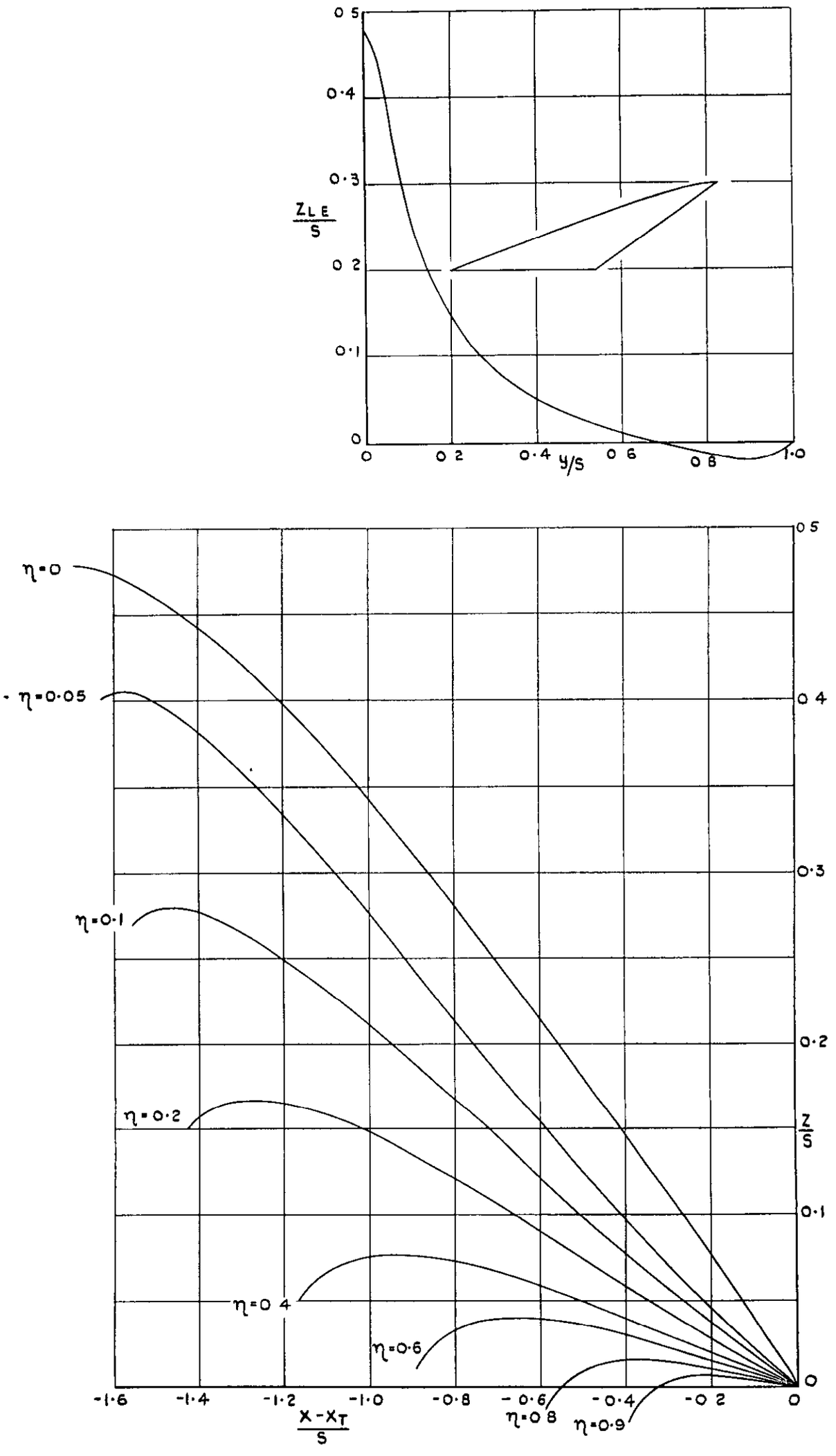

FIG.39. WING 33. $A = 2{\cdot}0$, $\varphi_0 = 70^\circ$, $\varphi_1 = 55^\circ$;
$-\Delta C_p = 0{\cdot}5 - 0{\cdot}5\,\xi$; $M_0 = 1{\cdot}2$.

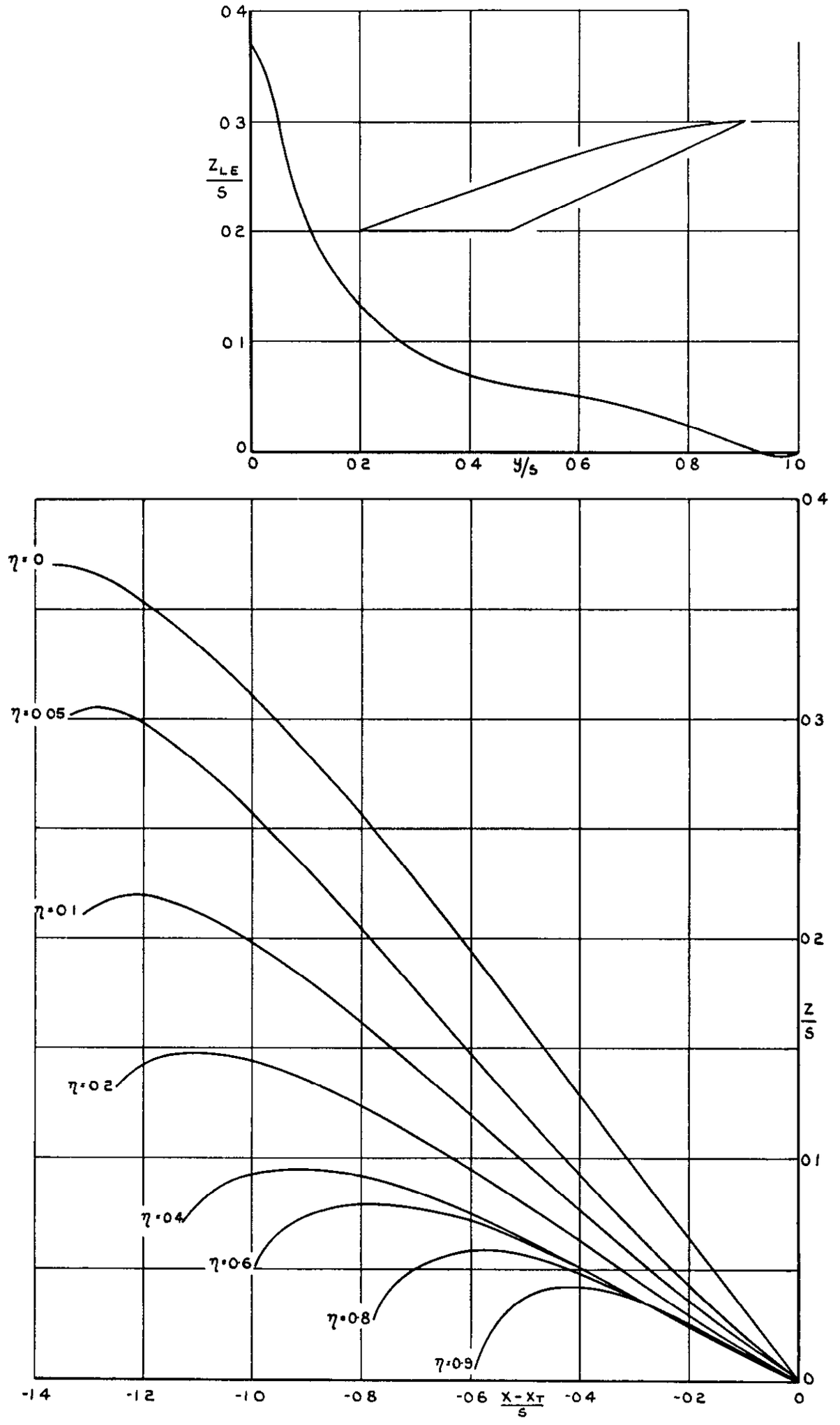

FIG. 40. WING 34. A=2·0, $\varphi_0 = 70°$, $\varphi_1 = 65°$;
$-\Delta C_p = 0{\cdot}5 - 0{\cdot}5\,\zeta$; $M_0 = 1{\cdot}2$.

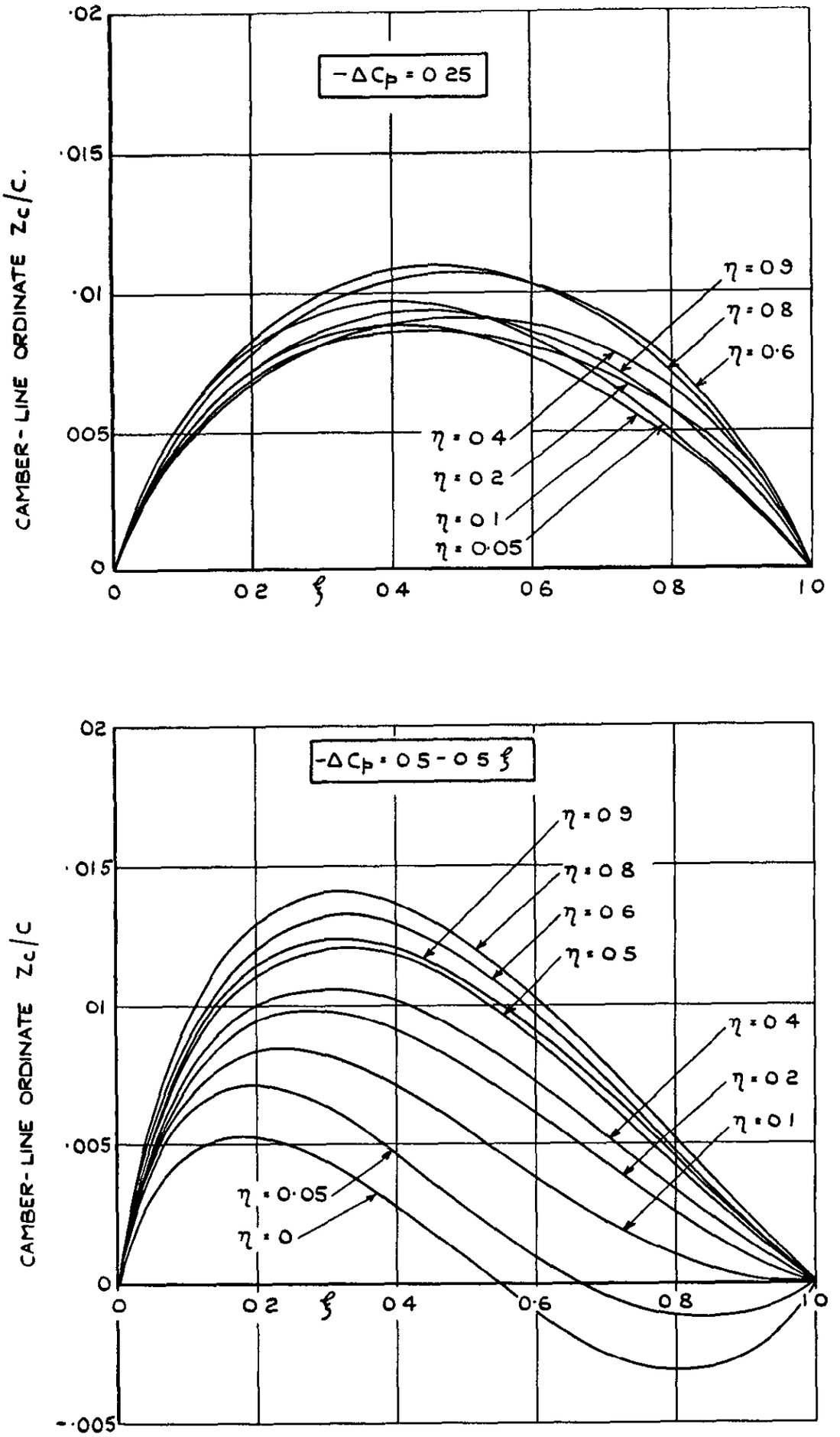

FIG. 42. WING 3. CAMBER-LINES FOR DIFFERENT LOADINGS.

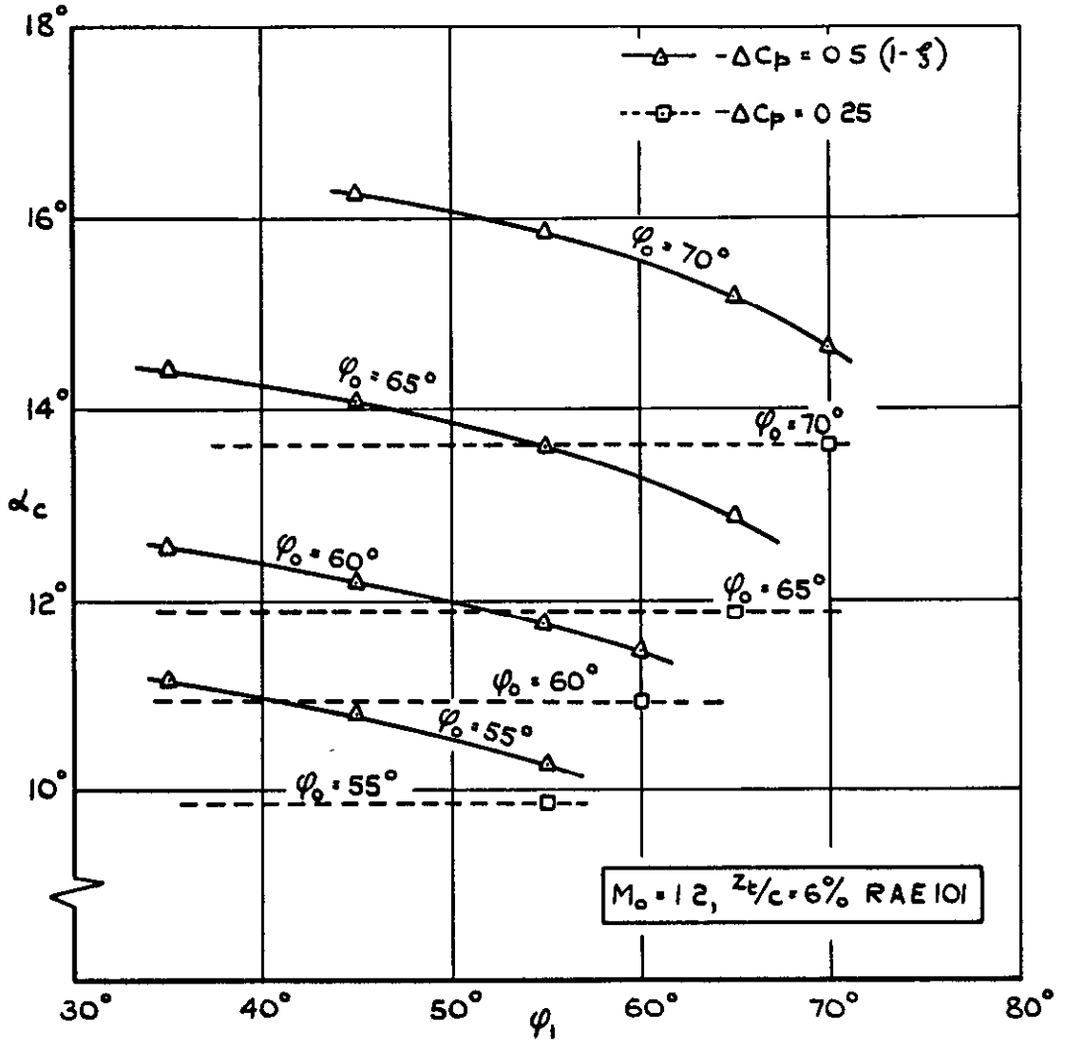

(a) VARIATION WITH WING SWEEP AND CHORDWISE LOADING.

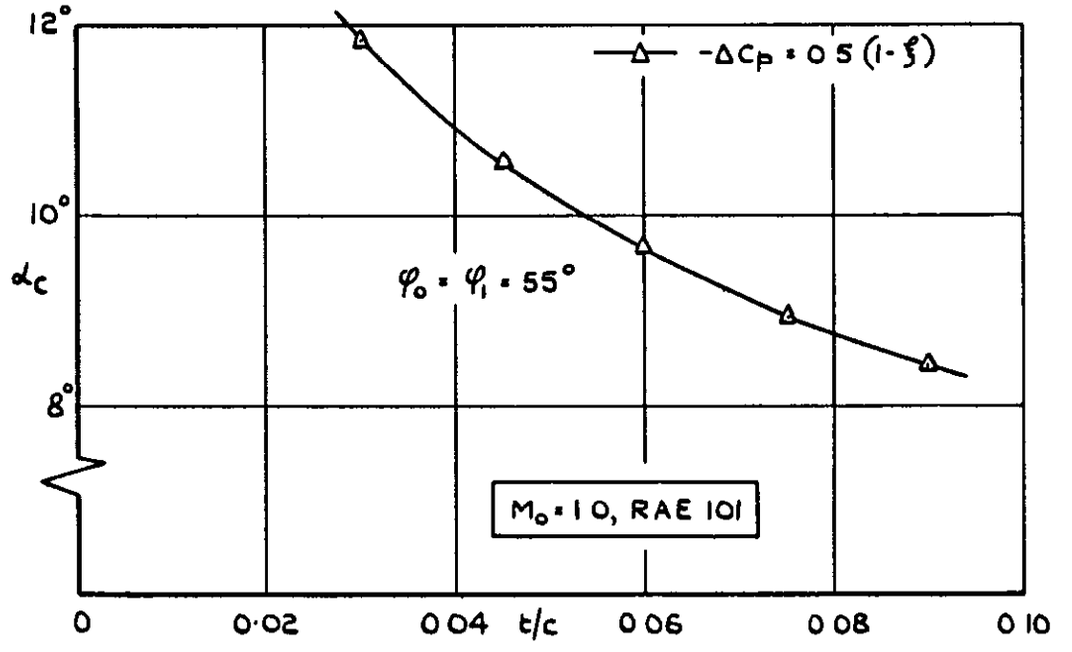

(b) VARIATION WITH WING THICKNESS.

FIG. 41.(a & b) CENTRE-LINE INCIDENCE.

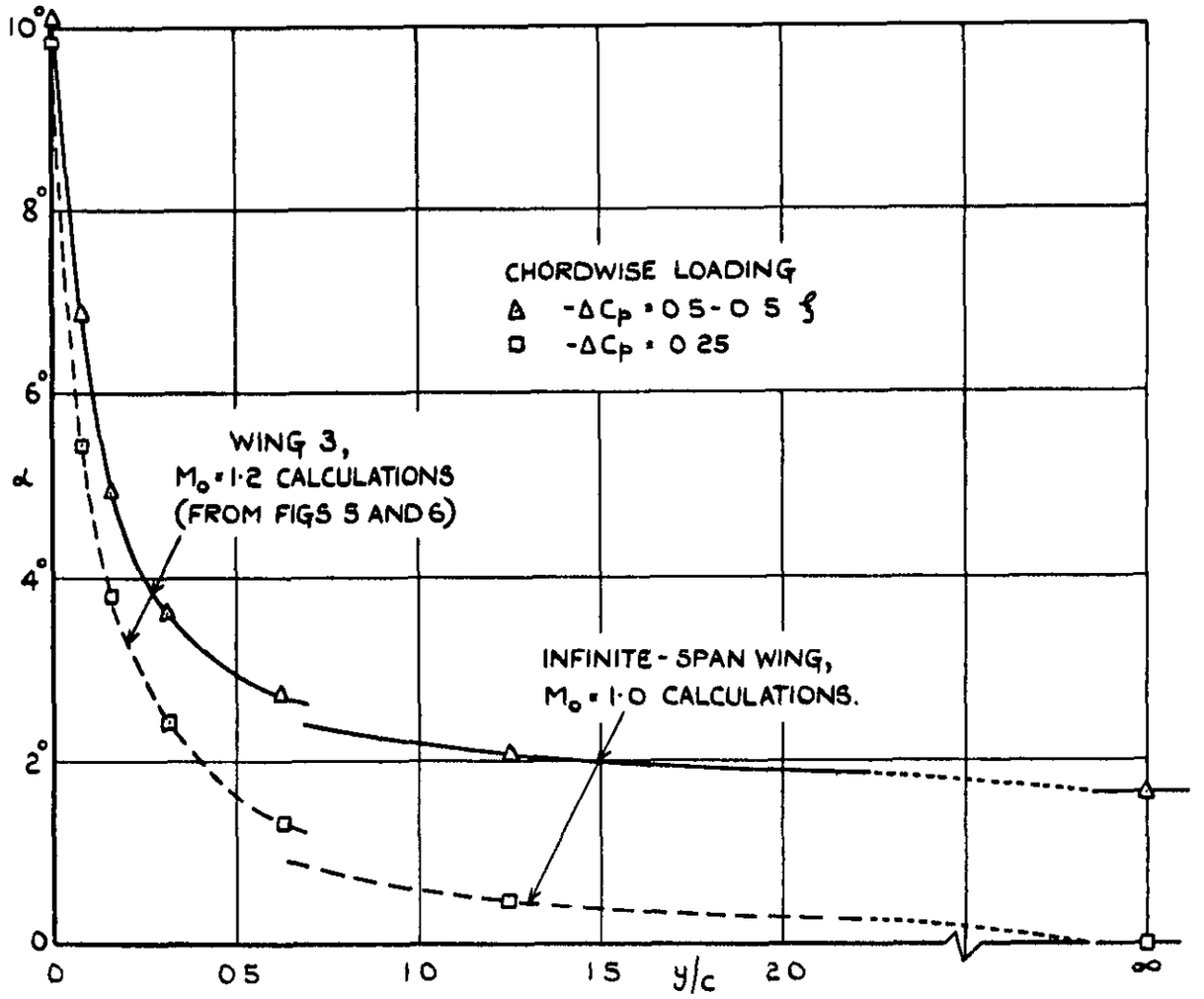

FIG. 43. SPANWISE VARIATION OF TWIST FOR DIFFERENT LOADINGS ON WINGS WITH $\varphi_0 = \varphi_1 = 55°$.

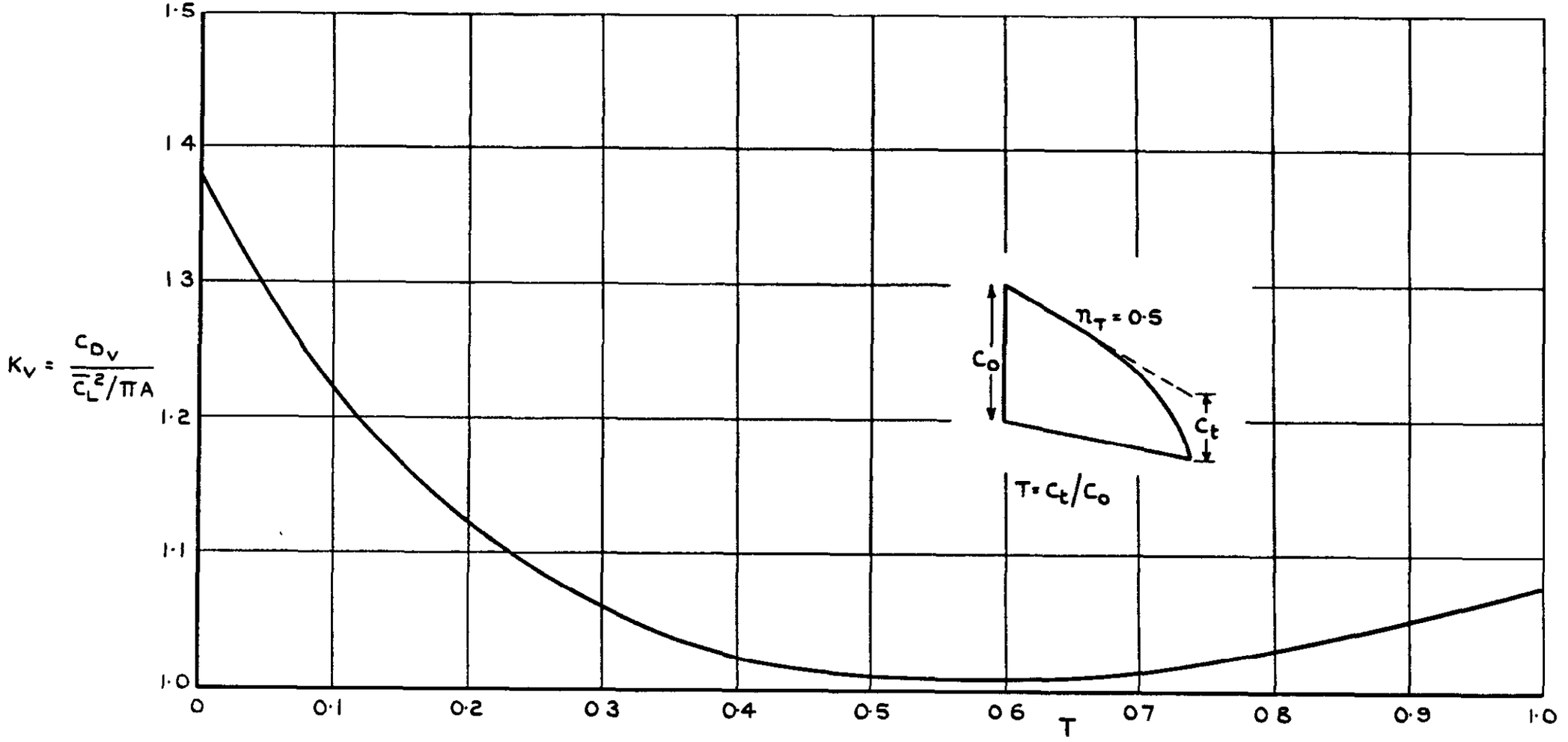

FIG. 44. VORTEX DRAG FOR WINGS IN FIG. 2, CAMBERED TO HAVE CONSTANT C_L ACROSS SPAN.

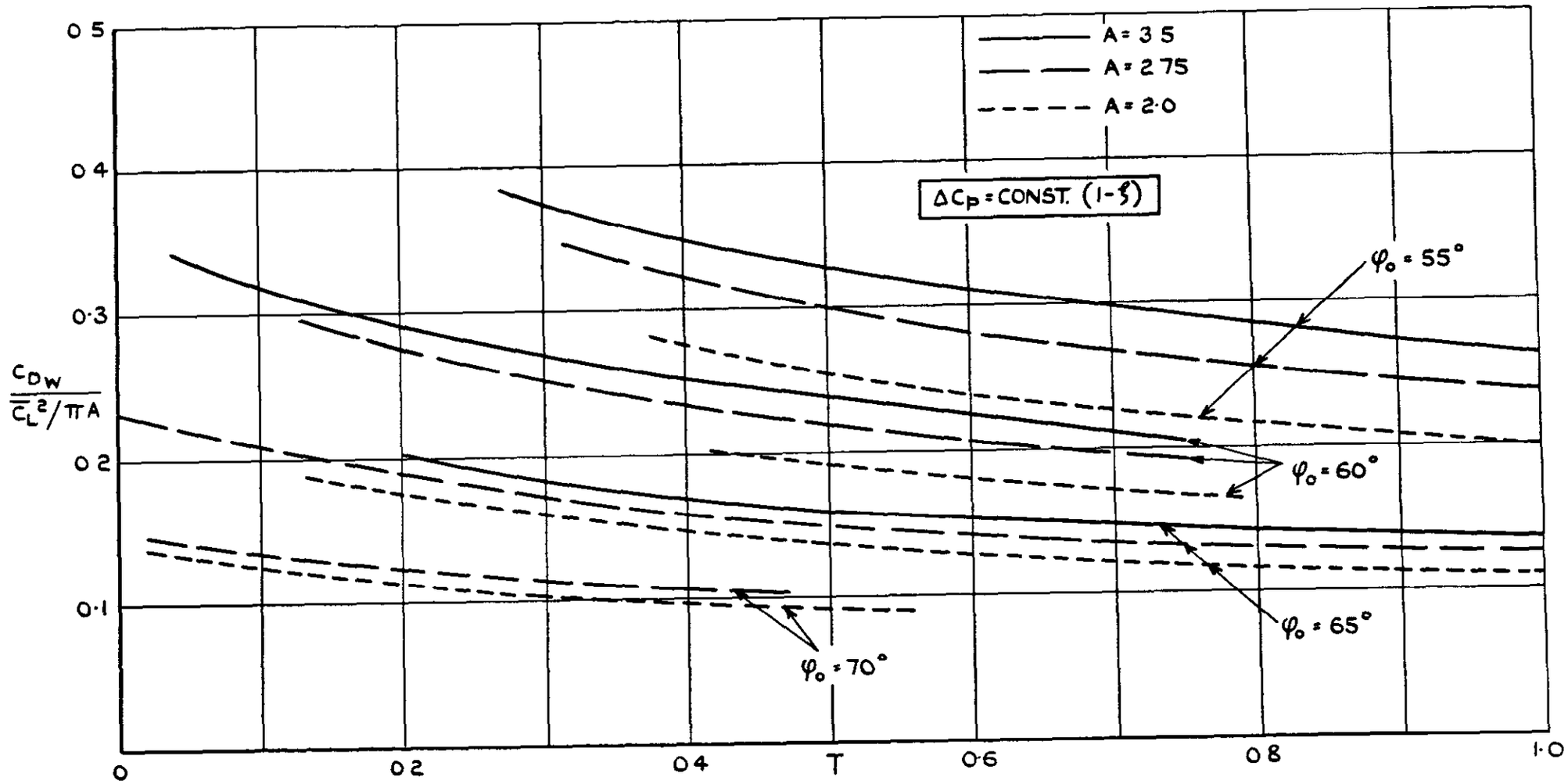

FIG. 45 (a) LIFT-DEPENDENT WAVE DRAG AT $M_0 = 1{\cdot}2$ FOR WINGS IN FIG. 2, CAMBERED TO HAVE CONSTANT C_L ACROSS SPAN AND TRIANGULAR CHORDWISE LOAD DISTRIBUTION.

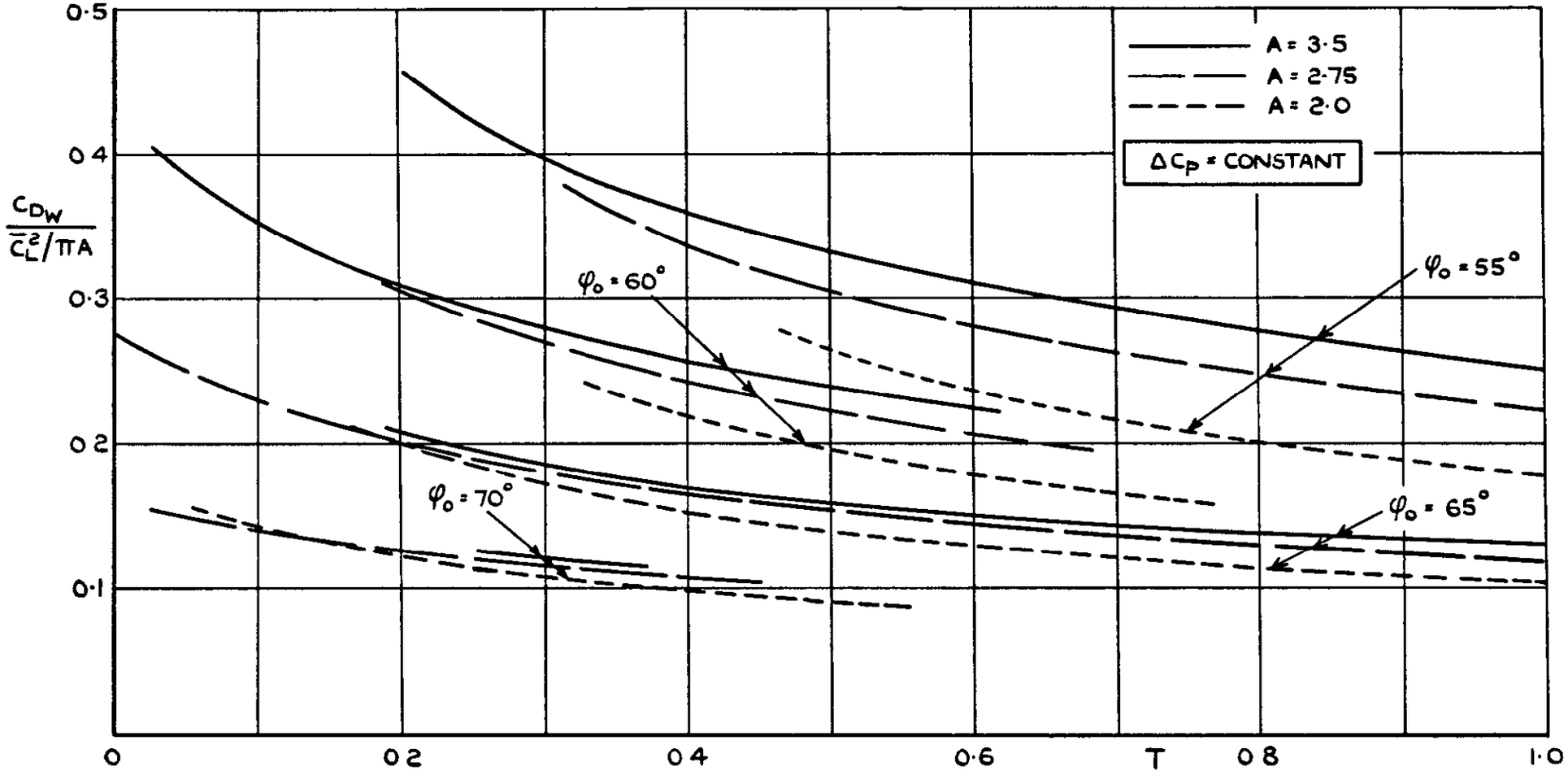

FIG. 45 (b) LIFT-DEPENDENT WAVE DRAG AT $M_o = 1{\cdot}2$ FOR WINGS IN FIG. 2, CAMBERED TO HAVE CONSTANT ΔC_p OVER WHOLE WING.

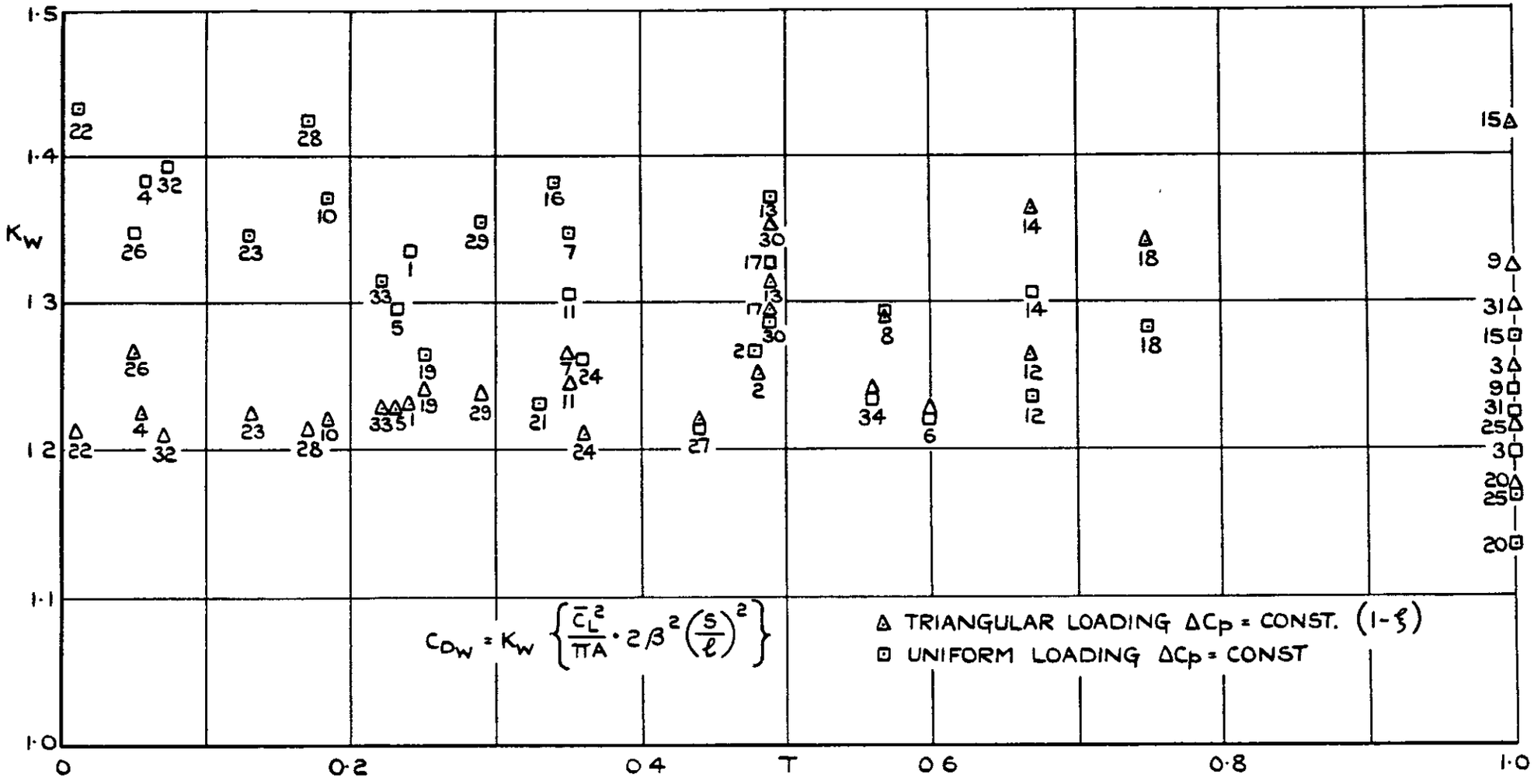

FIG. 46. LIFT-DEPENDENT WAVE DRAG FOR WINGS IN FIG. 2, CAMBERED TO HAVE CONSTANT C_L ACROSS SPAN.

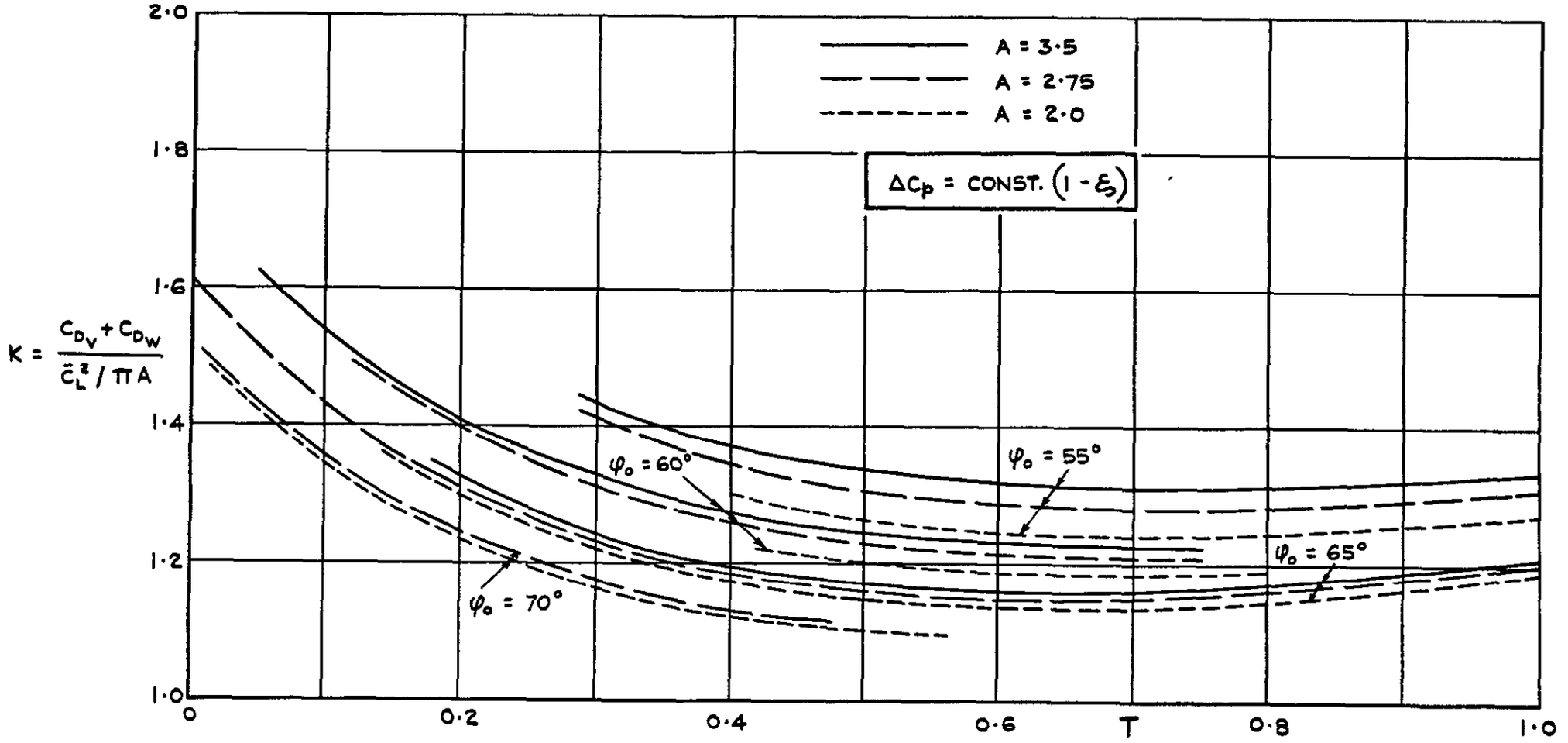

FIG. 47(a) TOTAL LIFT-DEPENDENT DRAG AT $M_o = 1·2$ FOR WINGS IN FIG. 2, CAMBERED TO HAVE CONSTANT C_L ACROSS SPAN AND TRIANGULAR CHORDWISE LOADINGS.

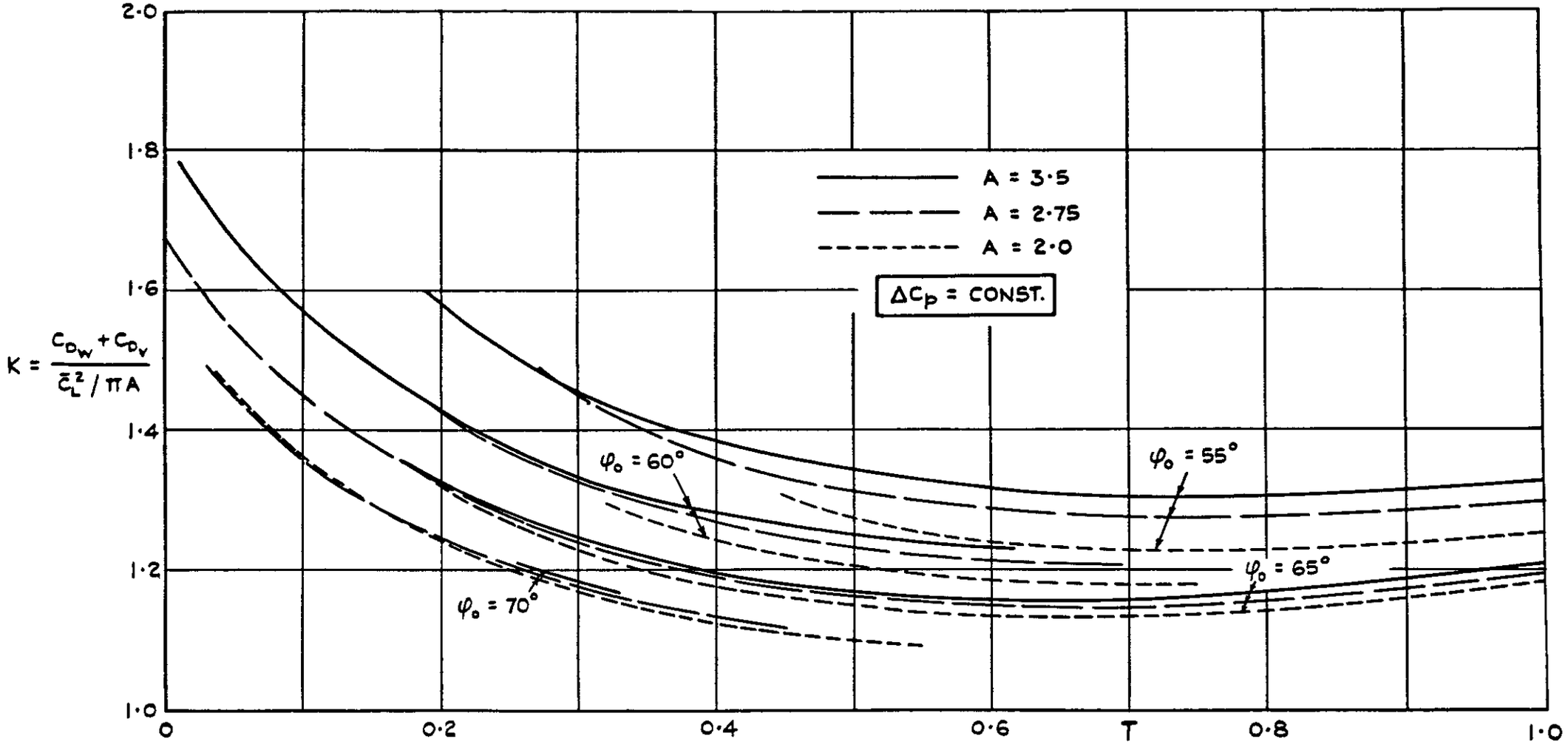

FIG. 47 (b) TOTAL LIFT - DEPENDENT DRAG AT $M_o = 1{\cdot}2$ FOR WINGS IN FIG. 2, CAMBERED TO HAVE CONSTANT ΔC_p OVER WHOLE WING.

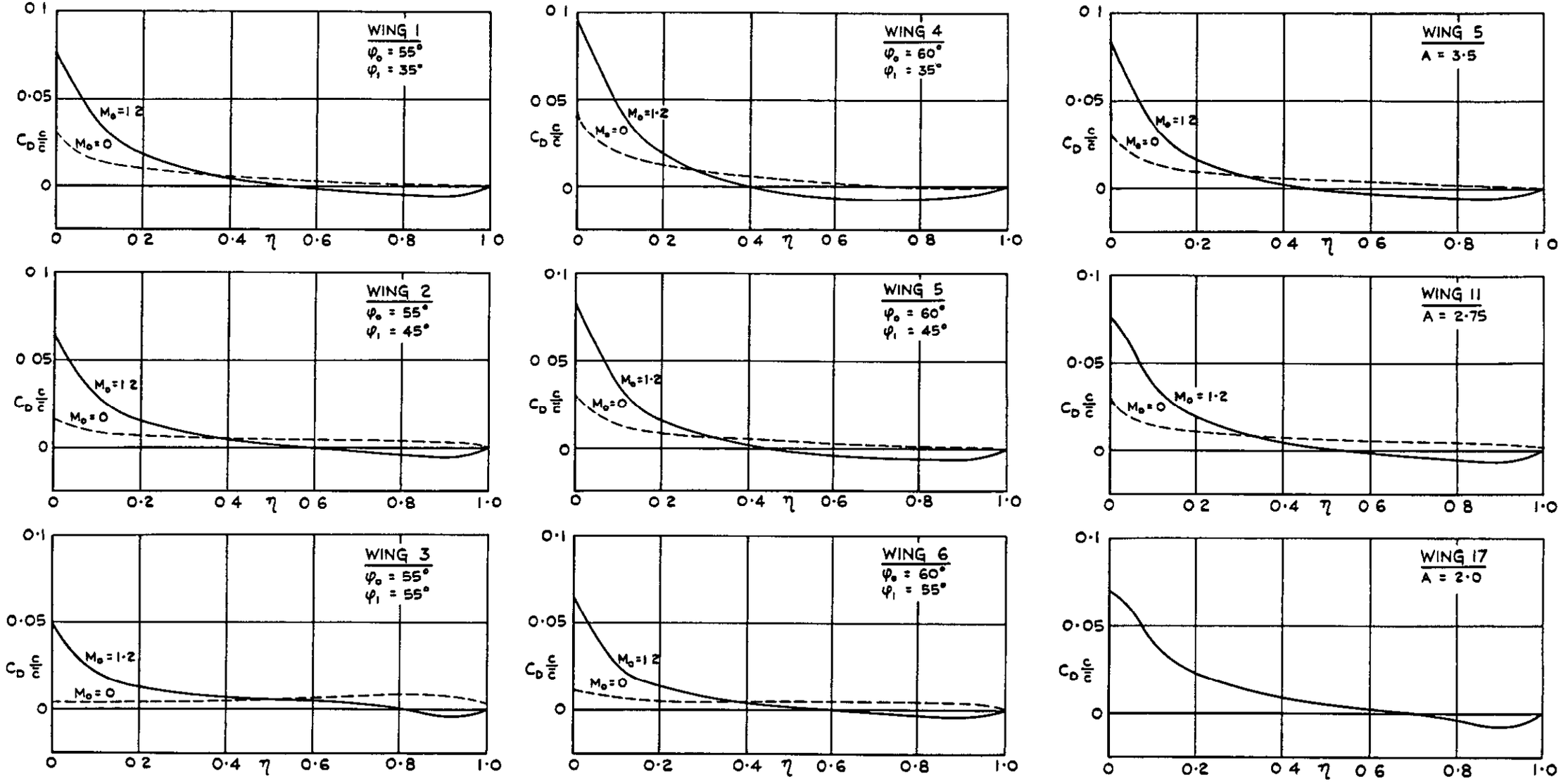

(a) WINGS OF A = 3·5

(b) WINGS WITH $\varphi_0 = 60°$, $\varphi_1 = 45°$

FIG. 48 (a & b) SPANWISE DRAG DISTRIBUTIONS FOR SEVERAL WINGS, WITH LOADING $-\Delta C_p = 0·5 - 0·5\,\xi$, DESIGNED FOR $M_0 = 0$ AND $M_0 = 1·2$.

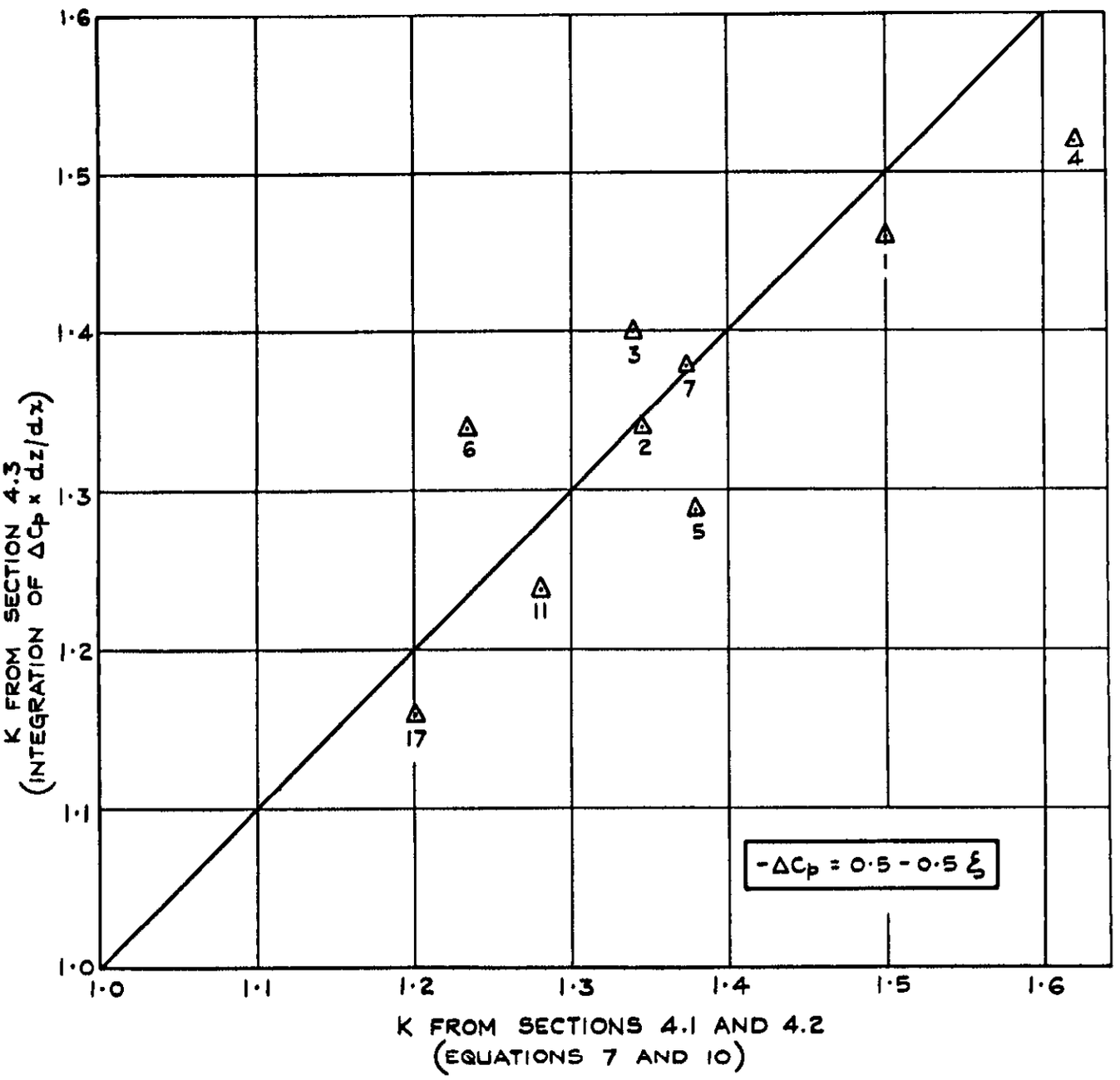

FIG. 49. COMPARISON OF LIFT-DEPENDENT DRAG FACTORS CALCULATED BY TWO METHODS ON SEVERAL WINGS.

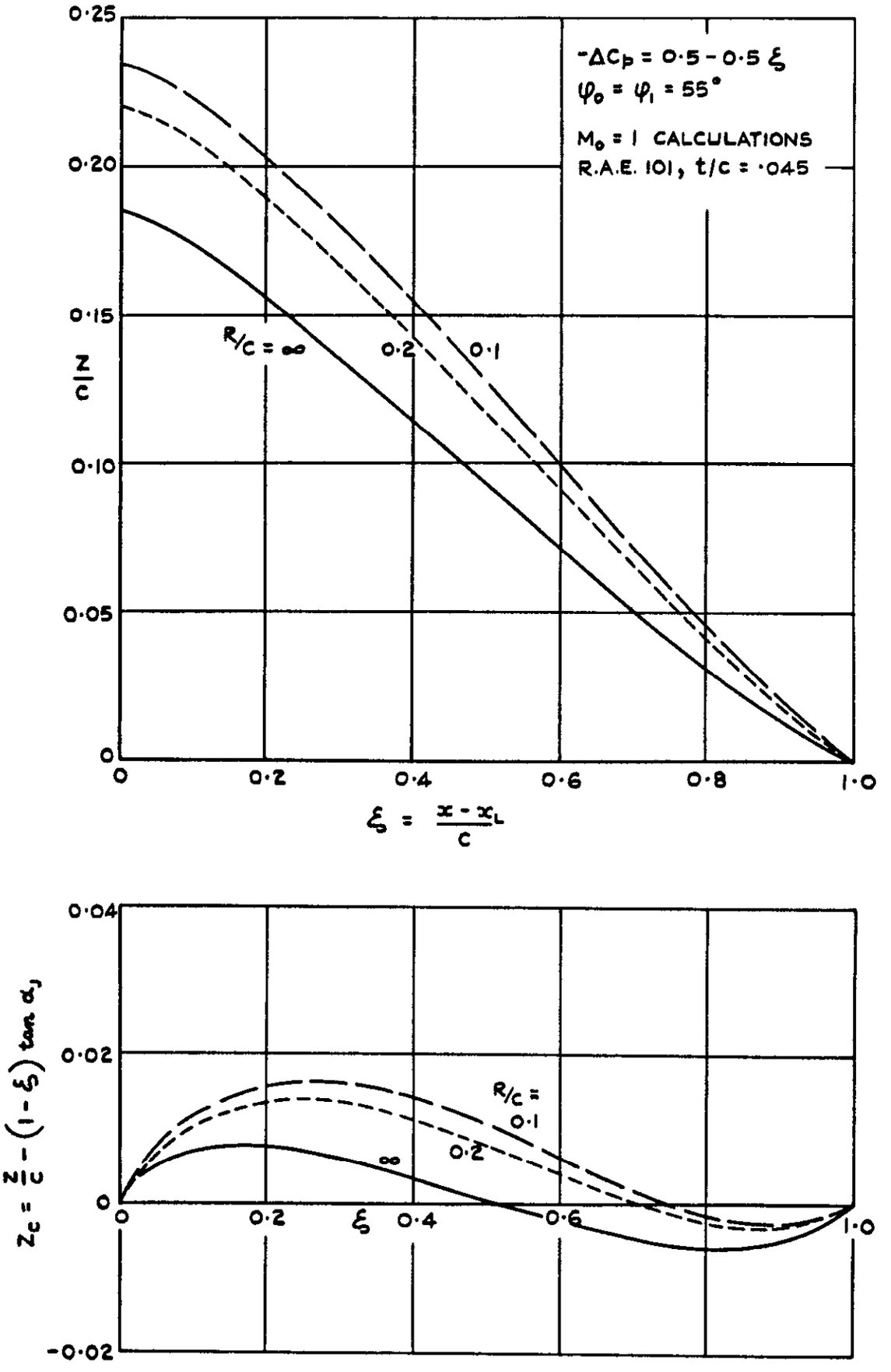

FIG. 50. WING - ROOT SECTIONS OF WING - FUSELAGE COMBINATIONS; TRIANGULAR CHORDWISE LOADING.

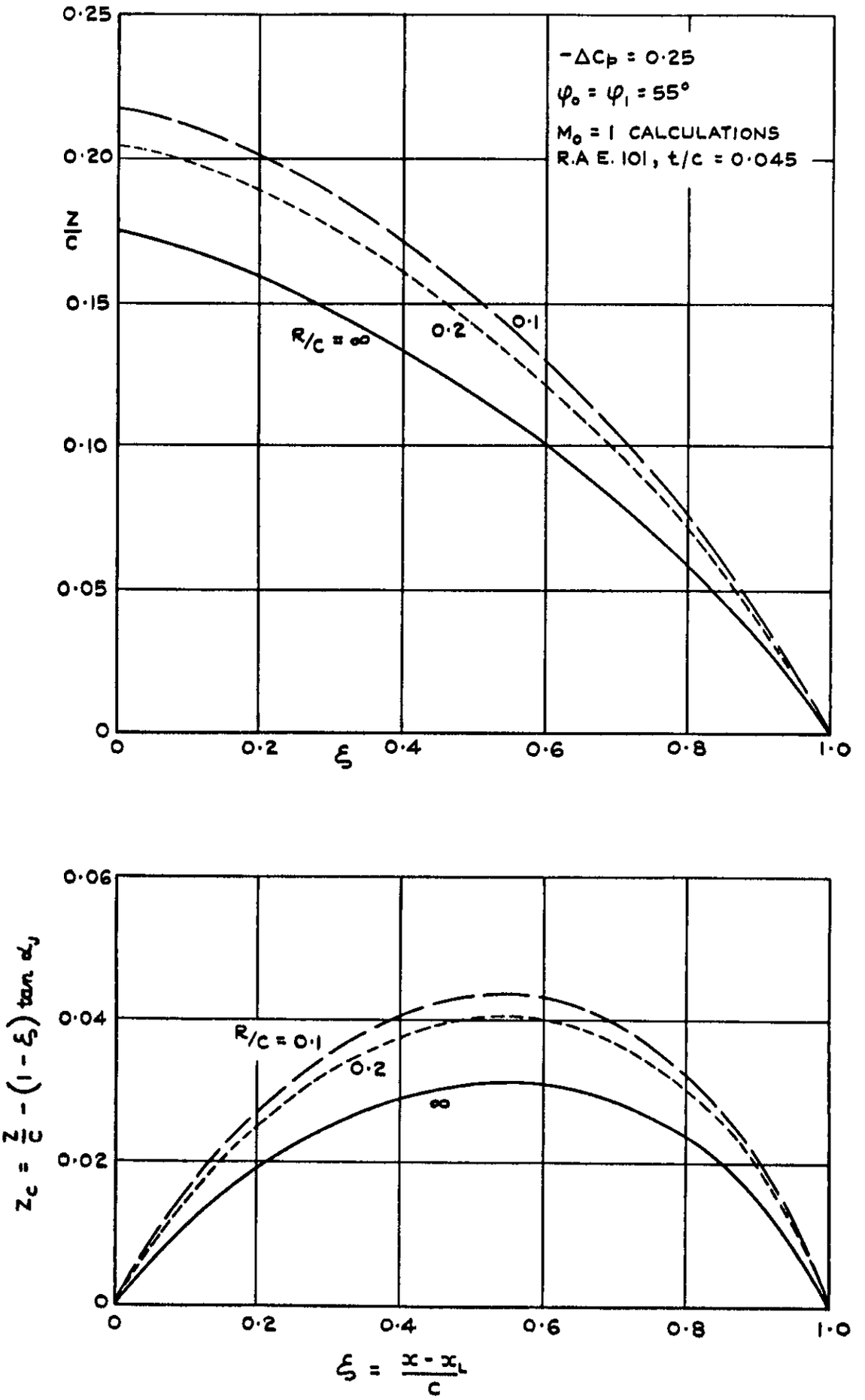

FIG. 51. WING - ROOT SECTIONS OF WING - FUSELAGE COMBINATIONS; UNIFORM CHORDWISE LOADING.

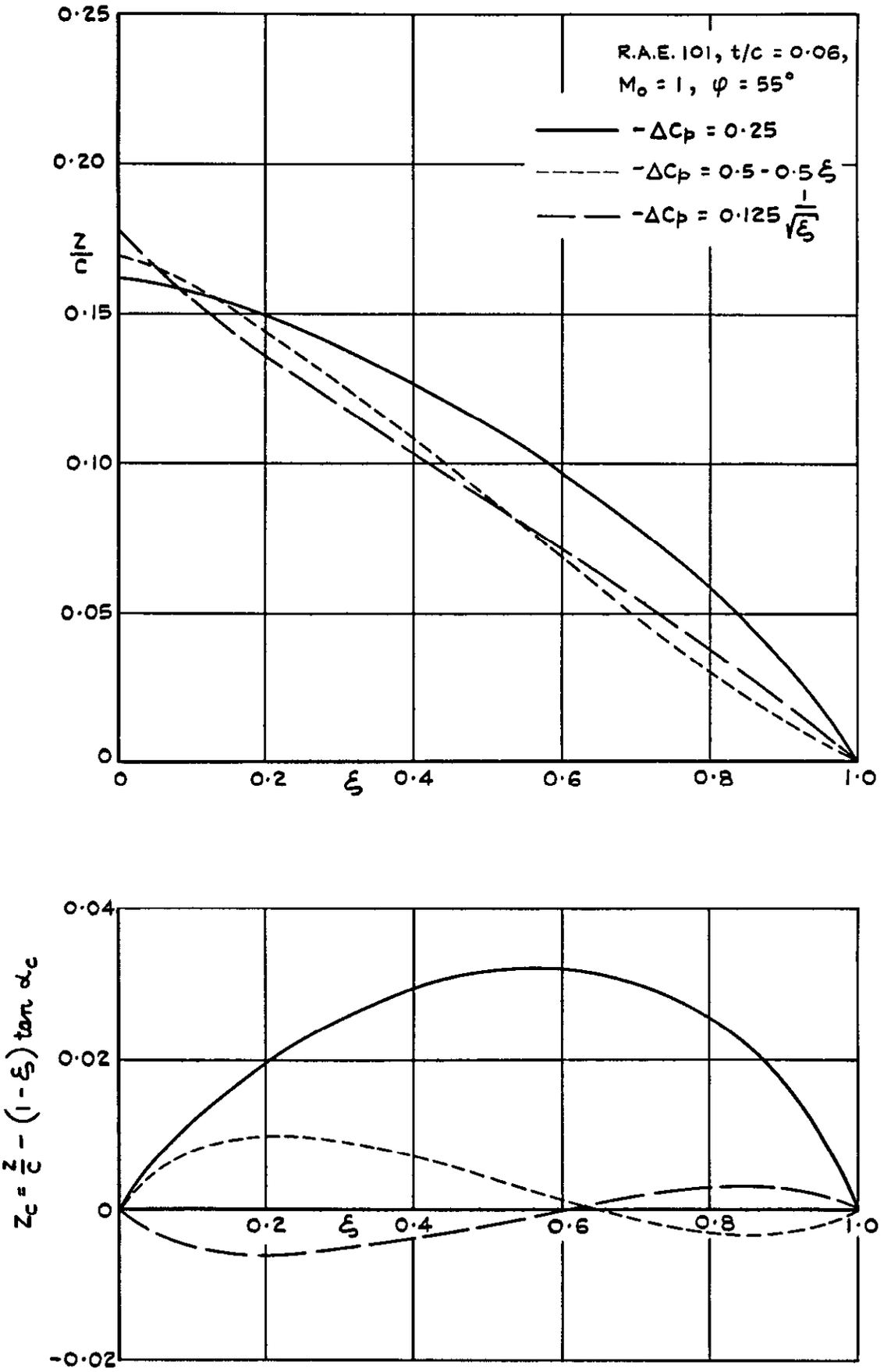

FIG. 52. CENTRE - SECTION SHAPES OF WINGS WITH VARIOUS CHORDWISE LOADINGS.

C.P. No. 512
(21,429)
A.R.C. Technical Report

Published by
HER MAJESTY'S STATIONERY OFFICE

To be purchased from
York House, Kingsway, London w.c.2
423 Oxford Street, London w.1
13A Castle Street, Edinburgh 2
109 St. Mary Street, Cardiff
39 King Street, Manchester 2
50 Fairfax Street, Bristol 1
2 Edmund Street, Birmingham 3
80 Chichester Street, Belfast 1
or through any bookseller

Printed in England

S.O. Code No. 23-9012-12

C.P. No. 512